The role of EBI-3 in a murine model of lung metastases of melanoma

Dissertation

zur Erlangung des Grades
„Doktor der Naturwissenschaften“

am Fachbereich Biologie
der Johannes Gutenberg-Universität Mainz

Kerstin Annika Sauer
geb. am 03.10.1977 in Schwetzingen

Mainz, im September 2007

Aus der I. Medizinischen Klinik und Poliklinik des Universitätsklinikums der Johannes Gutenberg-Universität Mainz

Dekan:

1. Gutachter:

2. Gutachter:

Tag der mündlichen Prüfung: 07.12.2007

Ich erkläre, dass ich die vorgelegte Thesis selbständig, ohne unerlaubte fremde Hilfe und nur mit den Hilfen angefertigt habe, die ich in der Thesis angegeben habe. Alle Textstellen, die wörtlich oder sinngemäß aus veröffentlichten oder nicht veröffentlichten Schriften entnommen sind, und alle Angaben, die auf mündlichen Auskünften beruhen, sind als solche kenntlich gemacht. Bei den von mir durchgeführten Untersuchungen habe ich die Grundsätze guter wissenschaftlicher Praxis, wie sie in der Satzung der Johannes Gutenberg - Universität Mainz zur Sicherung guter wissenschaftlicher Praxis niedergelegt sind, eingehalten.

Ort, Datum Kerstin Sauer

Diese Arbeit wurde in der Arbeitsgruppe für zelluläre und molekulare Immunologie der Lunge an der I. Medizinischen Klinik der Johannes-Gutenberg Universität in der Zeit von 01.10.2004 bis August 2007 angefertigt.

Teilergebnisse der Arbeit sind zur Veröffentlichung in Vorbereitung:

Sauer, K.A., Scholtes, P., Maxeiner, J.H., Karwot, R., Lehr, H.A., Birkenbach, M., Blumberg, R., Finotto, S. **Immunosurveillance of lung melanoma metastasis in EBI-3 deficient mice by IK-DC-induced CD8$^+$ T cells.**

Weitere Publikationen:

Maxeiner, J.H., Karwot, R., Hausding, M., **Sauer, K.A.,** Scholtes, P., Finotto, S. **A method to enable the investigation of murine bronchial immune cells, their cytokines and mediators.** Nature Protocols 2007; 2(1):105-12.

Sauer, K.A., Scholtes, P., Karwot, R., Finotto, S. **Isolation of CD4+ T cells from murine lungs: a method to analyze ongoing immune responses in the lung.** Nature Protocols 2006;1(6):2870-5.

Doganci, A., **Sauer, K.,** Karwot, R., and Finotto, S. **Pathological Role of IL-6 in the Experimental Allergic Bronchial Asthma in Mice.** Clinical Reviews in Allergy and Immunology 2005. **28**: 257-69.

Kongressbeiträge:

Sauer, K.A., Maxeiner, J.H., Scholtes, P., Karwot, R., Finotto, S. **EBI 3 deficient dendritic cells induce a CD8 mediated tumor cell death in a murine model of lung melanoma.** 4th annual symposium of the Association for Immunotherapy of Cancer as joint meeting with "Strategies for Immune Therapy" in Mainz on May 4th and 5th 2006

Sauer, K.A., Maxeiner, J.H., Scholtes, P., Karwot, R., Finotto, S. **EBI-3 deficiency protects from lung melanoma by upregulating IL-12 production in the airways in a murine model.** ATS 2006 in San Diego, May 19th -24th 2006

Sauer, K.A., Maxeiner, J.H., Scholtes, P., Karwot, R., Finotto, S. **EBI-3 deficiency protects from lung melanoma by inducing infiltration of dendritic cells in the tumor where they induce CD8 mediated tumor cell death.** ECI 2006, 16th European Congress of Immunology in Paris, September 6th – 9th 2006

Sauer, K.A., Scholtes, P., Maxeiner, J.H., Karwot, R., Lehr, H.A., Galle, P.R., Birkenbach, M., Finotto, S. **Immunosurveillance of lung melanoma metastasis in EBI-3 (-/-) mice by IKDCs- induced CD8^{+} T cells.** Immunology 2007, 9th Annual Meeting of the American Association of Immunologists in Miami Beach, May 18th-22nd 2007

Der Mensch hat 3 Wege, um zu lernen

Durch Nachdenken

- das ist der Edelste

Durch Nachahmung

- das ist der Leichteste

Durch Erfahrung

- das ist der Bitterste

(Konfuzius)

1 Introduction

1.1 Immune System

The mammalian immune system is an interactive network of lymphoid organs, cells, humoral factors and cytokines[1]. Its task is to protect the organism from abundant infectious microbes that possess a diverse collection of pathogenic mechanisms, at the same time avoiding responses pathological accompanied by excessive damage of self-tissue but recognize and eliminate mutated cells. The environment contains a wide range of pathogenic microbes that threaten the host by a broad selection of pathologic mechanisms. Therefore, the immune response uses a complex system of protective mechanisms to control and eliminate these organisms. All of these mechanisms rely on detecting structural features of the pathogens that mark them as distinct from host cells. This host-pathogen discrimination is essential to permit the host to eliminate the pathogen without excessive damage to its own tissues.

The mechanisms permitting recognition of microbial structures can be broken down into two general categories: the innate and the adaptive immune response.

The recognition molecules used by the innate system are expressed broadly on a large number of cells enabling this system to act rapidly after an invading pathogen is encountered thereby providing the initial host response. Because the adaptive system is composed of small numbers of cells with specificity for any individual pathogen, the responding cells must proliferate after encountering the pathogen to attain sufficient numbers to mount an effective response against the microbe. Thus, the adaptive response generally expresses itself temporally after the innate response in host defense. A key feature of the adaptive response is that it produces long-lived cells that persist in an apparently dormant state, but that can re-express effector functions rapidly after repeated encounter with an antigen. This provides the adaptive response with the ability to manifest immune memory, permitting it to contribute to a more effective host response against specific pathogens when they are encountered a second time, even decades after the initial sensitizing encounter[2].

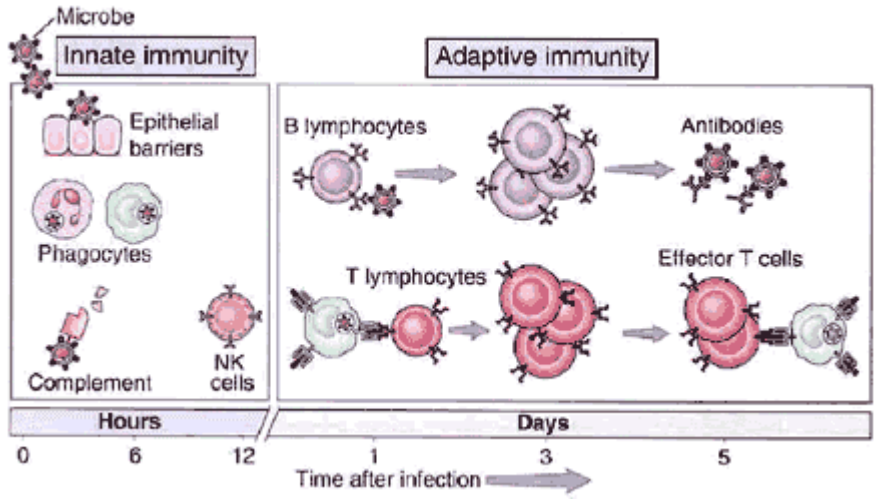

Figure 1: Innate and adaptive immunity. The mechanisms of innate and adaptive immunity provide the initial defense against infections. Adaptive immune responses develop later and consist of activation of lymphocytes[3].

1.2 The Lung

1.2.1 Anatomy of the Lung

The human lungs are located in the chest cavity on the left and right side of the heart. The left lung consists of two lobes while the right lung is divided into three lobes. As shown in Figure 2, the trachea splits into 2 primary bronchi that enter the roots of the lungs. Within the lungs these bronchi continue to divide into smaller units - called secondary and tertiary bronchi – creating a branching system in the lungs. Further divisions lead to the terminal bronchioles that end in the alveolar sacks which are comprised of clusters of alveoli that provide an enormous surface area and are wrapped in blood vessels[4, 5].

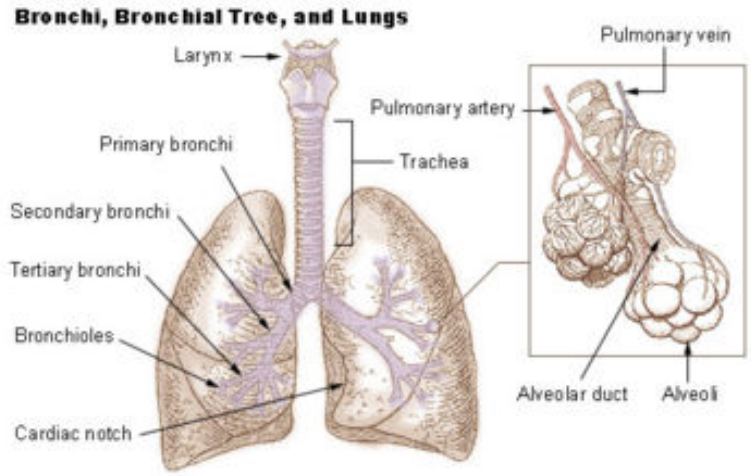

Figure 2: Anatomy of the lungs[4]. The left lung consists of two lobes and the right lung is divided into three lobes. The trachea splits into two bronchi that divide into smaller units within the lungs.

1.2.2 Function of the Lung

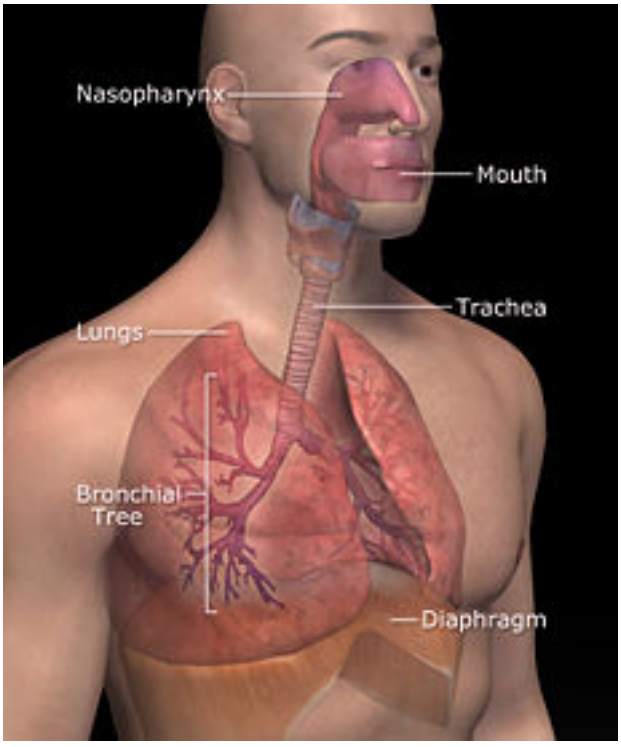

The main function of the lung is to deliver oxygen to the blood circulation and excrete carbon dioxide. Cells need oxygen for their energy production while carbon dioxide is the waste product that results from this process. Oxygen is brought into the airways via inhaling air through the mouth or the nose, both of which have effective filter systems that prevent irritants from accidentally entering the airways and causing a dangerous airway obstruction. The inhaled air flows through the branches of the respiratory tree into the alveolar sacks where a network of fine capillaries

Figure 3: Human respiratory system[4]. Oxygen is brought into the bronchial tree via inhaling air through the mouth or the nose.

allows the transport of blood over the surface of the alveoli. The exchange of oxygen and carbon dioxide takes place via diffusion across the alveolar membranes[4, 5].

1.3 Cancer

Cancer is a major health problem worldwide and one of the most predominant causes of deaths in children and adults. Transformed cells that show uncontrolled proliferation and spread of mutated clones, lead to cancer. Agents that are able to induce cellular transformation were all found to act on the level of DNA and are called carcinogens. Somatic mutations are the changes that can make a cell cancerous if the mutation leads to an abnormal chromosome that evades the regulating mechanisms of cell proliferation. However, several somatic mutations are necessary to cause cancer. Among the most potent triggers for somatic mutations are ultraviolet and ionizing forms of radiation, some organic and inorganic chemical compounds as well as many viruses[6]. The growth of malignant tumors is determined in large part by the proliferative capacity of the tumor cells and by the ability of these cells to invade host tissues and metastasize to distant sites. Although the immune system reacts against many tumors, one of the factors in the growth of malignant tumors is their ability to evade or overcome the mechanisms of host defense[7].

1.3.1 Tumor and Metastasis

The most life-threatening characteristics of malignant tumor cells are their abilities to detach from the primary tumor, invade into surrounding normal tissues and form metastatic growth at distant sites.

Transformed cells show genetic and phenotypic instability and have a higher tendency to undergo further mutations and phenotypic drifts than normal cells. The Darwinian selection – survival of the fittest – then meets the above described characteristics of cancer cells which logically creates cell populations that are resistant to the host's homeostatic growth controls, immune attack and environmental suppressions[8].

To develop successful treatment of cancer and its metastatic disease, it is necessary to understand the circumstances and mechanisms that cause one tumor to metastasize while another tumor does not. Eccles and Welch[9] described the basic mechanisms of metastasis (Figure 4) suggesting three possible ways that are not mutually exclusive but could all contribute.

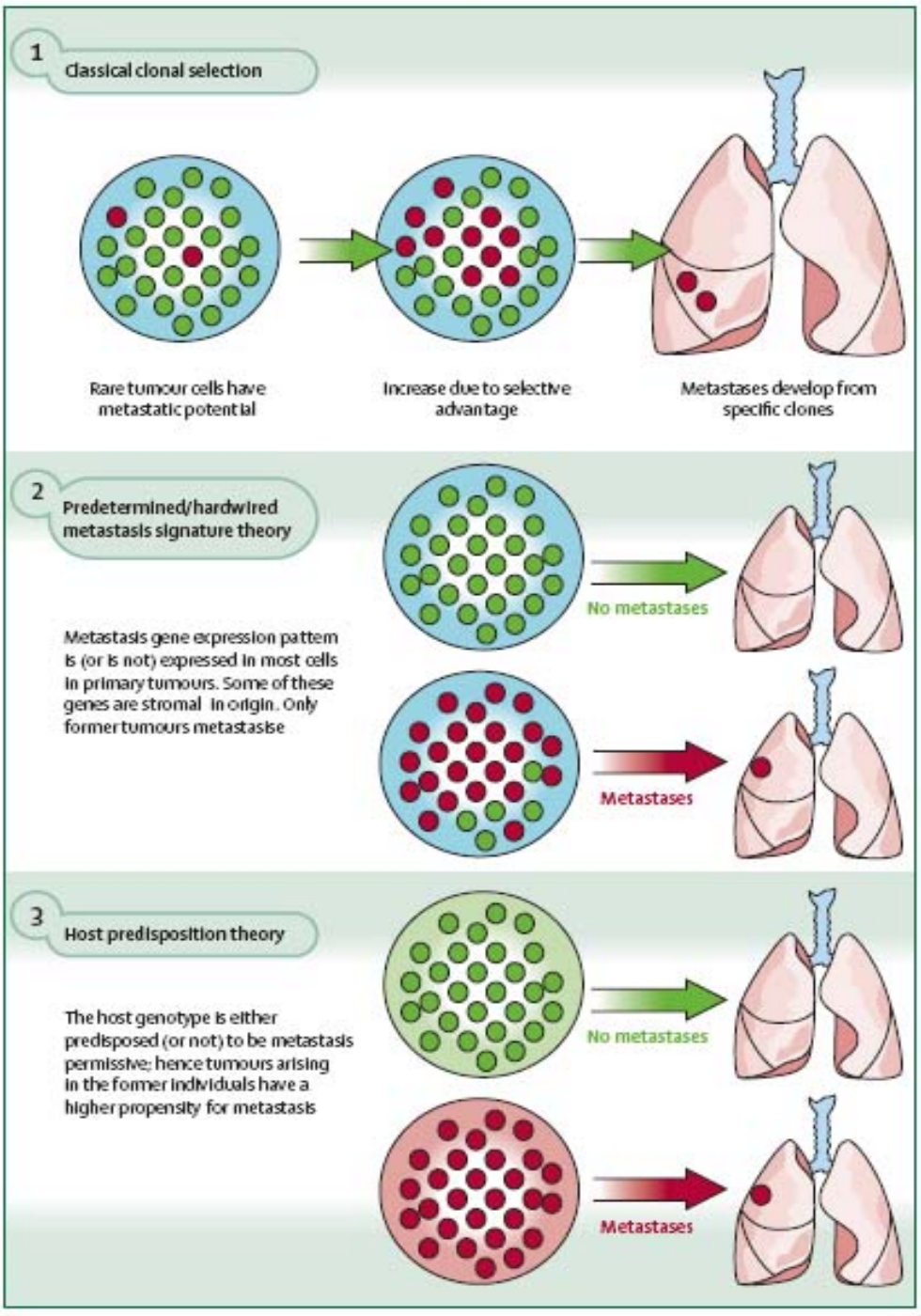

Figure 4: Basic mechanisms of metastasis[9]. The three suggested ways of metastasis are not mutually exclusive but could all contribute.

Keeping in mind the fact that cells which detach from tissue and therefore are disrupted from their correct substrate undergo programmed cell death, the organism per se are protected from cells establishing themselves outside their correct anatomical location. Therefore, resistance to apoptosis is essential for being able to disseminate

from the original tumor and reestablish cell growth at another site. The deregulation of apoptosis in metastases have been shown in many studies and included activation of survival pathways, overexpression of anti-apoptotic proteins and upregulation of metalloproteinases which induce the release of growth factors, down-regulate death receptors and condition extracellular matrix for invasion[10].

It is generally accepted that tumor growth depends largely on the tumor's ability to induce enormous and unusual vascularization of the tumor by overexpressing angiogenic cytokines like VEGF. The resulting very primitive vascular system is characterized by leaky capillaries which can simplify the process of cell dissemination and thereby support the formation of metastases[11]. Lymphangiogenesis is related to vascularization and its major cytokines, VEGF-C and VEGF-D, are linked to the poor prognosis of cancers involving lymph node metastasis[12].

In order to enter and exit the circulation, tumor cells need a variety of motility mechanisms that can, for example, be activated by endothelial cells during angiogenesis[13].

The summary above names numerous criteria that metastatic cells have to meet, but the question still remains whether the metastatic potential of certain cancers can be determined. Some cancers show a preference in metastasizing to certain tissues more commonly than others, as displayed in Figure 5. Partially this phenomenon can be explained by the blood flow, for example, the liver metastases from colorectal cancer, whereas in other cancers, this explanation fails (for example bone metastases from breast carcinoma)[14]. Several approaches to identify genes that are responsible for initiating metastases revealed a variety of genes that are common for metastases to all sites such as osteopontin. In addition, there are genes like CXCR4 that are only expressed in cell lines that have a predilection to grow in a certain tissue. These studies also pointed out that a combination of genes is necessary for successful metastasis to each site and that there are more than 20 genes which act as metastasis suppressors[15, 16]. Furthermore, the process of metastasizing depends on the tumor environment, although in many cases the tumor itself can condition the microenvironment and therefore tumor-host interactions in a way that benefits tumor growth[17].

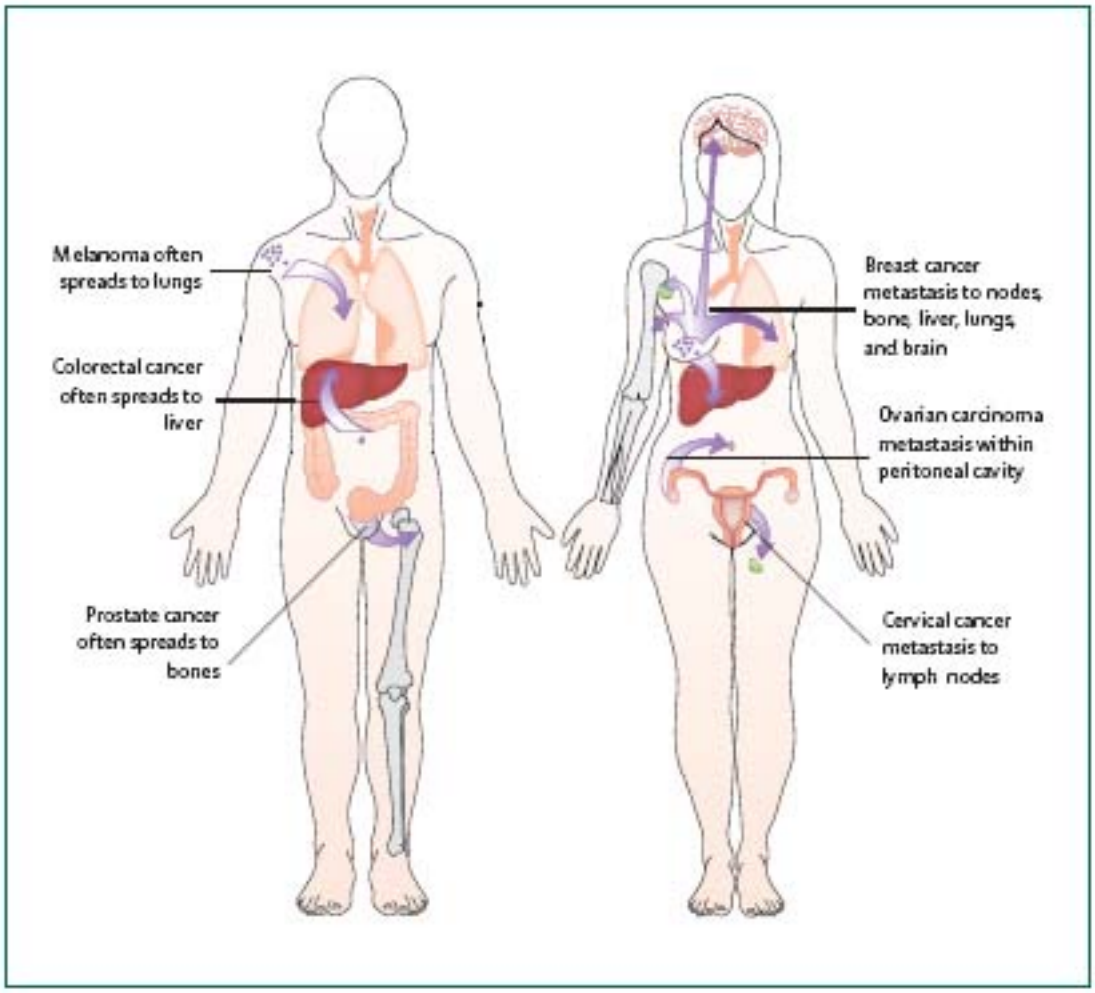

Figure 5: Can cancer spread be predicted?[9]. Some cancers that show a preference in metastasizing to certain tissues are displayed.

Since science has limited possibilities to prevent the spreading of cancer and the establishment of metastasis it is even more important to find ways to treat the metastatic disease effectively.

1.3.2 Malignant Melanoma

The World Health Organization describes malignant melanoma as the major cause of death from skin cancer, although it is far less prevalent than non-melanoma skin cancers. Since the early 1970s, malignant melanoma incidence has increased significantly. There has been an average four per cent (4%) increase every year in the United States. A large number of studies indicate that the risk of malignant melanoma

correlates with genetic and personal characteristics, as well as a person's Ultra Violet (UV) exposure behavior[18].

Figure 6: Examples of human malignant melanoma[18, 19].

Transformed melanocytes are the precursor of malignant melanoma. Normal melanocytes are specialized pigmented cells, particularly found in the basal layer of the epidermis of the skin, where they produce melanin and are responsible for skin and hair color. The ability of an individual to tolerate the sunlight is directly proportional to melanin pigmentation. Melanin is a complex polymer of tyrosine, which upon production from melanocytes is packaged in melanosomes that are transferred through dendritic processes into keratinocytes, where they provide photoprotection[20]. Upon UV radiation, keratinocytes produce factors that regulate the survival, differentiation, proliferation and motility of melanocytes, which then secrete melanin that leads to the tanning of the skin. Thereby, melanocytes protect the skin from damage by UV radiation[21]. To avoid UV light induced apoptosis, melanocytes express high levels of the anti-apoptotic protein Bcl-2 that forms a heterodimer with the pro-apoptotic protein Bax[22].

Cell proliferation is under the control of a series of positive and negative regulators that all come into action at sequential points throughout the cell cycle. Disturbance of these checks could contribute to cancer development by allowing excessive cell proliferation. The point in G1 at which cells commit to DNA synthesis is controlled by protein complexes consisting of cyclin-dependent kinases and cyclins. These complexes are inhibited by low molecular weight proteins, such as $p16^{INK4}$, $p15^{INK4B}$ and p18. Deletion or mutation of these cyclin-dependent kinase-inhibitors could lead to unchecked cell growth[23].

If the above described protection mechanism fails and melanocytes transform, malignant melanoma may arise. This process is described in Figure 7 showing normal skin in Figure 7a, that has dendritic melanocytes within the basal layer of the epidermis. Figure 7b displays increased numbers of dendritic melanocytes that occur in benign melanocytic naevi. These benign cells can progress to the radical-growth-phase melanoma shown in Figure 7c and may further advance to the vertical-growth-phase (Figure 7d), a dangerous stage of melanoma where cells have metastatic potential meaning that the vertical growth allows the melanocytes to access the blood vessels in the subcutaneous tissue.

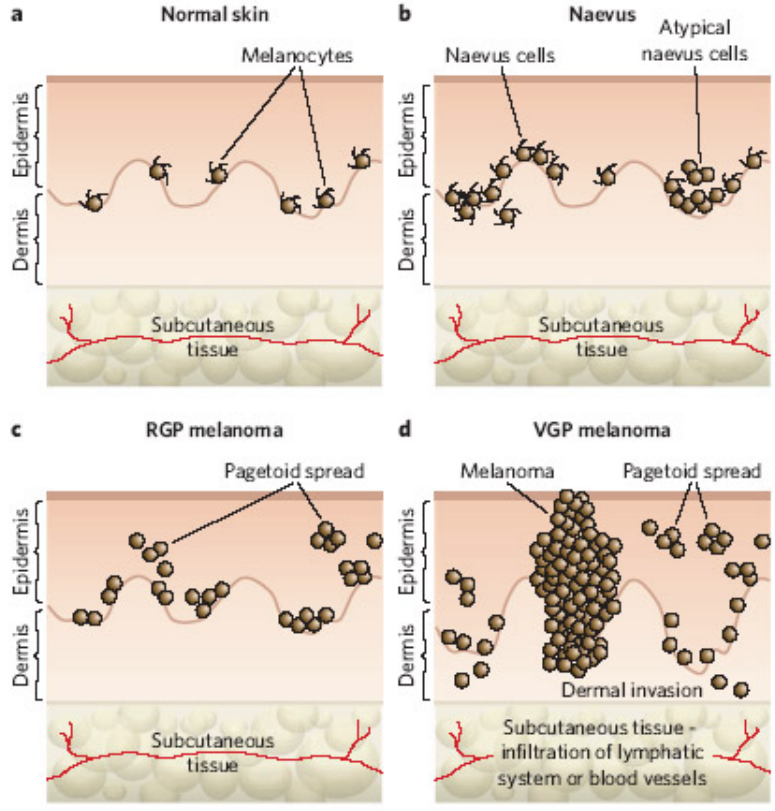

Figure 7: Progression of melanocyte transformation[21]. a) normal skin with melanocytes in the epidermis, b) benign melanocytic naevi that show increased numbers of dendritic melanocytes, c) melanocytes in the radical-growth-phase, d) melanoma progressed into the vertical-growth-phase.

1.3.3 Tumor Immunology

The immune system is able to distinguish “self” from “non-self” in order to protect the host from microbial infections. Cancers challenge the immune system in a different way, since this disease arises from the host’s own tissues, meaning that the genes which are

expressed by the tumor are also expressed by the host's normal tissue[24]. Paul Ehrlich described the inability to prevent immune recognition of the host's own tissue as "horror autotoxicus". To avoid autoimmune responses, developing T- and B-lymphocytes undergo an educative process in the bone marrow and thymus where the immature immune cells express an almost unlimited variety of receptors. If these receptors react with self-antigen expressed on antigen presenting cells (APCs) the immune cell is negatively selected, meaning it is deleted. This process is called central tolerance. Lymphocytes undergo positive selection and may further mature if their receptors do not recognize self-antigen[25]. But central tolerance is unable to remove all self-reactive T cells. Additional mechanisms to erase these cells now oblige to the peripheral tolerance. In secondary lymph tissue mature naïve T cells can undergo activation or tolerance upon antigen recognition. The pool of circulating T cells is influenced by extra-thymic self-antigens. High expression of antigen leads to activation of T cells via a process that is described later in this paragraph. Activated T cells, which are self-reactive, are then deleted. To do so, the immune system has many mechanisms available, one of which is the T cell subset called "regulatory T cells" that express the cell surface markers CD4 and CD25 and are able to effectively dampen the T cell response[26]. In contrast, antigen presentation at low levels may be ignored by the immune system and results in an immune repertoire of lymphocytes that remain inactivated but present in the periphery. If an altered form of the self-antigen occurs – e.g. transformed cells – and is highly expressed the lymphocytes will be activated and in consequence work against the self-antigen which leads to autoimmunity. Destruction of mutated tissue or cancer cells therefore is always connected with autoimmunity[24].

Adaptive immunosurveillance is able to trigger antigen-specific T cell responses, which are initiated by dendritic cells (DCs) as shown in Figure 8. Tumor cells secrete antigens that can be captured by immature DCs which are able to take up the antigen and start intracellular processing that leads to antigen presentation on the surface of the DCs by its major histocompatibility class (MHC) I and class II molecules. To efficiently activate the DCs and induce its maturation, tumor cells shed danger signals, e.g. heat shock proteins (HSP) or cytokines like IFN-α. During the process of ripening from an immature DC to a professional APC the cells also start to express the co-stimulatory B7 molecules, CD40 and the chemokine receptor CCR7 which directs their migration to

regional lymph nodes[27]. Naïve T cells in the lymph nodes express CCR7 also and can by down-regulating this chemokine migrate within the lymph node toward the activated DC. The likelihood of co-localization of DCs and T cells is thus increased. Once both cell types meet, the antigen presented on the MHC class I molecule is presented via direct physical interaction to the matching T cell receptor (TCR) of the $CD8^+$ T cell thereby activating the T cell[28]. Similarly, the TCRs of the $CD4^+$ T cells interact with the MHC class II molecules of the APCs. In addition, $CD4^+$ T cells express CD40 ligand on their surface, which binds the CD40 on the APCs. This linking procedure in turn further activates APCs. Ultimately, the activated $CD8^+$ T cells differentiate into cytotoxic T lymphocyte (CTLs) and migrate together with $CD4^+$ T helper cells out of the lymph node into the tissue and mount an attack against the tumor via tumor cell lysis. During this complex course of action many different cytokines are secreted by APCs as well as by T cells supplying help to the cellular immune response. The type of cytokine produced plays an important role in the decision of how the immune response is further built[29].

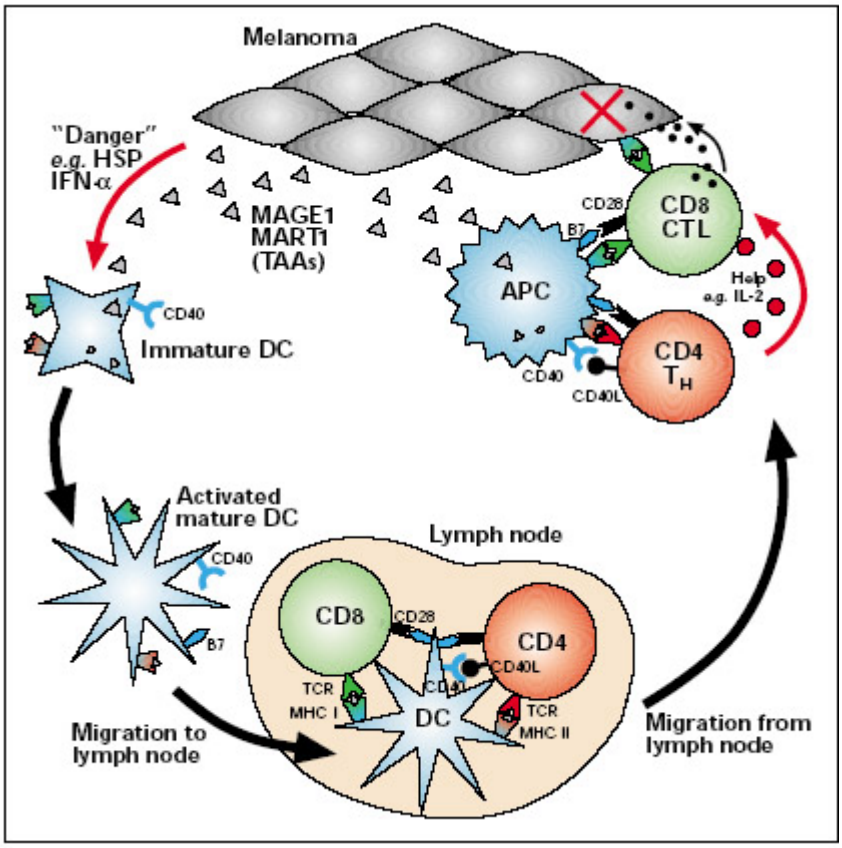

Figure 8: The adaptive immune response to tumor-derived tumor associated antigens (TAAs)[29]. Gray triangles depict the TAAs MAGE1 and MART1. Heat shock proteins (HSP) can act as danger signals. Red circles in mark secreted cytokines.

Recognition of transformed cells by the innate immune system involves natural killer (NK) cells which are able to kill MHC class I deficient tumor cells [30]. NK cells express a variety of surface receptors whose ligands are found on transformed cells. After binding the tumor cell via these receptor-ligand complexes, the NK cells secrete perforin and many cytokines including IFN-γ that lead to cytotoxicity. Among the many receptors on NK cells one is of special interest: the lectin-like NKG2D homo-dimer that associates with DAP10 and is broadly expressed on NK cells, macrophages and some T cell subsets. The NKG2D-DAP10 complex can interact with MHC class I related ligands on transformed cells[31-33]. NKT cells are a subset of T cells that also express some NK cell marker and have the ability to regulate CTL as well as NK cell mediated anti-tumor activity[34]. The invariant TCR of these cells recognize the MHC class I-like molecule CD1d. This stimulation leads to a rapid secretion of T helper 1 and 2 cytokines from the NKT cells, which provides help to the NK cells and connects the innate and the adaptive immune systems.

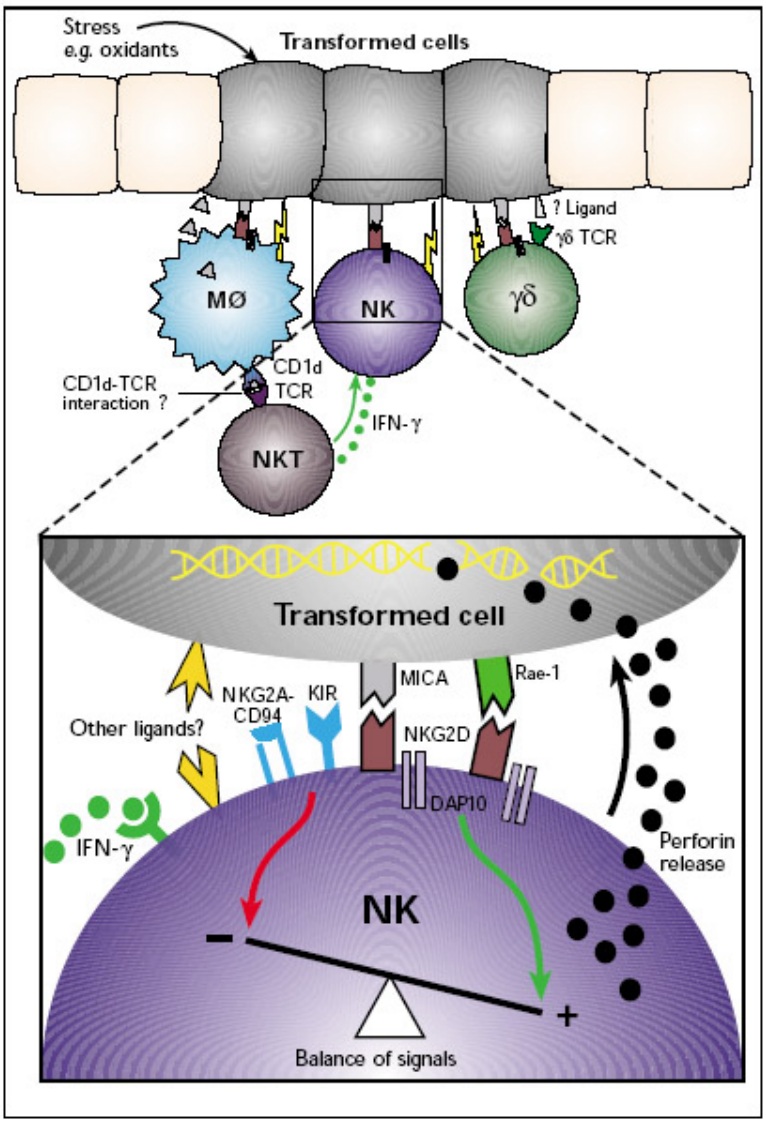

Figure 9: Recognition of transformed cells by the innate immune system[29]. Example of stress-induced transformed cells in an epithelial layer. Ligands that may lead to stress-induced cell transformation are MICA and Rae-1 which interact with the NKG2D-DAP10 complex. NK effector cells may also express inhibitory receptors among them KIR and CD94-NKG2A that send negative signals upon interaction with MHC class I molecules.

Innate and adaptive immunity cannot be seen as two independently working systems but they interact with each other to contribute to a more powerful immune response towards the cancer.

The significant reason why cancers are still resistant to most current treatments is their capability to evade the mechanisms of the immune system by various strategies. Since tumors develop from the host's own tissue they are usually tolerated by the

immune system because they express self-antigens and do not seem dangerous to the host's immune system. APCs then capture exosomes from living tumor cells or apoptotic bodies and present these antigens without co-stimulation which leads to an inappropriate activation of the corresponding T cells and finally to anergy or apoptotic death of these T cells. This process is shown in Figure 10b and results in T cell tolerance. The extremely fast proliferation of tumor cells leads to a rapid growth and spread of the tumors, which may overwhelm the capacity of the immune response to eradicate tumor cells. In addition, many tumor cells do not express MHC molecules as well as co-stimulatory molecules and are therefore not adequately recognized by $CD4^+$ and $CD8^+$ T cells. Another possibility is the loss of tumor antigens that are able to induce immune responses[24]. Immune recognition can also be evaded through more active mechanisms of the tumor cells such as secretion of immunosuppressive cytokines including TGF-β, IL-10 and prostaglandin E-2, as displayed in Figure 10a. These cytokines can act directly on $CD4^+$ and $CD8^+$ T cells or indirectly via APCs and suppress the anti-tumor response by stopping the proliferation of the antigen-specific T cells[27]. There are also a number of T cell subsets described which have regulatory or suppressor functions to maintain self-tolerance. These cells represent potential barriers to effective anti-tumor immune responses. Figure 10c shows how NKT cells can be stimulated via their T cell receptor that interacts with the CD1d molecule expressed on APCs. This stimulation induces the secretion of various cytokines many of which are anti-inflammatory and have the potential to inhibit activation and proliferation of tumor specific T cells[29, 34]. The inhibition of an anti-tumor response by $CD4^+CD25^+$ T cells is revealed in Figure 10d. This T cell subset is well characterized and has its major function as suppressor of autoimmune-responses. The antigen specific $CD4^+CD25^+$ T cells are able to down-regulate the cell-mediated immune response probably by interfering with the APCs[29, 35, 36]. Many tumor cells evade the immune response by developing dysfunctional apoptotic pathways. This can be accomplished using many different ways like increased expression of anti-apoptotic molecules as Akt, Bcl-2 and Bcl-xL or by down-regulating the expression of pro-apoptotic molecules Bax and Bak[37].

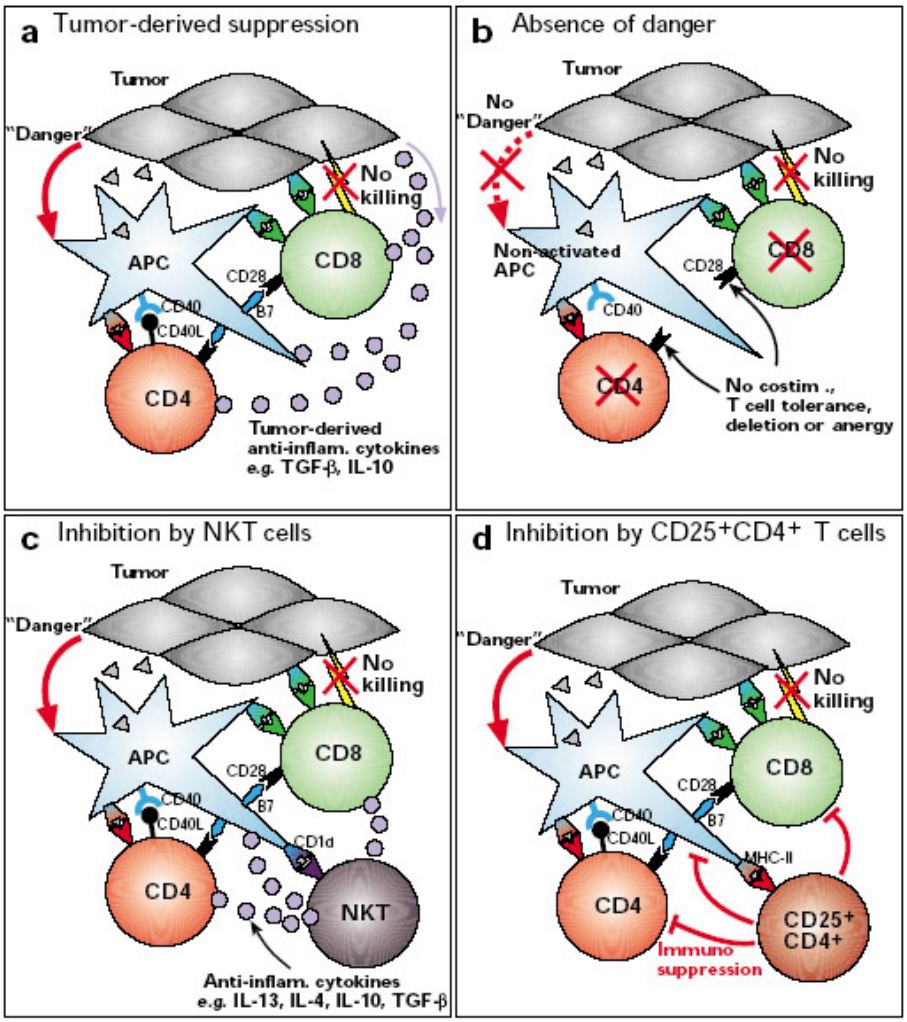

Figure 10: Mechanisms for tumor tolerance[29]. a) tumor-derived suppression by anti-inflammatory cytokines secreted from the tumor itself. b) Absence of danger occurs if the tumor does not send alarm signals. c) Inhibition by NKT cells that, when activated, produce a range of cytokines many of which have the ability to inhibit cell-mediated anti-tumor responses. d) Inhibition by antigen-specific $CD4^{+}CD25^{+}$ T regulatory cells.

1.3.4 Therapeutic Approaches

Classical therapies that treat cancer metastases are radiotherapy and chemotherapy, both targeting fast proliferating cells by inhibiting their DNA replication, DNA repair or the cell cycle. Receptor tyrosine kinases activate upon interaction with their ligand the Ras/Raf/MEK/ERK signaling. This pathway is a key regulator of cell proliferation and ERK is found overexpressed in up to 90% of human melanomas. Recently, therapies that focus on such specific molecules of the cancer are used in clinical trials. Small

molecule inhibitors and antibodies are targeting oncogenic signaling pathways like receptor tyrosine kinases (e.g. VEGFR-1 and VEGFR-2) and vascularization. Combination therapy of both molecular strategies and treatments combining anti-angiogenic and cytotoxic agents are used to find the best therapeutic effect[21].

Some of these therapies are mentioned in this chapter. In order to reach effective tumor-antigen specific cytotoxic T cell responses many strategies have been tested. Some of these approaches include the alteration of the peptide/TCR interface with the aim to develop high affinity T cells.

As a result of the success of vaccines in eliminating viral diseases, the interest in finding such therapies for cancer grew rapidly. Applying peptide-pulsed DCs to the patient is currently the most successful form of vaccination and treatment. Although hundreds of trials have been completed, it is still unclear how to create the best DC-based therapy[27, 38]. The use of peptides as vaccines that allow the hypothesis, that these peptides will be recognized and therefore are processed to create a strong immune response, is another possible treatment[24, 39]. In contrast, DNA vaccines contain various potential epitopes compared to peptide vaccines. A plasmid that encodes the antigen of interest is injected into the patient and will be taken up by professional APCs such as DCs[24]. Earlier studies used tumor cells as vaccines. Here, the advantages have to be balanced against the disadvantages. Theoretically, the tumor cell vaccines include all the relevant tumor antigens, which are needed to create a successful anti-tumor response. Furthermore, knowledge of the specific antigens is not necessary to develop the vaccine. However, autoimmunity is one dangerous side-effect and an increasing anergic status of the T cells may arise due to the lack of functional co-stimulatory molecules on the vaccine[39].

Targeting T regulatory cells with antibodies has been shown recently to eliminate the cell population that suppresses the immune system. Using an antibody against CTLA-4 which is expressed on the surface of this cell population showed some anti-cancer responses[40, 41]. Autoimmune diseases as side-effects were controllable while other antibodies, e.g. against the glucocorticoid-induced TNF receptor (GITR) lead to unacceptable side-effects[42]. IL-10 and TGF-β are two of the soluble, inhibitory cytokines produced by T regulatory cells. Their immunosuppressive function can be reversed upon blockade[43]. IL-2 is the best-studied cytokine for targeted

immunotherapy. The earliest investigations lead back to the 1980's when its role as activator and expander of tumor specific T cells was discovered and connected to the potency for immunotherapy. Unfortunately, IL-2 is the cytokine that is responsible for the growth and differentiation of all T cells thereby inducing autoimmunity. This limits the use of this cytokine[44]. Similarly, CD25 is expressed on T regulatory cells and targeting this cell surface molecule with an antibody is an approach to eliminate the $CD4^+CD25^+$ T regulatory cells. But CD25 is also expressed on newly activated $CD4^+$ T cells as well as on effector $CD8^+$ T cells[45]. Appropriate timing and dosage of IL-2 and anti-CD25 is therefore crucial to induce a beneficial immune response.

Monoclonal antibodies were first discovered in the late 1970`s and have become a standard therapy for several malignancies. Advantages are their high selectivity and safety and enhancement of the anti-tumor immune response. There are several classes of antibodies used. The first antibodies in therapy applied their anti-tumor effect via antibody-dependent cellular cytotoxicity or complement-dependent cytotoxicity. To date, many other classes of antibodies have been developed which are acting against a variety of cell signaling molecules and cellular targets like growth factors including VEGF and epidermal growth factor receptor (EGFR)[46, 47]. Table 1 summarizes some of the current cancer vaccine strategies.

Table 3. Cancer vaccines: strategies

I. Antigens alone with or without adjuvants
- Peptides
- Gangliosides
- Immunoglobulin idiotypes

II. Dendritic cells
- Peptides, immunoglobulin idiotype
- Tumor lysates
- DNA or RNA

III. Tumor cells unmodified or modified
- Autologous
- Allogeneic
- Mixed autologous-allogeneic

IV. Tumor-APCs hybrid

V. DNA alone (naked DNA), recombinant viruses (adenovirus, vaccinia, others)

Table 1: Examples of current cancer vaccine strategies[9]. Five groups of current vaccines strategies are displayed.

1.3.5 Mouse model of metastatic Melanoma

In order to obtain malignant melanoma cell lines of differing metastatic potential, Fidler et al.[48] used in vivo selection to enrich tumor cell populations with variants of high lung colonization abilities. The murine B16 melanoma cell line spontaneously arose in C57B/6 wild-type mice and showed low in vivo metastatic potential. Metastatic variants were selected for their abilities to implant, invade, survive, and grow to form gross lung tumor colonies after i.v. injection into syngeneic C57B/6 mice. Pulmonary tumor nodules were identified by their melanin pigmentation and removed from the lung for in vitro culture. The B16 cells that grew in culture after this first in vivo selection were designated as line B16-F1. These cells were harvested and injected i.v. into new groups of syngeneic animals to obtain the line B16-F2. After 10 selections, the B16-F10 line was obtained which was more metastatic when compared to the B16-F1 line in lung colonization[48] and spontaneous pulmonary metastasis assays[49].

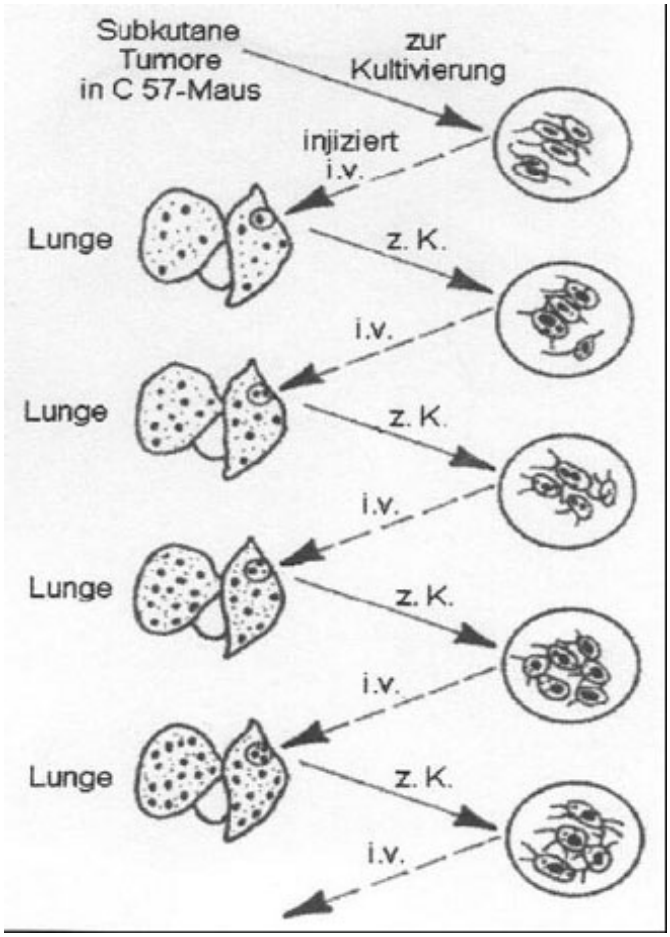

Figure 11: Selection of successive melanoma cell lines for metastasis[48]. Spontaneous melanoma of a C57B/6 mouse was cultured and injected i.v. into C57B/6 mice. Subsequent cell lines were selected for their ability to form pulmonary tumor nodules.

The B16-F melanoma system has proven particularly useful for studying tumor cell and host properties associated with metastasis. That the tumor arose spontaneously in the skin and is maintained in syngeneic hosts is one of the advantages of the system, as well as the fact that these tumors can be seen easily in the skin, lymph nodes, visceral organs and at other sites because of their high melanin pigment content. Furthermore, all B16 cell lines can be grown easily in tissue culture.

B16-F10 melanoma cells were labeled with [^{125}I]-5-iodo-2`-deoxyuridine in order to be able to follow the kinetic distribution after i.v. and i.c. melanoma cell injection and to assure lung specificity of the cell line[50]. In the case of i.c. injection, extrapulmonary arrest, detachment and recirculation are necessary to reach the lung microcirculation. Two minutes after injection of the B16-F10 cell line via these two routes, analysis of organs and blood showed a different kinetic distribution of the blood-borne cells while one day later the same numbers of viable B16-F10 cells were found in the lungs of both i.v.- and i.c.-injected animals. Two weeks after melanoma cell injection the mice were sacrificed and tumor nodules in different organs were counted and found that the same numbers of pulmonary metastases developed in the mice that received the melanoma cells via the tail vein or the left ventricle[50]. Extrapulmonary metastases were not found upon B16-F10 cell injection, indicating that initial blood-borne tumor cell distribution and arrest may have little consequence on subsequent metastatic colonization. From the highly metastatic line B16-F10 significantly more cells implanted, survived and grew to detectable lung metastases compared to line B16-F1.

The differences between the B16-F10 and B16-F1 cell line in their ability to form gross lung tumors where still significant but decreased with long-term in vitro culture under non-selecting conditions. To retain the stability of the cell lines it may prove necessary to start fresh cultures from early passaged cells or to repeat in vivo selection procedures to prevent loss of phenotypic properties in tissue culture.

1.4 Interleukin-27 and its signaling

1.4.1 The heterodimeric cytokine IL-12

Interleukin-12 was discovered in 1989 and considered as the cytokine produced by cells of the innate immune system like activated macrophages and DCs. IL-12 secretion from

these cells can be activated by the interaction of LPS with its receptor TLR4. All mammalian TLRs signal through the adaptor protein MyD88, the protein kinase IRAK, and the ubiquitin E3 ligase TRAF6. Activation of TRAF6 leads to the induction of NFκB. TLR4, in addition to engaging a MyD88-dependent pathway, also activates a second adaptor protein, TIRAP. The MyD88-independent signaling pathway downstream of TLR4 also activates NFκB. Active NFκB then leads to gene transcription which encodes for IL-12. Both pathways are shown in Figure 12.

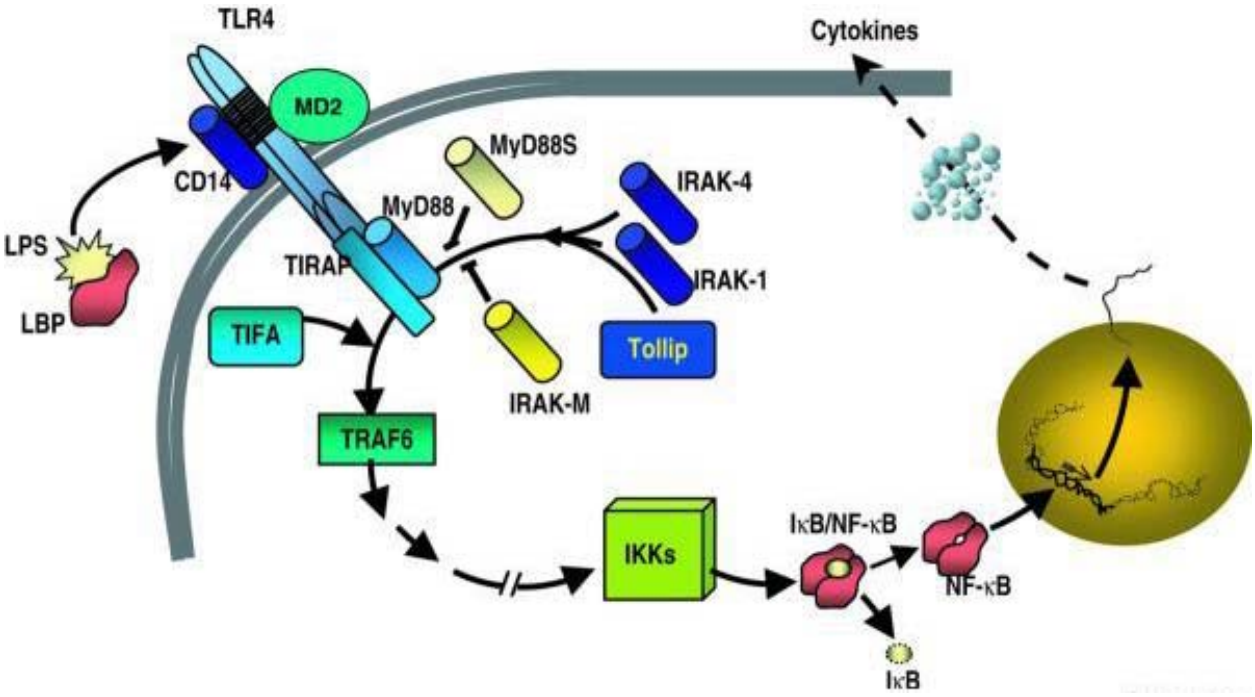

Figure 12: Pathway of TLR stimulation[51]. LPS-induced TLR stimulation activates a complex pathway that results in the secretion of IL-12.

IL-12 was found to influence the cell mediated immunity of the adaptive immune system by controlling the differentiation of naïve $CD4^+$ T cells after antigen encounter. The cytokine belongs to the type I cytokines that are a superfamily of immune modulators showing common structural motifs in ligands as well as in their receptors, e.g. the four-helix bundle and the hematopoietin receptor domain. The two subunits IL-12p35 and IL-12p40 form the complete cytokine. The p35 subunit is homologous to type I cytokines like IL-6 while the p40 subunit shows a close relation to the soluble IL-6 receptor (IL-6R) and the extracellular domains of other hematopoietic cytokine receptors. To gain biological activity, the co-expression of both IL-12 subunits on one cell is necessary but secretion of p40 is always higher than secretion of the p35 subunit.

If p40 is expressed alone, it can either be secreted as a disulfide-linked homodimer or as a monomer. In the case of expression of p35 alone, the cytokine subunit is not secreted. IL-12 mediates its biological effects through a high-affinity IL-12 receptor that activates the Janus kinase/signal transducer and activator of transcription (Jak/STAT-4) pathway of signal transduction in activated T cells, NK cells and some DCs. The receptor consists of the two subunits IL-12Rβ1 and IL-12Rβ2, which are both related to the signal transducing receptor gp130 and therefore resemble members of the class I cytokine receptors.

The discovery of IL-23 and IL-27, two IL-12 related cytokines, has led to intensify the studies on the role of these cytokines in T helper (Th) cell regulation in order to gain a deeper understanding of how the immune system responds to pathogens. Figure 13 displays the IL-6/IL-12 family of cytokines with receptors and ligands[52].

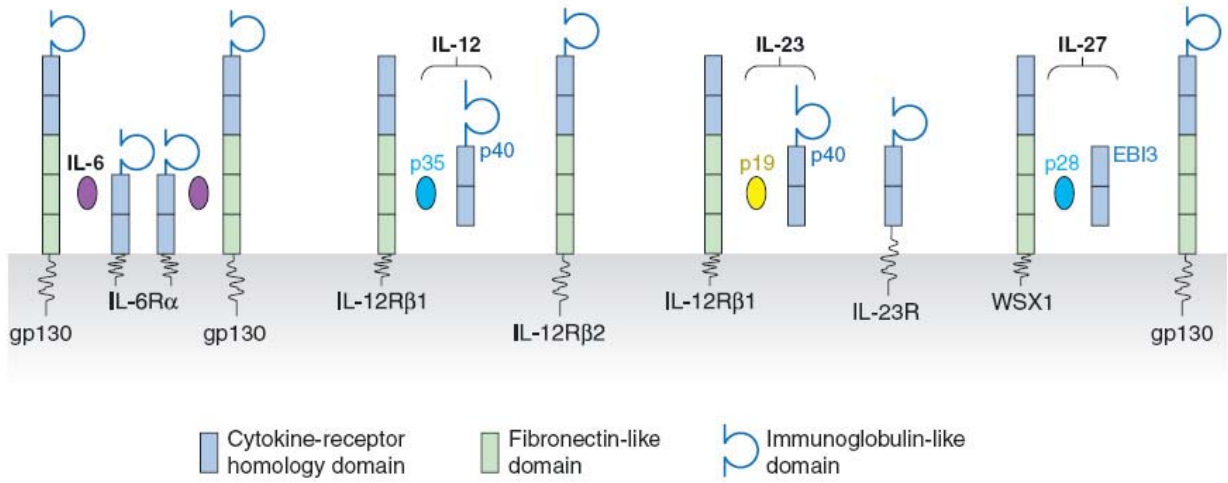

Figure 13: The IL-6/IL-12 family of cytokines[52]. The Interleukins IL-6, IL-12, IL-23 and IL-27 belong to one family of cytokines that all share structural motifs in ligands and receptors.

1.4.2 Interleukin-23

The discovery of IL-23 in the late 1990's showed a molecule with a novel four-helix bundle cytokine named p19 and the IL-12p40 subunit. While the p40 subunit is identical to the IL-12 cytokine, the p19 subunit of IL-23 resembles the IL-12p35 subunit.

Like IL-12, the Interleukin-23 is mostly expressed on activated DCs and its p40 subunit binds to the IL-12Rβ1. The second part of the receptor is unique for IL-23 and therefore named IL-23R, which is expressed on activated memory T cells as well as on T cell clones and NK cell lines. It belongs to the class I cytokine receptors although

structurally it lacks the three characteristic membrane-proximal fibronectin type III-like domains[52].

1.4.3 Interleukin-27

Interleukin-27 was discovered almost simultaneously with IL-23 and is the pairing of a helical protein, which is called IL-27p28 with a soluble cytokine receptor-like protein, the Epstein-Barr virus induced gene 3 (EBI-3) (Figure 13).

EBI-3 is an IL-12p40 homologue originally found secreted from Epstein-Barr virus transformed B cells. But the protein is ubiquitously expressed on a range of activated immune cells like B cells, monocytes, DCs and epithelial cells upon stimulation with lipopolysaccharide (LPS), CD40 ligation or exposure to inflammatory cytokines. It contains two cytokine binding domains but fails to have membrane anchoring motifs and a cytoplasmic tail.

The dimeric partner of EBI-3 to form bioactive IL-27 is the IL-27p28 which is a helical cytokine closely related to the IL-12p35 and IL-6. The gene transcription of IL-27p28 is securely regulated and the protein is best secreted when co-expressed with IL-12p40 or EBI-3 then forming IL-27. Similar to IL-12, the transcription of the soluble receptor component of IL-27, namely EBI-3, is always increased compared to the helical p28 subunit. Speculations about other partners for EBI-3 besides p28 are therefore not surprising. However, except for the binding to IL-12p35, which did not lead to a distinct function, any other interactions with EBI-3 have not been demonstrated.

Biological active IL-27 signals through its receptor consisting of two subunits. WSX-1, formerly called T cell cytokine receptor (TCCR), is a type I cytokine receptor with four positionally conserved cysteine residues and a C-terminal WSXWS protein sequence motif. The second part of the receptor that is necessary for the function is gp130 which is also part of the IL-6R complex. Co-expression of both, WSX-1 and gp130, to form the IL-27R complex is greatest on NK and T cells. In general, the binding of IL-27 to the IL-27R induces the Jak/STAT signaling cascade. To be more precise, ligation of the two molecules on T cells leads to phosphorylation of Jak1, STAT1, STAT3, STAT4 and STAT5 while in NK cells STAT4 is not activated by IL-27. The binding of IL-27 to monocytes directs phosphorylation of STAT1 and STAT 3 whereas in mast cells only STAT3 is activated by this cytokine. The capability to stimulate the

Jak/STAT pathway implies that the major function of the IL-27R is in the regulation of immune processes.

Considering the cells expressing IL-27 and its receptor, both are mainly found in the spleen, thymus, lungs, intestine, liver, peripheral blood and lymph nodes as in these sites immune cells occur on high rates[53].

T helper cells are T cells expressing the CD4 molecule on their cell surface and are therefore restricted to MHC class II expressing APCs. Under the influence of different cytokines these $CD4^+$ Th cells can be skewed into the development of diverse but specific immune responses. As demonstrated in Figure 14, naïve T cells can develop into different populations of effector T cells depending on the cytokine milieu present during antigen presentation. IL-12 together with IL-27 is critical for generating Th1 cells while IL-27 at the same time inhibits the newly described Th17 differentiation normally induced by TGF-β and IL-6. TGF-β alone promotes the production of T regulatory (Treg) cells and secretion of IL-4 activates the Th2 pathway[54].

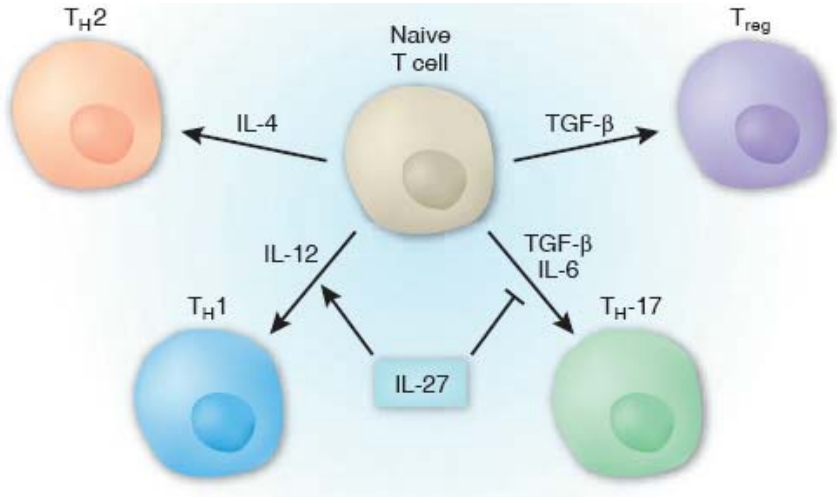

Figure 14: Regulation of CD4+ T cell differentiation by IL-27[54]. Naïve $CD4^+$ T cells can differentiate into either effector Th1 cells, effector Th2 cells, T regulatory cells or Th17 cells dependent on the cytokine profile during differentiation.

The above-described family of IL-12 cytokines promotes the initiation of a Th1 immune response. Figure 15 illustrates the influence of each of these cytokines within the signaling pathway. Infection or pathogen uptake (green symbols in APC) induces the secretion of several cytokines from APCs. IL-27R is expressed on naïve T cells (Th0) and ligation of IL-27 to its receptor is the first step to initiate the subsequent upregulation of IL-12Rβ2. The synergistic effect of IL-27 and IL-12 enables IL-12 to

become active and via binding to its receptor induces Th1 effector immune responses which are characterized by intracellular upregulation of T-bet, a Th1 specific T-box transcription factor, and secretion of high amounts of IFN-γ. IL-12 also stimulates the expression of IL-18R so that the IL-1 related and IFN-γ stimulating cytokine IL-18 can contribute to the maintenance of the Th1 effector response. Within this pathway homodimeric p40 has two opposing functions. It can either block IL-12 at its receptor or support the Th1 activation by interacting with IL-12Rβ1. The further development of Th1 effector cells into Th1 memory cells seems to be regulated exclusively by IL-23[55].

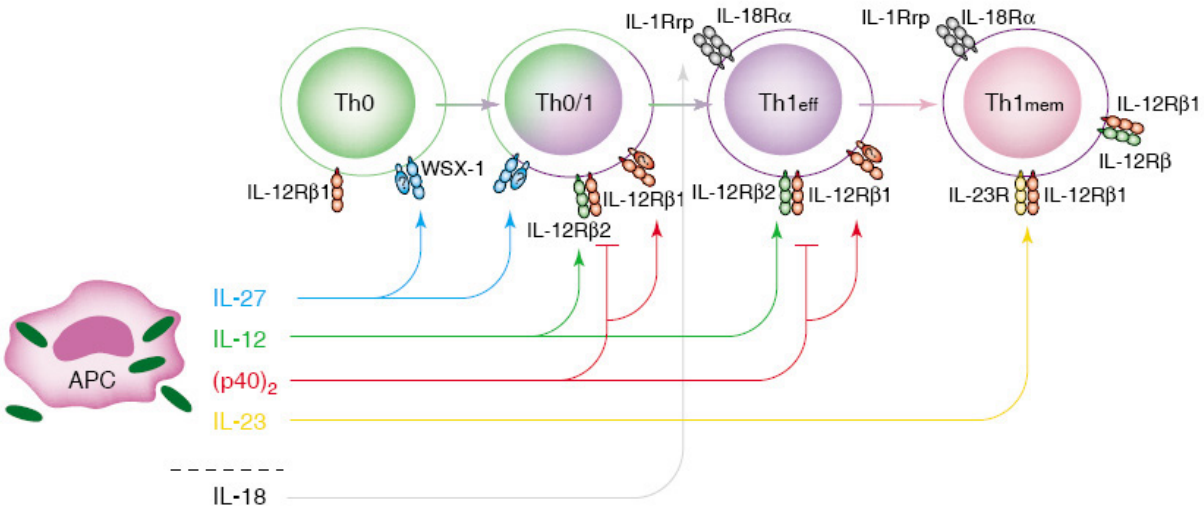

Figure 15: Regulation of Th1 development by IL-12 family members and IL-18[55]. IL-27 acts on naïve T cells initiating the Th1 differentiation that is proceeded by IL-12. The p40 homodimers can either support the Th1 activation or block the IL-12R. IL-23 contributes to the development of Th1 memory cells.

Th cell differentiation is very much influenced by activating as well as inhibitory members of the IL-12 cytokine family most of them contributing to a Th1 development at diverse stages of the differentiation process. EBI-3 alone without its binding partner p28 acts as a Th2 inducing factor (Figure 16). Nieuwenhuis and colleagues showed after targeted deletion of the EBI-3 gene in a mouse model that EBI-3 stimulates the growth and activation of invariant NK cells which then produce IL-4, the Th2-initiating factor[56].

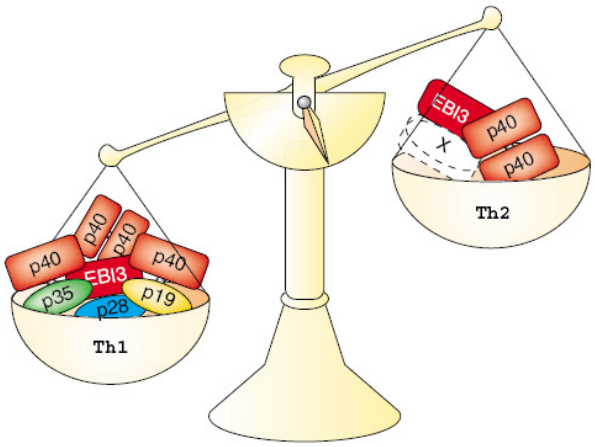

Figure 16: Regulation of Th cell differentiation by members of the IL-12 family[55]. Most IL-12 cytokine family members contribute to the Th1 development during T cell differentiation. EBI-3 alone without p28 acts as a Th2 inducing factor.

1.4.4 The paradoxical pro- and anti-inflammatory properties of IL-27

Many studies within recent years have identified that the binding of IL-27 to its receptor complex affects numerous types of immune cells, resulting in initiating either pro- or anti-inflammatory immune responses. Figure 17 displays a summary of the effects of IL-27 treatment or IL-27 receptor deficiency on $CD8^+$ T cells, $CD4^+$ T cells, NKT cells, NK cells, monocytes and mast cells. The results of studies including IL-27 and/or the IL-27 receptor can be summarized by pointing out that IL-27 influences infection induced immune responses as well as autoimmunity. Although IL-27 does not necessarily dictate the polarity of the Th differentiation, it is more likely to result in suppression of cell mediated inflammatory responses[53].

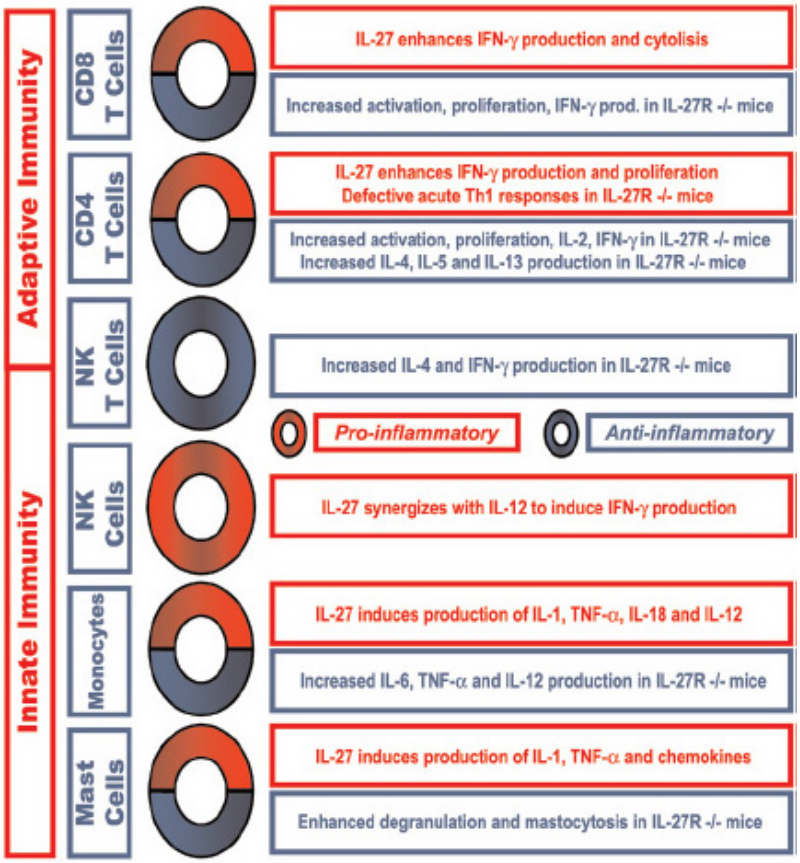

Figure 17: The paradoxical pro- and anti-inflammatory properties of IL-27[53]. The effects of IL-27 treatment or IL-27 receptor deficiency on $CD8^+$ T cells, $CD4^+$ T cells, NKT cells, NK cells, monocytes and mast cells.

2 Definition of the Project

EBI-3 was discovered in the late 1990s as a soluble cytokine receptor that together with p28 forms the Interleukin-27. Many studies were designed to identify the function of the protein, thereby discovering that EBI-3 is much more widely expressed than its partner p28. This led to the assumption that EBI-3 might have a function different from IL-27.

EBI-3 deficient, as well as EBI-3 transgenic mice, were created to clarify the many questions on the role of EBI-3. To date, the expression of EBI-3 and IL-27 are very well known and their roles in inflammatory diseases have been extensively studied.

It yet remains to determine the effect of the lack of EBI-3 in metastatic cancers. Since EBI-3 is expressed by activated antigen presenting cells it is a potential candidate to influence antigen presentation during tumor development and the metastatic spreading of the disease.

In this thesis the murine B16-F10 melanoma cell line was used in a model of EBI-3 deficient mice in order to first determine if the lack of EBI-3 affects the development of tumor metastases and then focus on the changes in the immune response of B16-F10 lung melanoma bearing EBI-3 deficient mice compared to C57B/6 wild-type mice.

3 Materials and Methods

3.1 Materials

3.1.1 Chemicals and Reagents

Acetic Acid	E. Merck AG, Darmstadt
Acetone	Carl Roth GmbH, Karlsruhe
Accutase	PAA Laboratories GmbH, Pasching, Austria
Agarose	Sigma-Aldrich Chemie GmbH, Taufkirchen
Ammoniumchloride (NH_4Cl)	Riedel-de Haen, Seelze
Ammoniumperoxidsulphate (APS)	Carl Roth GmbH, Karlsruhe
Aprotinin from bovine lung	Sigma-Aldrich Chemie GmbH, Taufkirchen
Aqua dest.	Braun, Melsungen
Assay Diluent for Elisa	BD Biosciences, Heidelberg
Bovine Serum Albumine	Sigma-Aldrich Chemie GmbH, Taufkirchen
Buffer solution, pH 7,00	E. Merck AG, Darmstadt
Buffer solution, pH 4,00	E. Merck AG, Darmstadt
Casy Ton	Schärfe System GmbH, Reutlingen
Casy Clean	Schärfe System GmbH, Reutlingen
Citric acid-Monohydrate	E. Merck AG, Darmstadt
Collagenase Type II	Worthington Biochemical Corporation, Lakewood, NJ
Disodium-EDTA	Gerbu Biotechnik, Gaiberg
Di-Sodiumhydrogenphosphate (Na_2HPO_4)	E. Merck AG, Darmstadt
DNase	Roche Diagnostics GmbH, Mannheim
Dimethylsulfoxid (DMSO)	E. Merck AG, Darmstadt
Dulbecco`s modified eagle medium (DMEM)	Gibco, Invitrogen Corp, Grand Island, NY
ECL Western blotting detection system	Amersham Pharmacia Biotech, UK

Ethanol (EtOH)	E. Merck AG, Darmstadt
Ethidiumbromide (EtBr)	Carl Roth GmbH, Karlsruhe
Ethylendiamintetraacetate (EDTA)	Gerbu Biotechnik, Gaiberg
Farblösung für Proteinassay nach Bradford	Biorad, München
Fetal Calf Serum (FCS)	Biochrom KG, Berlin
Formaldehyde	E. Merck AG, Darmstadt
Gelatine	E. Merck AG, Darmstadt
Gene Ruler^{TM} 1 kb DNA Ladder	MBI Fermentas Molecular Biology, St. Leon-Rot
Glycerin	E. Merck AG, Darmstadt
Glycin	Carl Roth GmbH, Karlsruhe
HRP Streptavidin	Dako, Glostrup, Dänemark
Hydrochloric Acid (HCl) 25%	E. Merck AG, Darmstadt
Hydrogen Peroxide	E. Merck AG, Darmstadt
Kaleidoscope prestained standards	Biorad, München
LPS (E. coli 0111:B4 LPS)	Invivo Gen, San Diego, USA
Magnesiumchloride ($MgCl_2$)	
Methanol	Carl Roth GmbH, Karlsruhe
Non fat dry milk	Applichem, Darmstadt
Nonidet P 40	Fluka, Buchs, Schweiz
OCT compound	Sakura Finetek, Zoeterwonde, NL
Paraformaldehyde	SERVA Electrophoresis GmbH, Heidelberg
Phosphate buffered Saline (PBS)	Biochrom KG, Berlin
PBS EDTA pH7,5	Cambrex Bio Science, Verviers
Penicillin/Streptomycin (P/S)	Gibco, Invitrogen Corp, Grand Island, NY
Pentobarbital (Narcoren)	Merial, Rohrdorf
Polyacrylamid 40%	Carl Roth GmbH, Karlsruhe
Potassiumhydrogencarbonat ($KHCO_3$)	Sigma-Aldrich Chemie GmbH, Taufkirchen
Potassiumhydroxide (KOH)	E. Merck AG, Darmstadt

Proteinase K	Roche Diagnostics GmbH, Mannheim
RPMI 1640 Medium	Gibco, Invitrogen Corp, Grand Island, NY
Sodium-dodecylsulfate (SDS) ultra pure	Carl Roth GmbH, Karlsruhe
Sodium Azide (NaN_3)	Sigma-Aldrich Chemie GmbH, Taufkirchen
Sodiumcarbonat (Na_2CO_3)	E. Merck AG, Darmstadt
Sodiumdihydroenphosphat (NaH_2PO_4)	E. Merck AG, Darmstadt
Sodiumhydrogencarbonat ($NaHCO_3$)	E. Merck AG, Darmstadt
Sodiumhydroxide	E. Merck AG, Darmstadt
Sterofundin	Braun, Melsungen
Streptavidin-Cy2	Dianova, Hamburg
Streptavidin-Cy3	Dianova, Hamburg
Sulfuric Acid (H_2SO_4)	E. Merck AG, Darmstadt
TEMED	Carl Roth GmbH, Karlsruhe
3,3,5,5- Tetramethylbenzidin (TMB)	Fluka, Buchs, Schweiz
Tricin	Carl Roth GmbH, Karlsruhe
Tris	Carl Roth GmbH, Karlsruhe
Tris-hydrochloride (Tris-HCl)	Carl Roth GmbH, Karlsruhe
Trypan blue stain 0.4%	Gibco, Invitrogen Corp, Grand Island, NY
Trypsin-Inhibitor	Sigma-Aldrich Chemie GmbH, Taufkirchen
Trypsin/EDTA 0.05%	PAA Laboratories GmbH, Pasching, Austria
Tween 20	E. Merck AG, Darmstadt

3.1.2 Equipment

Arpege 70, cryo tank	Air Liquide Deutschland, Düsseldorf
AxioCam MRc	Carl Zeiss GmbH, Jena
Biometra DOC Analyzer	Biometra GmbH, Göttingen
Cell counter CASY TT	Schärfe System GmbH, Reutlingen
Centrifuge Minifuge T	Heraeus Instruments, Hanau
Centrifuge Megafuge 1.0R Sorvall	Heraeus Instruments, Hanau

Incubator 1, Binder CB210	Binder GmbH, Tuttlingen
Incubator 2, Cellstar	Nunc, Wiesbaden
Dispergiergerät Miccra D1	ART Labortechnik, Müllheim
Electrophoresis System Mini-Protean	Biorad, München
ELISA-Reader	Dynex Technologies, Chantilly, VA
FACS Calibur	BD PharMingen, Heidelberg
Glass ware	Schott, Mainz
Kompaktschüttler KS 15A	Johanna Otto GmbH, Hechingen
Laminar flow box 1 Holten Laminair 1.5	Thermo Fisher Scientific
Laminar flow box 2 Topsafe 1.5	Nunc GmbH Wiesbaden
Magnetrührer MR 3001	Heidolph, Schwabach
Microscope IX 70	Olympus, Hamburg
Microscope Nikon TMS S3	Cambridge Scientific Products
Microscope Axioskop 2 mot plus	Carl Zeiss GmbH, Jena
Neubauer-chamber	Roth, Karlsruhe
OctoMACS Separation Unit	Miltenyi Biotech, Bergisch Gladbach
PH-Meter	InoLab, Weilheim
Photometer	Biochrom, Berlin
Pipetten Eppendorf Reference	Eppendorf, Hamburg
Pipettierhilfe Pipettus	Hirschmann Laborgeräte
QuadroMACS Separation Unit	Miltenyi, Bergisch Gladbach
Refrigerators	Liebherr, Bosch
Schweißgerät Futura Jr.	Audion Elektro, Weesp, NL
Stereo microscope Stemi 200-C	Carl Zeiss GmbH, Jena
Thermomixer	Eppendorf, Hamburg
Tischzentrifuge, gekühlt Biofuge fresco	Heraeus Instruments, Hanau
Transferkammer Trans Blot Cell	Biorad, München
Ultrasound bath Sonorex RK 510S	Bandelin Elektronic, Berlin
Vaacumpump MINI VAC E1	PEQLAB Biotech, GmbH, Erlangen
Vortexer Reax Control	Heidolph, Schwabach
Waagen AE50, PM300	Mettler, Basel
Waterbath	Köttermann, Uetze/Hänsingen

3.1.3 Applied equipment

Glassware was sterilized prior to use by 20 min autoclavation at 121°C.
Plastic material like cell culture flasks, cell culture dishes, pipette tips were purchased as aseptic material.

Cellcultureplate Cellstar TC-Plate 24 wells	Nunc, Wiesbaden
Cellcultureplate Cellstar TC-Plate 48 wells	Nunc, Wiesbaden
Cellcultureplate Cellstar TC-Plate 96 wells	Nunc, Wiesbaden
Cellstar PP-tubes 50 ml, 15 ml	Greiner, Frickenhausen
Cell strainer 40 µm Nylon	BD Falcon, Bedford, MA
Cryotubes	Nunc, Wiesbaden
ELISA-Plate PS Microplate 96 wells	Nunc, Wiesbaden
FACS tubes	Becton Dickinson, Franklin Lakes, NJ
Films Biomax ML	Kodak, Rochester, NY
Glasplatten für Mini-Protean	Biorad, München
Kamm	Biorad, München
Kanülen, Sterican 0,45x12mm	Braun, Melsungen
Kapillarspitzen 200 µl	Biozym, Oldendorf
MACS MS Separation columns	Miltenyi, Bergisch Gladbach
MACS LS Separation columns	Miltenyi, Bergisch Gladbach
Magnetstäbchen	Roth, Karlsruhe
Microküvette Nr.1201	Ratiolab, Dreieich
Microscope cover glasses	Menzel Gläser, Braunschweig
Nitocellulosemembran Protran	Schleicher + Schuell, Dassel
Parafilm	American National Can, Chicago, IL
Petri dish	Nunc, Wiesbaden
Pinzette	FST, Heidelberg
Pipetten mit Spitze, steril	Sarstedt, Nümbrecht
Pipettenspitzen Standartips	Eppendorf, Hamburg
Polysine-Objektträger	Menzel, Braunschweig
Reaktionsgefäße	Eppendorf, Hamburg
Röntgenkassette	Röntgen Bender, Baden-Baden

Scissors	FST, Heidelberg
Skalpelle, aseptic	Feather Safety Razor Co, Köln
Spatel	Merck, Darmstadt
Sterilisationsfilter 22 µm:	Millipore, Bedford, MA
Syringe, Injekta F 1 ml	Braun, Melsungen
Syringe, Injekta F 10 ml	Braun, Melsungen
Syringe, Omnican 1 ml	Braun, Melsungen
Whatman Filterpapier	Whatman, Maidstone, UK

3.1.4 Antibodies

β-Actin	Santa Cruz, Heidelberg
CD28	BD Biosciences, Heidelberg
CD3ε	BD Biosciences, Heidelberg
TNF-α	R&D Systems, Wiesbaden
Bcl-2	Santa Cruz, Heidelberg
Bcl-xL	Santa Cruz, Heidelberg
CD8	Santa Cruz, Heidelberg
GATA-3 (HG3-31)	Santa Cruz, Heidelberg
Flk-1	BD Biosciences, Heidelberg
TRAIL	R&D Systems, Wiesbaden
VEGF	Santa Cruz, Heidelberg
TGF-β1	BD Bioscience, Heidelberg

Horseradish Peroxidase labeled secondary antibodies:

Anti-goat Ig	Amersham Bioscience, Buckinghamshire
Anti-mouse Ig	Amersham Bioscience, Buckinghamshire
Anti-rabbit Ig	Amersham Bioscience, Buckinghamshire

Biotinylated secondary antibodies:

Anti-goat IgG	Vector Laboratories Inc, Burlingame, CA
Anti-mouse IgG	Vector Laboratories Inc, Burlingame, CA
Anti-rabbit IgG	Vector Laboratories Inc, Burlingame, CA

Fluorochrome-labeled FACS antibodies:

CD1d FITC	eBioscience, San Diego, CA
CD3ε PE	eBioscience, San Diego, CA
CD4 (L3T4) APC	BD Biosciences, Heidelberg
CD4 (L3T4) FITC	BD Biosciences, Heidelberg
CD4 (L3T4) PE	BD Biosciences, Heidelberg
CD4 (L3T4) PE-Cy7	eBioscience, San Diego, CA
CD8α (Ly-2) PE	BD Biosciences, Heidelberg
CD8α (Ly-2) APC	BD Biosciences, Heidelberg
CD11c-APC	eBioscience, San Diego, CA
CD11c-FITC	BD Biosciences, Heidelberg
CD25 PE-Cy5.5	Caltag Invitrogen GmbH
CD31 PE-Cy7	eBioscience, San Diego, CA
CD40 PE	eBioscience, San Diego, CA
CD44 (Pgp-1, Ly-24) PE-Cy5	BD Biosciences, Heidelberg
CD45R PE-Cy5.5	eBioscience, San Diego, CA
CD49d PE	eBioscience, San Diego, CA
CD69 (H1.2F3) FITC	BD Biosciences, Heidelberg
CD80 PE	eBioscience, San Diego, CA
CD86 PE-Cy5	eBioscience, San Diego, CA
CD106 FITC	eBioscience, San Diego, CA
CD120b PE	BD Biosciences, Heidelberg
CD122 (TB b1) PE	BD Biosciences, Heidelberg
Fas FITC	BD Biosciences, Heidelberg
FasL PE	eBioscience, San Diego, CA
Foxp3 (FJK-16a) APC	eBioscience, San Diego, CA
H-2Db MHC1 PE	Caltag Invitrogen GmbH
ISO IgG2a (KLH) FITC	BD Biosciences, Heidelberg
ISO IgG2b (eB149/10H5) FITC	BD Biosciences, Heidelberg
ISO IgG2a (KLH) PE	BD Biosciences, Heidelberg
ISO IgG2b (eB149/10H5) PE	BD Biosciences, Heidelberg
IFN-γ (XMG1.2) FITC	BD Biosciences, Heidelberg

MHC Class II-FITC	eBioscience, San Diego, CA
NK1.1 APC	Caltag Invitrogen GmbH, Karlsruhe, Germany
PDCA-1 PE	Miltenyi Biotech, Bergisch Gladbach

3.1.5 Beads

CD4 (L3T4) microbeads	Miltenyi Biotech, Bergisch Gladbach
CD8 (Ly-2) microbeads	Miltenyi Biotech, Bergisch Gladbach
CD11c (N418) microbeads	Miltenyi Biotech, Bergisch Gladbach

3.1.6 Commercial Kits

Annexin V: FITC Apoptosis Detection Kit I	BD Biosciences, Heidelberg
Foxp3 Fixation/Permeabilization Concentrate and Diluent	eBioscience, San Diego, CA
GolgiStop Protein Transport Inhibitor Kit	BD Biosciences, Heidelberg
Mouse IL10 Elisa Set (BD OptEIA^{TM})	BD Biosciences, Heidelberg
Mouse IL-12p40 Elisa Set (BD OptEIA^{TM})	BD Biosciences, Heidelberg
Mouse IL-12p70 Elisa Set (BD OptEIA^{TM})	BD Biosciences, Heidelberg
Mouse IL-17 Elisa mouse Set (DuoSet®)	R&D Systems, Wiesbaden
Mouse IFNγ Elisa Set (BD OptEIA^{TM})	BD Biosciences, Heidelberg
Mouse TNF-α Elisa Set (BD OptEIA^{TM})	BD Biosciences, Heidelberg
Mouse VEGF Elisa mouse Set (DuoSet®)	R&D Systems, Wiesbaden
Mouse VCAM-1 Elisa mouse Set (DuoSet®)	R&D Systems, Wiesbaden
10x Permeabilization Buffer	eBioscience, San Diego, CA

3.1.7 Buffers and solutions

Buffers and solutions for ELISA

Carbonate Coating Buffer	0.356 g Na_2CO_3 0.84 g $NaHCO_3$ ad 100 ml Aqua dest.

	titrate to pH 9.5
Phosphate Coating Buffer	1.18 g Na_2HPO_4 1.61 g NaH_2PO_4 ad 100 ml Aqua dest. titrate to pH 6.5
TMB solution	120 mg 3,3´5,5´-Tetramethylbenzidin Dilute in 2,5 ml Acetone 22.5 ml EtOH add 150 µl H_2O_2 30%
Substrate Buffer	6.3 g Citric Acid-Monohydrate ad 1000 ml Aqua dest. Titrate to pH 4.1 using 4N KOH
Stop Solution	28 ml H_2SO_4 (97%) ad 500 ml Aqua dest.
Wash Buffer	0.005% Tween 20 in PBS

Buffers and solutions for FACS

FACS Buffer	PBS EDTA pH7.5 0.5% BSA
Fixation Buffer PFA 4%	40 g Paraformaldehyde ad 800 ml PBS titrate to pH 7.0-7.4 dilute at 60°C over night cool to RT ad 1 l PBS

Buffers and solutions for cell isolation and cell culture

All buffers and solutions used in cell culture were sterilized prior to use by filtration over a 0.22 µm filter under aseptic conditions.

ACK-lyse Buffer	8.29 g NH_4Cl 1.0 g $KHCO_3$ 0.367 g Na_2EDTA ad 1 l H_2O titrate to pH 7.2-7.4 using NaOH
Coating Buffer	$NaHCO_3$ (0.1M), pH 8.2
MACS Buffer	PBS EDTA pH7.5 0.5% BSA
Cell culture media for isolated cells	5% FCS 1% Penicillin/Streptomycin in RPMI
Cell culture media for B16-F10 cells	10% FCS 1% Penicillin/Streptomycin in DMEM

Buffers for genotyping of mice

TAE Buffer (50X)	2 M Tris 0.05 M EDTA titrate to pH 8.0 using Acetic Acid
PCR Buffer	1.87 g KCl 5 ml 1M Tris-HCl 255 mg $MgCl_2$ 50 mg Gelatine

	2.25 ml Nonidet P 40 2.25 ml Tween 20 ad 500 ml Aqua dest.

Buffers for Western Blot

Inhibitormix	325 µl PBS 25 µl Aprotinin 25 µl Trypsininhibitor (5mg/ml) 25 µl 10% Nonidet P40
Gel Buffer	3M Tris-HCl 0.3% SDS ad 100 ml aqua dest. Titrate to pH 8.45
Separation Gel (10%) Stock Solution	10 ml Gel Buffer 7.3 ml Polyacrylamid 40% 8.7 ml aqua dest.
Stacking Gel (5%) Stock Solution	3.1 ml Gel Buffer 1.2 ml PAA 40% 4 g Glycerin 8.2 ml aqua dest.
Separation Gel (10%) Solution for use	10 ml stock solution 10 µl TEMED 100 µl APS
Stacking Gel (5%) Solution for use	5 ml Stammlösung 5 µl TEMED 50 µl APS

Cathode Buffer	0.1 M Tris-HCl 0.1 M Tricin 0.1% SDS titrate to pH 8.5
Anode Buffer	0.2 M Tris-HCl titrate to pH 8.9
Transfer Buffer	3.03 g Tris 14.4 g Glycin 200 ml Methanol 3.3 ml SDS (10%) ad 1 l Aqua dest. titrate to pH 8.1
Blotto	5% Magermilchpulver 0.05% Tween 20 PBS
Wash Buffer	0.05% Tween 20 PBS
Stripping Buffer	0.1 M Glycin titrate to pH 2.8

3.2 Methods

3.2.1 Mice

C57B/6 mice were obtained from Charles River Laboratory and Jackson Laboratory. They were bred and maintained under specific pathogen-free conditions in our animal facility. EBI-3 (-/-) mice have been generated by targeted deletion described previously[56, 57]. Shortly, the ebi-3 gene was disrupted by homologous recombination in 129SvJ embryonic stem cells (Figure 18). These embryonic stem cells were injected into C57B/6 blastocysts thereby generating chimeric mice. Heterozygous offspring of one chimeric founder were identified by PCR amplification of genomic DNA and interbred to generate homozygous animals of mixed C57B/6 and 129SvJ background.

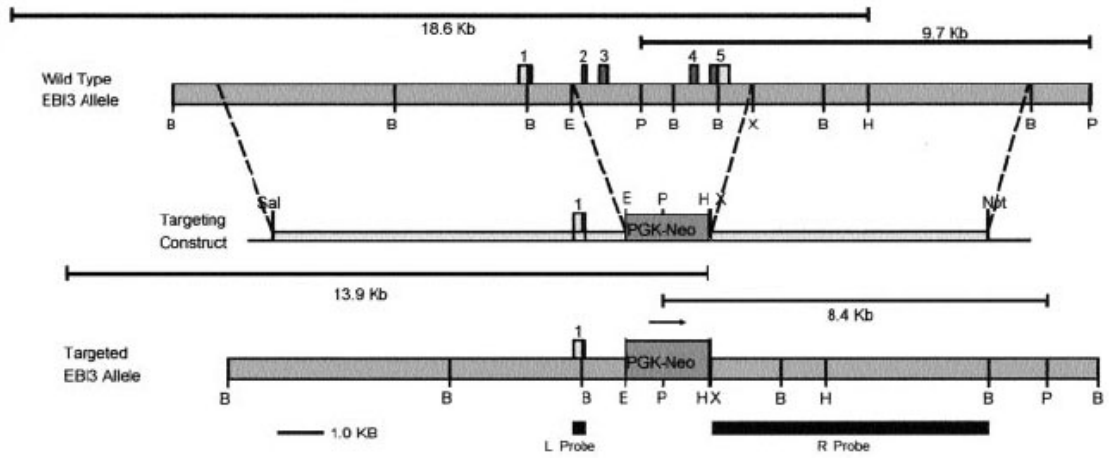

Figure 18: Generation of the EBI-3 deficient mouse strain[56]. The Exons 2-5 encode for the amino acids 24-228 of the EBI-3 protein and were replaced by the Neo gene cassette under control of the phosphoglycerate kinase promoter (PGK-Neo) that was inserted in the same orientation as the ebi-3 gene.

Prof. Richard S. Blumberg from Boston generously provided the EBI-3 deficient mice. Animals were backcrossed to a C57B/6 background and bred and maintained under specific pathogen-free conditions in our animal facility. Mice were treated according to institutional animal care and use guidelines. Mice were 6 weeks old when experiments were started. The animals remained in the animal facility until they were sacrificed for the removal of organs.

EBI-3 deficient mice were routinely genotyped by polymerase chain reaction (PCR). Therefore biopsies were taken from the ear of each mouse and digested in 200

µl PCR buffer and 7 µl Proteinase K at 55°C over night. Afterwards the proteinases were inactivated by keeping the samples at 95°C for 10 minutes (min.) Primer sequences and conditions used for genotyping EBI-3 are described later on in this chapter.

All experiments were undertaken with approved license from the Ethical Committee of Rheinland-Pfalz (Mainz, Germany).

3.2.2 DNA isolation and PCR

1983 Kary Mullis invented the polymerase chain reaction (PCR), which is a rapid and simple method in biochemistry, and molecular biology for isolating and exponentially amplifying a specific DNA sequence without using living organisms (such as E. coli or yeast). Today it is a common technique used for example, to sequence genes or create transgenic organisms, where it is necessary to amplify DNA fragments up to 10 kilo base pairs.

The PCR usually consists of a series of 20 to 35 cycles and is carried out in three steps. Prior to the first cycle, an initialization step is used to heat the sample to a temperature of 94-96°C for 1-9 minutes. This ensures that most of the DNA template and primers are denatured which means that the DNA is melted by disrupting the hydrogen bonds between complementary bases of the DNA strands with two single strands of DNA as a result. The cycling now begins with the denaturation step at 94-98°C for 20-30 seconds.

The denaturation is followed by the annealing step where the temperature is lowered to 50-64°C for 20-40 seconds so that the primers can anneal to the single-stranded DNA template. DNA-DNA hydrogen bonds are constantly formed and broken between primer and template. Polymerase attaches and begins DNA synthesis only when stable bonds are formed and that is when the primer sequence very closely matches the template sequence.

The extension step continues the reaction during which the DNA polymerase synthesizes new DNA strands complementary to the DNA template strands. The temperature at this step depends on the DNA polymerase used but is mostly of about 72°C. The hydrogen bonds between the extended primer and the DNA template are now strong enough to tolerate the forces of high temperature. Primers that have

annealed to DNA regions with mismatching bases dissociate from the template and are not extended. The DNA polymerase condenses the 5'-phosphate group of the primers with the 3'-hydroxyl group at the end of the extending DNA strand. The extension time depends both on the DNA polymerase used and on the length of the DNA fragment to be amplified.

The PCR now uses an elongation step of 5-15 minutes, which depends on the length of the DNA template and makes sure that any remaining single-stranded DNA is fully extended.

The DNA of ear biopsies of EBI-3 deficient mice was obtained as described above and three primers were used in PCR to identify the EBI-3 gene disruption. The primer sequences used are as follows:

EBI-3-NEO1	5`>ATT CGC AGC GCA TCG CCT TC<3´
EBI-3-2	5´>AGC TAG CAC CAT TCT GTG TC<3´
EBI-3-3	5´>TGC GGG GCT TTG TGA ACT<3´

PCR cycler was programmed for the amplification of these primers as described below:

95°C for 5 min

33 cycles of 95°C for 45 seconds

58°C for 45 seconds

72°C for 2 min

72°C for 10 min

8°C forever (in order to keep samples cool until probed on the gel)

After amplification of the gene of interest, the PCR samples were loaded onto a gel of 2% agarose in TEA buffer containing Ethidiumbromide. Applying 100 V to the gel for 1h separated the DNA sequences by its molecular size. This is due to the fact that if the pH of a solution is neutral the 5'-phosphate group of the nucleic acids are ionized and as a consequence the molecules can migrate through the electric field. The actual size of DNA fragments in the gel is determined by a DNA-standard marker of known size that is also applied to one chamber of the gel. The length of the PCR product is 500 kb for the knock-out and 633 kb for wild-type. The DNA pattern on the gel is detected under UV-light at 245 nm wavelengths.

3.2.3 Design of standard experiments

Mice were divided into 4 groups each group consisting of 5 mice.

Group 1: C57B/6 wild-type mice

Group 2: EBI-3 deficient mice

Group 3: C57B/6 wild-type mice

Group 4: EBI-3 deficient mice

Group 1 and 2 were treated as described in the experimental design in Figure 19. Mice from groups 3 and 4 were not injected with tumor cells but otherwise treated exactly like their littermates from groups 1 and 2.

More precisely, on day 0 the mice of group 1 and 2 were injected intravenously into the tail vein with $2x10^5$ B16-F10 cells resuspended in 200 µl Sterofundin. Mice of all groups including the untreated controls were sacrificed either by cervical dislocation or by intraperitoneal injection of 200 µl of Narcoren solution (diluted 1:4 in phosphate buffered saline [PBS]) at the indicated time points five, ten, 14 and 21 days after B16-F10 cell injection. The bronchoalveolar lavage fluid (BALF) of these mice was obtained as described later. Lungs and spleens were surgically removed by opening the chest of the mice with anatomical scissors. Pictures were taken of the lungs under the stereo microscope followed by either storing the lungs in 10% buffered formalin or freezing the tissue in optimal cutting temperature (OCT) compound for creating histological sections. Alternatively, lungs were frozen in liquid nitrogen or cells were isolated from the organs for further investigations.

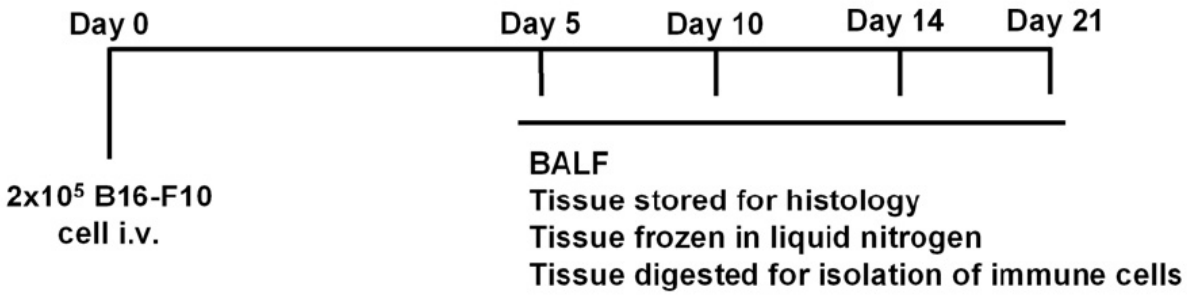

Figure 19: Design of standard experiments. $2x10^5$ B16-F10 cells were injected into EBI-3 deficient and B6 wild-type mice at day 0. At days 5, 10, 14 and 21, the BALF was taken from these mice. Additionally, lung tissue was stored in formalin as well as in liquid nitrogen and tissue was digested for isolation of immune cells. Untreated tumor-free controls were treated equally.

3.2.4 Design of cell transfer experiments

In order to analyze the function of certain cell populations of EBI-3 deficient mice an adoptive transfer experiment was designed as shown in Figure 20.

The cell types of interest were isolated from lungs of mice that have been injected with $2x10^5$ B16-F10 cells five days before. Each B6 wild-type recipient mouse was intravenously injected with a suspension containing $2x10^5$ B16-F10 cells and $5x10^5$ $CD11c^+$ / $1x10^6$ $CD4^+$ / $1x10^6$ $CD8^+$ cells either isolated from lungs of B6 wild-type or EBI-3 deficient mice. The control group consisted of B6 wild-type mice that were injected with $2x10^5$ B16-F10 cells at the day of the adoptive transfer.

At days 10 and 14 after the cell transfer the recipient mice were sacrificed and BALF was obtained before surgically removing the lungs for further investigations of the immune response in the recipient mice.

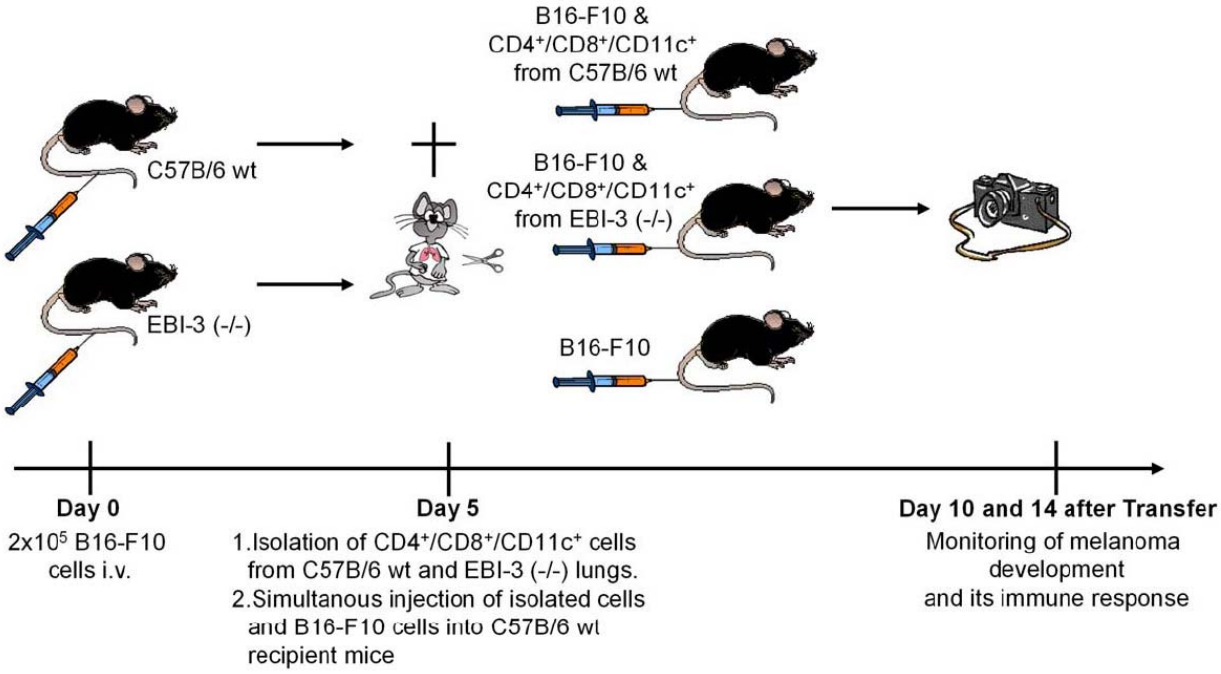

Figure 20: Design of adoptive cell transfer experiment. $2x10^5$ B16-F10 cells were injected into EBI-3 deficient and B6 wild-type mice at day 0. At day 5, either $CD4^+$ or $CD8^+$ or $CD11c^+$ cells were isolated from the lungs of the B16-F10 injected mice. $5x10^5$ isolated cells of both B6 wild-type and EBI-3 (-/-) lungs together with $2x10^5$ B16-F10 cells were intravenously transferred into B6 wild-type mice. Untreated tumor bearing control received $2x10^5$ B16-F10 cells. At day 10 and 14, melanoma development was monitored.

3.2.5 Bronchoalveolar Lavage Fluid (BALF)

Monitoring the complete immune response within the murine airways is an essential step in immunologic research of the lung and its diseases. As a consequence, the collection of the BALF has become an important routine method in laboratories investigating the immune function in different lung diseases and is a possibility to answer the question about how the breathing problems of affected patients occur. It also sheds light on the mechanism underlying the immune response.

Therefore, the bronchoalveolar lavage fluid (BALF) of the right lung was performed according to standard protocols in our laboratory as described by Maxeiner et al.[58].

Similar to human medicine the murine lungs are floated with Sterofundin and the liquid is regained then containing cells and cytokines of the airways. In contrast to patients the mice have to be anesthetized and a tracheal tube is surgically implanted into the trachea in order to be able to inject a liquid into the airways. Anesthetizing of the mice is performed by i.p injection of a Narcoren solution. Immediately after the mouse motionless tolerates surgery the dissection is started to avoid changes in the airway environment due to the dying organism. The tissue covering the trachea is removed using surgical scissors, two tweezers and a scalpel. The trachea then has to be fixed on a flat surface, which is accomplished by pushing a spattle under the trachea. To complete the surgery a cut is performed into the trachea and a tracheal tube is put into the cut followed by binding the tube to the trachea. To inject the Sterofundin and collect the BALF a syringe plus a needle is adapted to the tracheal tube. The BALF is collected by injecting 1 ml of Sterofundin into the prepared trachea to float the airways. The liquid is regained by winding up the syringe while simultaneously massaging the thorax of the mouse. After transfer into a Greiner tube and centrifugation by 1500 rotations per minute (rpm) for 5 min, the resulting BALF supernatant can be stored for cytokine detection by ELISA and the resuspended cell pellet can be used for generation of cytospins, FACS analyses and cell viability checks.

3.2.6 Surgical removal of organs

On the day of the experiment, the mice of all groups including the untreated controls were sacrificed. Depending on the design of the experiment this was performed either

by cervical dislocation or by intraperitoneal injection of 200 µl of Narcoren solution (diluted 1:4 in PBS). 70% ethanol was used to wet the chest and to prevent infections in the wound of the mice, which were then opened with anatomical scissors. The lung is then removed by means of anatomical scissors and tweezers. The spleen is removed in a similar way by performing a cut into the right flank of the mice and delocalizing the organ from its natural environment. In case of cell isolation the lungs and spleens are removed under aseptic conditions and transferred into a centrifugation tube containing RPMI with 5% FCS and 1% P/S.

3.2.7 Quantification of tumor mass

Removed lungs were photographed under the stereomicroscope Stemi 200-C with AxioCam MRc. The lungs were then transferred into a petri dish and pictures were taken from both sides of the lungs. The pictures were imported to a computer by Axiovision 4.2. from Carl Zeiss Vision GmbH. The metastases of each lung were marked both on the front- and backside pictures with the tools of the computer program that allowed quantification of the area of each lung that is covered by melanotic metastases. The total melanotic area was compared to the size of the whole lung by using an Excel computer program. Results are shown in percentages.

3.2.8 Lung histology

Histology allows studying the microscopic anatomy of tissue that is sectioned into thin slices. By using immunohistological protocols, proteins and cell surface molecules of the tissues or cells can be stained by antigen-antibody interaction and are visualized either by direct labeling of the antibody or by use of a secondary labeling method.

Paraffin sections

Lung histology was generously analyzed in cooperation with Prof. Dr. Hans-Anton Lehr. Thus, lung samples were stored in 3-5% PBS buffered formalin before embedding in paraffin in accordance to standard protocols in the pathological department of the Centre Hospitalier Universitaire of Lausanne, Switzerland.

Lung histological images of paraffin sections in this thesis were stained and quantified in the pathological department at the University of Lausanne, Switzerland and imported in Photoshop (Adobe systems Inc. version 7.0, San Jose, CA) as previously described[59]. Space bars in Figure 25 correspond to 2.5 mm for the histological overviews and 200 µm for the high magnification images on the right. The staining was performed with hematoxylin and eosin, which allows the detailed analysis of the histological structure of the lung and revealed the tumor mass within lung tissue and the migration of the injected B16-F10 cells from the vessels to the pleura of the lung.

Frozen sections

Lungs were embedded in OCT compound and stored at –80°C until lung sections of 5 µm thicknesses were generated with a Cryostat kept constantly at –20°C. The gained sections were transferred to a Polylysin-coated microscope slide and kept at –20°C until further use.

Before the immunohistochemical staining procedure is started, the lung has to be exempted from the surrounding OCT compound. For this purpose, the slides were kept in Acetone at –20°C for 20 minutes. This procedure was followed by a 20 min fixation of the tissue in 4% Paraformaldehyde and a washing step in 0,05M Tris-hydrochloride. After additional washing in PBS the sections were incubated with the primary antibody in accordance with manufacturers` information. This step was performed over night at 4°C. Unbound primary antibody was washed off with PBS and a corresponding biotinylated secondary antibody was diluted (1:1000) in PBS and pipetted onto the samples where it remained at room temperature for 1 hour (h). The last step consists of incubation with streptavidin-conjugated Cy2 or Cy3 at room temperature again for 1h. This allows the detection of the stained molecules under the fluorescence microscope (Olympus).

3.2.9 Cell isolation from spleens and lungs

The isolation of different subsets of immune cells is an essential basic method in immunological science. In the first step, the generation of a single cell suspension is required and created from the tissue that is to be analyzed.

Protocols for total cell isolation from lungs and spleens vary because of the collagen that fixes lung cells in the tissue and that needs to be degraded prior to further isolation steps.

Spleens were removed from mice at the indicated time points and filtered through a 40 µm nylon filter with the help of a sterile syringe top and RPMI media in order to remove tissue fragments. The filtrate was centrifuged (300 g, 5 min) and the cell pellet washed once with RPMI 1640. Erythrocytes were removed from spleen cell suspension by hypotonic lysis in ammonium chloride and potassium chloride (ACK) buffer. After 2 washes in PBS, the cell pellet was resuspended in 10 ml MACS buffer for further isolation of cell subsets and the cell number was determined. Alternatively the cell suspension was resuspended in RPMI media for cell culture.

Lungs were treated like the spleens but prior to filtering the cells through the nylon mesh, the lungs were cut into small pieces of approximately 1–2 mm^2 with a scalpel. The tissue pieces were suspended in PBS (5 ml per lung) containing 300 U/ml of collagenase type II and 0.001% DNase. The suspension was incubated at 37°C for 1 hour with constant shaking. Afterwards, cell isolation proceeded as described for splenocytes and was either used for FACS analysis, cell culture experiments or further cell purification.

3.2.10 $CD4^+/CD8^+/CD11c^+$ cell purification from spleens and lungs

The $CD11c^+$ lung or spleen cells were directly purified from isolated lung or spleen cell suspension by incubation at 6-12°C for 15 minutes with 100 µl of anti-mouse $CD11c^+$ (N418) microbeads per 10^7 total cells and positively sorted in a multiparameter magnetic cell sorter system according to manufacturers` instructions as follows. This reaction was stopped by adding 1-2 ml of MACS buffer per 10^8 cells followed by a 10 min centrifugation at 1500 rpm. Supernatants were completely pipetted off and the cell pellets were resuspended in 500 µl of MACS buffer per 10^8 cells. During the above described incubation the column was placed in the magnetic field of the separation unit and prepared by rinsing with 500 µl MACS buffer. Afterwards the sample solution was applied onto the column and the column was washed 3 times with 500 µl MACS buffer. The effluent was collected in a centrifugation tube and contained the unlabeled cell fraction. To gain the positive cell fraction, the column was removed from the magnetic

field and placed on a suitable tube. 1 ml MACS buffer was pipetted into the reservoir of the column and the liquid was immediately forced through the column by using the plunger that is provided with the column. The effluent contains the purified $CD11c^+$ cells.

The $CD4^+$ and $CD8^+$ lung cells were directly purified from isolated lung cell suspension by incubation with 10 µl of anti-mouse $CD4^+$ (L3T4) / anti-mouse $CD8^+$ (CD8a Ly-2) microbeads per 10^7 total lung cells at 4°C for 15 minutes and positively sorted in a multiparameter magnetic cell sorter system as described previously[60].

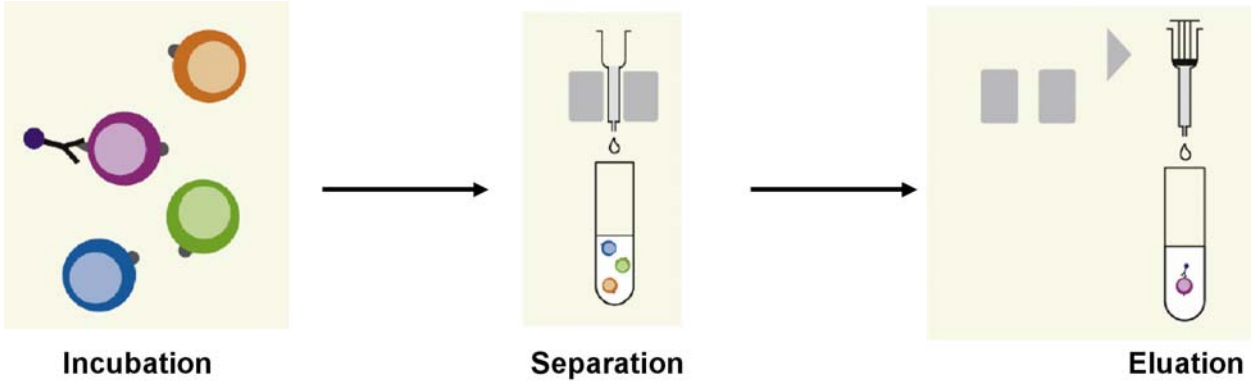

Figure 21: Scheme of cell isolation with MACS®[61].

3.2.11 Cell culture

B16-F10 melanoma cell culture

The cell line was kindly provided by Prof. Laurie H. Glimcher and grown in cell culture flasks containing DMEM with adjuvants as described above. The adherent cells were passaged at a density of 60%, which was achieved every second day after splitting in a 1:10 ratio. The splitting procedure was performed by removing the media from the flask and rinsing the adherent cells with 10 ml PBS that was discarded. To detach the cells from the culture flask 2 ml of a Trypsin/EDTA solution or alternatively Accutase was pipetted into the flask and distributed by gently shaking the flask. When the solution covered the ground of the culture flask completely the flask was incubated at 37°C for approximately 5 minutes and cells were detached by dashing the flask against a table. The cells were resuspended in 10 ml culture media and transferred into a tube, which was centrifuged at 1500 rpm and 4°C for 5 min. After discarding the supernatant, the cell pellet was resuspended in 10 ml culture media and a single cell suspension was created by gently pipetting the suspension up and down. Finally 1 ml of the single cell suspension was transferred into a new culture flask and 35 ml of culture media was

added. Until the next passaging step, the cells were incubated at 37°C and 5% CO_2 in an atmosphere saturated with water vapor.

B16-F10 cells were cultured for a maximum of 3 weeks as described above. To assure a permanent high quality of cells, the cell line was frozen in liquid nitrogen after only few passages. The cell splitting was accomplished until detaching the B16-F10 cells and centrifugation. $1x10^6$ B16-F10 cells were then resuspended in 1.8 ml of a mixture of 90% FCS and 10% DMSO and immediately stored at –20°C. After 4-5h the tubes were transported to –80°C and where they were kept over night. The next day the frozen B16-F10 cells were stored in liquid nitrogen until further use.

Culture of isolated $CD4^+$ and $CD8^+$ cells

After 3 washes in complete medium, the $CD4^+$ / $CD8^+$ T cells were cultured with 5 µg/ml plate-bound anti-CD3 antibody at a density of 10^6 cells/ml. The culture was maintained in an incubator for 24 h under the following conditions: 37°C, 5% CO_2, atmosphere saturated with water vapor.

Alternatively, EBI-3 deficient $CD8^+$ T cells were co-cultured with B16-F10 cells in a 1:1 ratio, 5 µg/ml plate-bound anti-CD3 antibody and different doses of anti-TNF-α antibody were supplemented.

The cell culture plate was coated with anti-CD3 antibody prior to adding the cells and culture medium. Resuspending 50 µl anti-CD3 antibody in 5 ml aseptic NaHCO3 solution and applying 200 µl of this mixture into each well of a 24 well-plate accomplished this. The plate was then incubated for 1 h under the above described conditions followed by 2 washing steps with 1 ml PBS. The presence of anti-CD3 antibody in the T cell culture stimulates the T cell receptor of the cultured cells and increases cytokine production of the cells.

Culture of isolated $CD11c^+$ cells

After 3 washes in RPMI medium, the $CD11c^+$ cells were cultured at a density of 10^6 cells/ml for 24 hours. The cell culture media was supplemented with 1 µg/ml LPS to mimic antigen presence in the culture which stimulates dendritic cell activities.

If $CD11c^+$ lung cells were cultured for intracellular FACS staining, the cells were cultured at a density of 10^6 cells/ml over night in a cell culture plate with 1 µg/ml LPS as

stimulating factor. The next morning, the medium was replaced by RPMI containing 1 µg/ml LPS and 0.5 ng/ml Phorbol-myristat-Acetate (PMA) plus 500 ng/ml Ionomycin and 4 µl Monensin/6ml medium. The cell culture plate was incubated for another 5 h.

Culture of total lung cells

Total lung cells were either cultured under the conditions for stimulating dendritic cells or activating T cells as described for the isolated cell fractions above.

If total lung cells were cultured for intracellular FACS staining, the cells were cultured at a density of 10^6 cells/ml overnight in a cell culture plate that was coated with anti-CD3 antibody. Additionally, 2.5 µg/ml anti-CD28 antibody was supplemented. The next morning, the medium was replaced by RPMI containing anti-CD3 and anti-CD28 antibodies plus 0.5 ng/ml Phorbol-myristat-Acetate (PMA) plus 500 ng/ml Ionomycin and 4 µl Monensin/6ml medium. The cell culture plate was incubated for another 5 h.

3.2.12 FACS staining and analysis

Fluorescence-activated cell sorting (FACS) is a method to quantify surface molecules and intracellular proteins of a single cell suspension. The technique bases on antigen-antibody reactions whereby the used antibodies are labeled with a fluorochrome. The flow cytometer is an instrument that is able to send the cells of the suspension one at a time through a fluorimeter with a laser-generated incident beam. The electrons of the fluorochrome are activated to a higher energetic level by the monochromatic laser beam. By emitting energy the electrons return to their original status. The emitted energy is detected and is proportional to the amount of antibody that is bound to one cell. It is possible to detect several different molecules simultaneously by using different fluorochromes, which are activated at a common wavelength but each have a different but characteristic emission spectrum.

In addition, information on the cell size and granularity of the cell is also provided by light scattering and diffraction[62].

FACS staining with cell surface molecules

To assure the purity of isolated cells or to analyze different cell subsets within the total lung cell suspension the samples were stained with up to four different fluorochrome-

labeled antibodies for surface molecules. Routinely, $5x10^5$ cells were washed with 1 ml PBS then incubated for 30 min at 4°C in 100 µl PBS containing 5 µg/ml of each antibody. The cells were then washed with 1 ml of PBS and resulting cell suspensions were resuspended in FACS buffer. In addition, unstained samples, as well as samples stained with only one of each antibody have to be provided in order to program the FACS Calibur correctly.

The measurement was performed by FACS Calibur and subsequently analyzed by using Cell Quest Pro version 4.02 (BD PharMingen, Heidelberg, Germany). A typical dotplot of a measurement of total lung cell suspensions is shown in Figure 22. Lung cell suspensions include a wide range of cell types that vary in size and granularity. This phenomenon is depicted in the left graph of Figure 22 showing the cells in the forward scatter (FSC) and side scatter (SSC) of the FACS Calibur. Such a graph allows the localization of different subpopulations of lung cells, e.g. lymphocytes (Gate 1) and DCs (Gate 2), due to their size and granularity. The following explanation only refers to the gate for lymphocytes but can be performed with the gate for DCs as well. To calculate the percentage of cells expressing certain surface markers – here CD8, CD44 and CD49d – the gated population of lymphocytes was further analyzed and only $CD8^+$ lymphocytes were gated (Figure 22). In the last step the $CD8^+$ lymphocytes were analyzed for the expression of CD44 and CD49d. By using isotype controls and samples that were stained with only one fluorochrome-labeled antibody the area were $CD44^+$ and $CD49d^+$ cells are located can be defined. The percentage of $CD8^+$ cells expressing both CD44 and CD49d was the calculated.

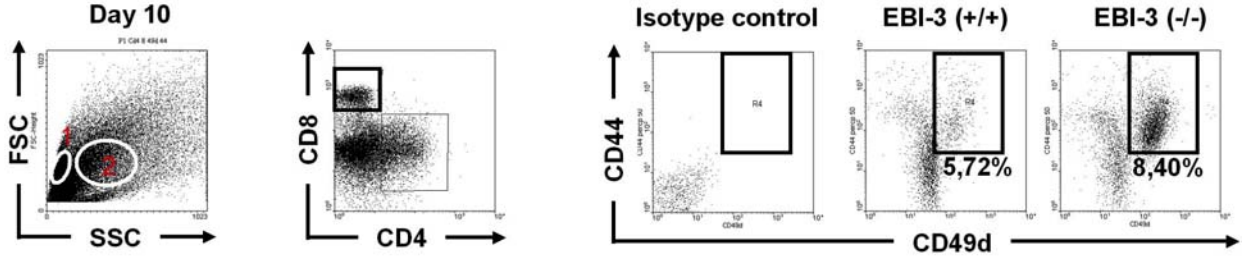

Figure 22: Example of total lung cells analyzed by FACS. The left graph displays a dotplot of total lung cell suspension. Gate 1 encloses the population of lymphocytes and Gate 2 is placed were DCs are found. Gate 1 for lymphocytes was selected for the graph in the middle. $CD8^+$ cells were then gated and the final analysis shown on the right refers to the selected $CD8^+$ lymphocytes.

The FACS analysis of cell suspensions from draining lymph nodes was performed according to lung cell analysis described above. However, the gate for DCs in DLNs was selected differently as shown in Figure 23.

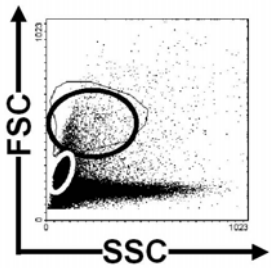

Figure 23: Example of cell suspension from DLN analyzed by FACS. The white circle encloses the population of lymphocytes while the black circle is placed were $CD11c^+$ cells are found in DLN.

Intracellular FACS staining

Intracellular FACS staining was performed for the cytokine IFN-γ and the transcription factor Foxp3. For this method it is necessary to make the cell membranes permeable for the antibodies. However, the intracellular staining was always combined with staining of surface molecules, which must be performed prior to the intracellular staining. Therefore, the cell suspension that was gained from the overnight cell culture as described above was first incubated with the cell surface markers and after the last washing step resuspended in 200 µl Foxp3 Fixation/Permeabilization Concentrate and Diluent instead of FACS buffer. The Foxp3 Fixation/Permeabilization Concentrate and Diluent solution was purchased ready to use and the 45 min incubation time at 4°C made the cell membranes permeable. The samples were then centrifuged and incubated with 1 µl of anti-IFN-γ or anti-Foxp3 diluted in 60 µl 1x Permeabilization Buffer. This suspension was incubated at 4°C for 30 min and the reaction was ended by adding 300 µl 1x Permeabilization Buffer and centrifuging the samples. This washing step was repeated prior to resuspending the cells in 300 µl of FACS buffer. Unstained samples and samples stained with only one kind of fluorochrome labeled antibody has to be provided as described for the staining with surface molecules. It is especially important to prepare these controls the same way the samples are prepared.

3.2.13 ELISA

An enzyme-linked immunosorbent assay (ELISA) uses antibody-antigen reactions to detect the amount of antigen in a sample. The antibody is therefore coupled to an enzyme that has the capability to convert the clear substrate into a colored product whereby the color can be detected with a spectro-photometer. The sandwich ELISA that is commonly used in our laboratory consists of two reactions with different antibodies that bind to two different epitopes of the same antigen.

In the first step a fixed amount of one antibody is incubated in plastic microtiter wells in order to attach to the plate. This antibody captures the antigen from the sample whose antigen concentration needs to be determined. In addition, a series of standard solutions with known concentration are added to some wells for allowing the creation of a reference curve at the end of the assay. Unbound antigen is removed by washing steps. Now the second antibody, which is covalently linked to an enzyme – mostly horseradish peroxidase – is incubated with the samples. It is also important that the second antibody binds to an epitope that does not overlap with the epitope recognized from the first antibody since an overlapping would circumvent the binding of the second antibody which in consequence leads to the detection of lower amounts of antigen as actually present.

To finally detect the amount of antigen, a substrate solution is added to all wells that causes a change in pH and therefore, a color reaction to the enzyme. Since the amount of enzyme-labeled antibody is proportional to the amount of antigen in the sample, the intensity of the color reaction also depends on the amount of antigen and is measured with a spectro-photometer[62].

The detection of the cytokines displayed in this thesis was performed by sandwich ELISA in accordance to manufacturers` instructions. Only TGF-β was not purchased as an ELISA Kit and the protocol used is as follows:

3 µg/ml Capture antibody were diluted in 10 ml Phosphate Buffer that was titrated to pH 9.3. Each well of a 96 well plate was coated with 100 µl of this dilution and incubated at 4°C over night. After three washing steps with PBS containing 0.05% Tween 20 the reaction was blocked with 1% BSA in PBS at 37°C for 1h.

During blocking incubation time each 200 µl sample is diluted with 10 µl HCl to switch the pH to approximately pH3. This solution is incubated at 37°C for 30 min and the neutralized with 10 µl NaOH.

After blocking, the plate is washed again three times and samples as well as standards are added to the wells and incubated at 37°C for 2h followed by washing steps. 40 µl of the biotinylated secondary antibody are diluted in 10 ml blocking buffer and pipetted into the wells. Incubation time is 1h at 37°C and ends with 5 washings. Horseradish peroxidase is diluted in Blocking Buffer and applied onto the samples and standards and kept under constant shaking for 30 min at room temperature in the dark. After 5 washings the TMB substrate solution is added to the wells and the reaction is stopped when the lowest standard concentration is slightly visible as blue staining in the well. H_2SO_4 is used to convert the blue color of the wells into yellow that is detectable with the ELISA reader.

3.2.14 Protein isolation and Western Blot analysis

A western blot is a method to detect a specific protein in a sample of tissue homogenate and was first used by George Stark at Stanford University. It uses gel electrophoresis to separate denatured proteins by their size. After separation the proteins are transferred to a nitrocellulose membrane, where they are detected by using antibodies that are specific for the target protein.

The method begins with the preparation of samples from whole tissue – in my case, lung tissue - or from cell culture. Samples are reduced to extremely small pieces using a homogenizer. Usually detergents are added to fasten cell lysis and to solubilize proteins. The task of protease inhibitors is preventing the digestion of the sample by its own enzymes. Centrifugation is then used to separate the cell compartments from the protein containing supernatants.

The proteins of the samples are then separated by gel electrophoresis. This technique is based on the isoelectric point and the molecular weight of the proteins, which means that proteins move in an electric field dependent on their size and their electric charge. Commonly, a polyacrylamide gel is prepared including buffers loaded with sodium dodecyl sulfate (SDS). Thereby the proteins are covered with the negatively charged SDS so that their own charge is no longer detectable and the

movement of the proteins to the positively charged electrode is only due to the size of the molecules. Therefore small proteins migrate faster through the gel than larger proteins and this mechanism separates the proteins. The concentration of acrylamide determines the resolution of the gel. Large concentrations of acrylamide lead to better resolutions of proteins with high molecular weight.

The samples are loaded into the wells in the gel. A commercially available mixture of proteins with defined molecular weights, that are usually stained to show visible bands, is loaded to one well and is later used to identify the size of the proteins. Except for the marker the separated proteins are not yet visible. A transfer from the gel onto nitrocellulose membrane makes the proteins accessible to antibody detection. The membrane is placed on top of the gel, and a stack of tissue papers placed on top of that. The entire stack is placed in a transfer buffer solution, which uses electricity to pull proteins from the gel into the nitrocellulose membrane. The proteins have now moved from within the gel onto the membrane while maintaining the organization they had within the gel. As a result of this "blotting" process, the proteins are exposed on a thin surface layer for detection.

Prior to applying antibodies to the membrane, steps must be taken to prevent interactions between the membrane and the antibody, which is used for detection of the target protein. This is necessary because the membrane has the ability to bind protein, and both the antibodies and the target are proteins. Blocking of non-specific binding is achieved by placing the membrane in a solution of protein – typically Bovine serum albumin (BSA) or non-fat dry milk including a small percentage of detergent such as Tween 20. The protein in the solution attaches to the membrane in all places where the target proteins have not attached. Thus, when the antibody is added, there is no room on the membrane for it to attach other than on the binding sites of the specific target protein. This reduces the “background” in the final product of the Western blot, leading to clearer results, and eliminates false positives.

The primary antibody can be diluted in the blocking buffer and is incubated with the membrane under gentle agitation from 30 minutes to overnight depending on the temperature during incubation. After rinsing the membrane to remove the unbound primary antibody, the membrane is exposed to another antibody that is directed at the species-specific portion of the primary antibody. The so-called secondary antibody is

usually linked to either biotin or to an enzyme such as horseradish peroxidase. Several secondary antibodies will be able to bind to one primary antibody, which enhances the signal. The membrane is then incubated with a chemiluminescent agent that reacts with the enzyme and causes a luminescence in proportion to the amount of bound protein. In the dark, a photographic film is placed on the membrane, and the luminescence from the reaction creates an image of the antibodies bound to the blot. This image becomes apparent after developing the film with standard photographic devices and can be analyzed by densitometry, which evaluates the relative amount of protein staining and quantifies the results in terms of optical density. So-called "enhanced chemiluminescent" (ECL) detection is considered to be among the most sensitive detection methods for blotting analysis and was used for detection of proteins in this work.

The Western blots shown in this thesis were performed as described above and analyzed by comparing the density of the protein staining on the film to the density of staining with β-Actin as reference. To assure the loading of equal amounts of protein from each sample the concentration of protein was determined by the colorimetric method of Bradford. The extinction of each sample is measured with a photometer and quantified using a reference curve.

3.2.15 Statistical evaluation

All experiments were repeated three times in order to gain n ≥ 15 individual measurements per group. The results were used to calculate the mean and the standard error of mean (SEM). Differences were evaluated for significance ($P < 0.05$) by the Student's two-tailed t test for independent events (Excel, PC). All data are given as mean values ± SEM and significance is marked as listed below:

* $P<0.05$

**$P<0.01$

***$P<0.001$

4 Experiments and Results

4.1 Development of B16-F10 induced lung melanoma in EBI-3 deficient and C57B/6 wild-type mice

4.1.1 Development of B16-F10 induced lung metastasis of melanoma

Melanoma is a malignant skin tumor that can metastasize to any organ, including the brain and the lung[21]. Cutaneous malignant melanoma is a highly aggressive, potentially fatal malignancy often resistant to current available therapy[63].

To start to analyze the role of EBI-3 in a murine model of metastatic melanoma, I studied the development of melanotic colonies in EBI-3 deficient and C57B/6 wild-type mice after intravenous injection of $2x10^5$ B16-F10 cells into the tail vein at day 0. To monitor the development of the lung melanoma, I sacrificed the mice at different time points after B16-F10 melanoma cell injection and removed the lungs in order to analyze and count lung colony formation by means of a stereomicroscope in both EBI-3 deficient and B6 wild-type mice as shown in Figure 24. Starting at day 10, a significant increase in melanotic lung colonies was detected in the B6 wild-type mice compared to EBI-3 deficient B16-F10 injected mice. This difference was maintained until day 21.

As described by Fidler the F10 clone of the B16 cell line is very aggressive and specific for its ability to form only pulmonary tumor nodules upon intravenous injection of the in vitro cultured cell line[50]. Consistently with this observation, I did not locate colonies of melanoma in any other organs of these mice other than the lung.

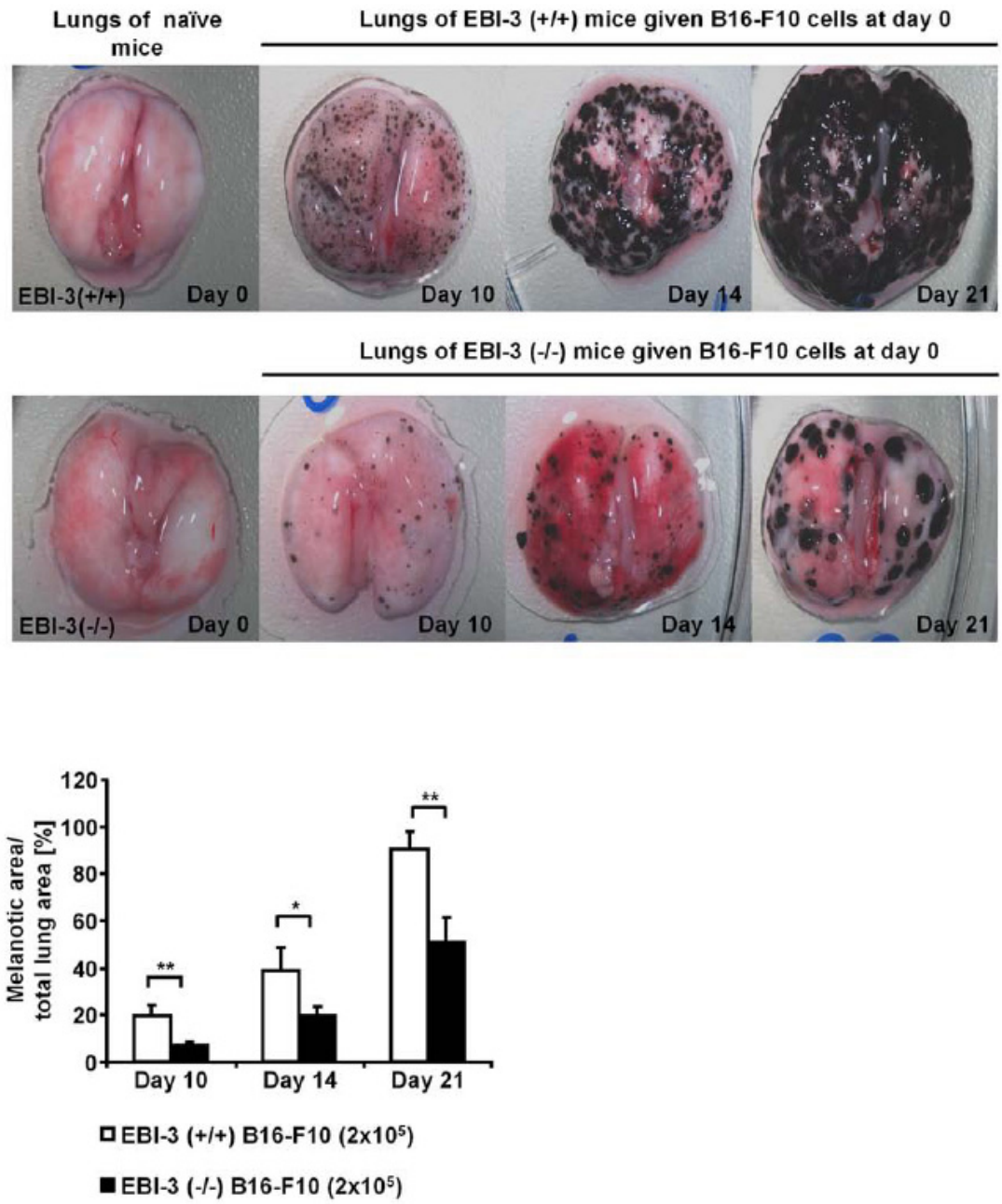

Figure 24: Development of B16-F10 induced lung melanoma in EBI-3 deficient and C57B/6 wild-type mice. Intravenous injection of $2x10^5$ B16-F10 melanoma cells leads to a time dependent development of the melanoma in the lungs of B6 wild-type mice (upper panels) as well as in EBI-3 (-/-) lungs (lower panels). Quantification analysis shows that the area of the lungs covered with melanotic colonies on days 10, 14 and 21 is significantly reduced in EBI 3 (-/-) lungs.

The upper two panels of Figure 25 show representative sections of the B16-F10 injected lungs using hematoxylin and eosin staining. The development of melanoma was visible as dark purple cells in the lung tissue. The finding displayed in Figure 24

was confirmed after histological quantification of the hematoxylin and eosin stained lung sections (graph in Figure 25) where at day 5 melanoma formation was visible in sections of B6 wild-type mice while the corresponding sections of the EBI-3 deficient mice remained without tumor. Starting from day 10 EBI-3 deficient mice exhibited melanoma colonies but at all indicated time points, the melanoma growth in the EBI-3 deficient mice was to a significantly lesser extent than in their wild-type littermates. In both type of mice the preferential localization of metastases was found in the sub-pleural areas and the confluence of tumor colonies increased to large conglomerates at later time points.

To confirm the assumption that the intravenously injected B16-F10 cells remain in the blood stream until they reach the lung where they have to find their way to the surface of the lung, I took histological lung sections of B16-F10 injected mice. The microscopic slides were stained with hematoxylin and eosin in order to be able to follow the migration of the B16-F10 cells. The lower right panel of Figure 25, which is marked with the letters A-D, is showing tumor cells adherent to the endothelium of a large vessel (A). This status is followed by emigration of the melanoma cells from a vessel filled with tumor cells (B), which leads to tumor cell entry into the lung microvessels closer to the surface of the lung – the pleura(C). (D) Finally, B16-F10 tumor cells are adhering to the pleura and further building a tumor microenvironment that allows unlimited tumor growth.

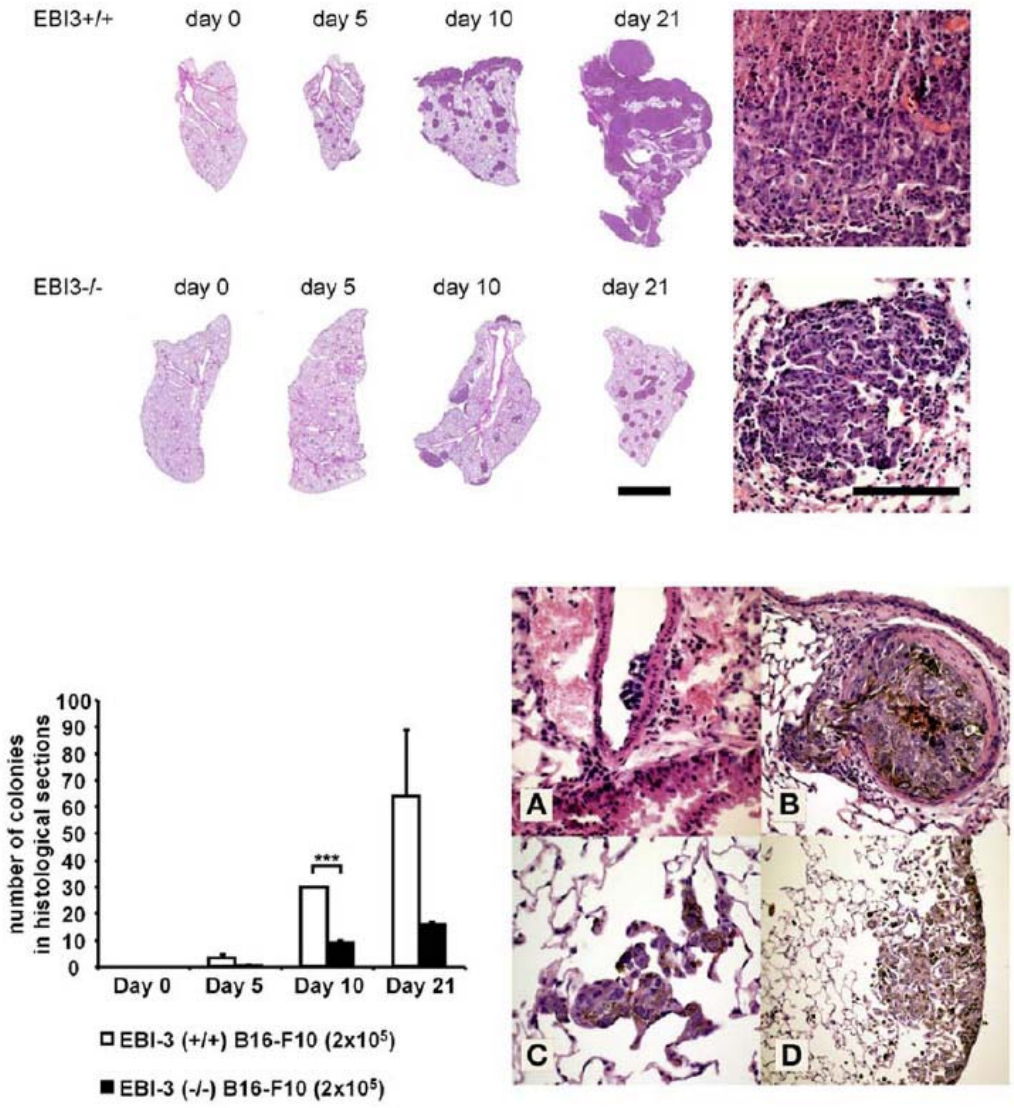

Figure 25: Lung histology after B16-F10 cell injection. Representative histological sections across lungs of wild-type (upper images) and EBI-3 (-/-) mice (lower images) are displayed after staining with hematoxylin and eosin. Sections were taken at the indicated time points 0, 5, 10 and 21 days after tumor cell injection. The higher magnification images rendered on the right side of the image show representative sections of melanoma metastases. Space bars correspond to 2.5 mm for the histological overviews and 200 µm for the high magnification images on the right. Quantification analysis of histological sections showed a decreased number of melanotic colonies in the tumor bearing lungs of EBI-3 (-/-) mice compared to the wild-type mice. (A-D) Histological slides stained with hematoxylin and eosin showing tumor cells adherent to the endothelium of a large vessel (A), emigration from a vessel filled with tumor cells (B), and tumor cell entry in the lung microvessels (alveolar capillaries)(C). (D) Tumor cells adhering to the pleura.

4.1.2 Survival of mice with B16-F10 induced lung melanoma

It was found that targeted deletion of EBI-3 results in a suppressed growth of the B16-F10 induced lung metastasis of melanoma. Nevertheless, it remained unclear whether the protection from tumor growth seen in EBI-3 deficient mice was a temporary effect or whether the slower tumor growth continued in these mice leading to a long lasting protection. EBI-3 deficient mice that were injected with $2x10^5$ B16-F10 cells at day 0 showed an increased survival compared to the B6 wild-type littermates (Figure 26). Specifically, a dramatic drop in the survival of B6 wild-type mice started at day 21 after intravenous injection of B16-F10 cells, whereas one hundred percent of the EBI-3 deficient mice survived until day 28. At this specific time point fifty percent of the B6 wild-type mice bearing tumor were already dead. At day 33, one hundred percent of the B16-F10 cell injected B6 wild-type mice were dead, whereas 50% of EBI-3 deficient mice were still alive. Although tumor mass in the lungs of EBI-3 deficient mice increased dramatically over time, it never caught up with the enormous tumor growth in the B6 wild-type littermates.

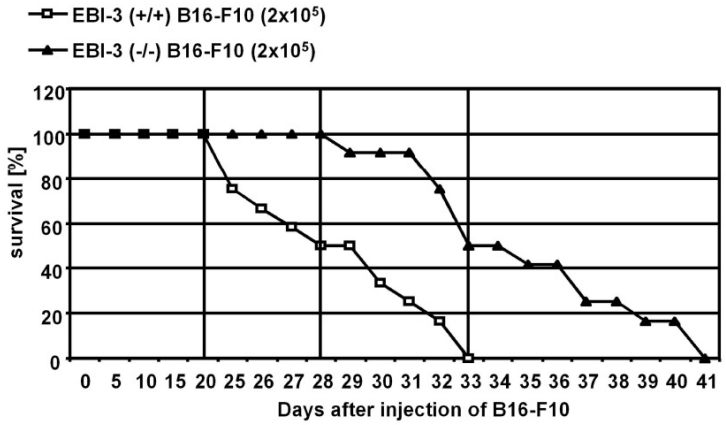

Figure 26: Survival of EBI-3 deficient and C57B/6 wild-type mice after B16-F10 melanoma cell injection. Intravenous injection of $2x10^5$ cells of the B16-F10 cell line leads to increased survival of EBI-3 (-/-) lung melanoma bearing mice.

These findings indicate that targeting EBI-3 in patients of metastatic melanoma could be a promising approach for the therapy of this disease. But to develop effective therapies, it is necessary to demonstrate the mechanisms, which are used by the EBI-3 deficient immune system to target the B16-F10 tumor cells. I therefore studied various anti-tumor mechanisms noted in publications. The following studies focused on cell

mediated anti-tumor responses but also included the quantification of growth factors and anti-apoptotic proteins.

4.2 Analysis of EBI-3 deficient tumor vascularization

Many tumors are characterized by enormous vascularization. The newly built vessels in and around the tumor are often due to a high expression of growth factors from the tumor cell itself. The major factor detected in tumor tissue is the vascular endothelial growth factor (VEGF) that creates an enormous development of abnormal neovascularization although its structures are very simple and unorganized. The main purpose of the many new vessels is thought to supply the tumor with oxygen and nutrients. Therefore, the new vessels are extremely permeable in order to allow the nutrients to leave the blood stream and immigrate into the tumor tissue. As a result, the pressure in the tumor tissue increases due to the constant influx of substances. Consequently, the tumor reduces the pressure by allowing tumor cells to leave the original tumor site and enter the blood stream by which VEGF enables metastatic seeding since the tumor cells are now able to migrate to new locations where they build metastases of the primary tumor[64].

4.2.1 VEGF expression in the lungs of B16-F10 injected mice

Since I used only one cell line for the establishment of the metastatic lung colonies of melanoma in the EBI-3 deficient and B6 wild-type mice, it is very unlikely that the expression of VEGF from the tumor cells varies in the two types of mice. But the suppressed growth of melanoma in the EBI-3 deficient mice could still be the result of a decrease in the expression of VEGF in the lung. This effect would lead to a reduced maintenance of the newly established tumor and finally lead to retarded tumor growth.

To analyze the amount of VEGF in the tumor bearing lungs of EBI-3 deficient and B6 wild-type mice I took the bronchoalveolar lavage fluid (BALF) and collected the supernatants after centrifugation for cytokine analysis. VEGF detection in the BALF by ELISA revealed a very low overall expression of the growth factor in the lungs of these mice and showed that VEGF expression remains unchanged throughout tumor development. In addition, as demonstrated in Figure 27 the comparison between B6

wild-type and EBI-3 deficient mice did not show differences in the amount of VEGF detected. But supernatants of B16-F10 in vitro cell culture displayed enormous amounts of VEGF (data not shown).

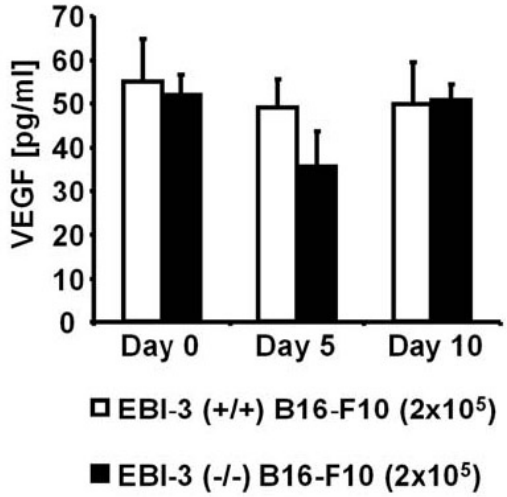

Figure 27: VEGF production in BALF of EBI-3 deficient mice. The BALF was taken from EBI-3 (-/-) and B6 wild-type mice at the indicated time points and supernatants were taken for cytokine analysis. VEGF was found to be equally released in the BALF of EBI-3 deficient and B6 wild-type mice at all investigated time points.

The supernatants of the BALF contain the whole spectrum of substances produced in the lung, but unfortunately in the BALF, the concentration of most cytokines and proteins is not very high. Due to this experience I was looking for an additional way to detect VEGF in the lung and decided on protein isolation from lung tissue. When using 700 µg of total lung protein per sample in an ELISA assay the amount of VEGF detected was clearly increased (Figure 28). Except for day 14, when surprisingly VEGF was increased in EBI-3 deficient mice compared to the B6 wild-type littermates, the expression of VEGF was still found to be equal within the two types of mice.

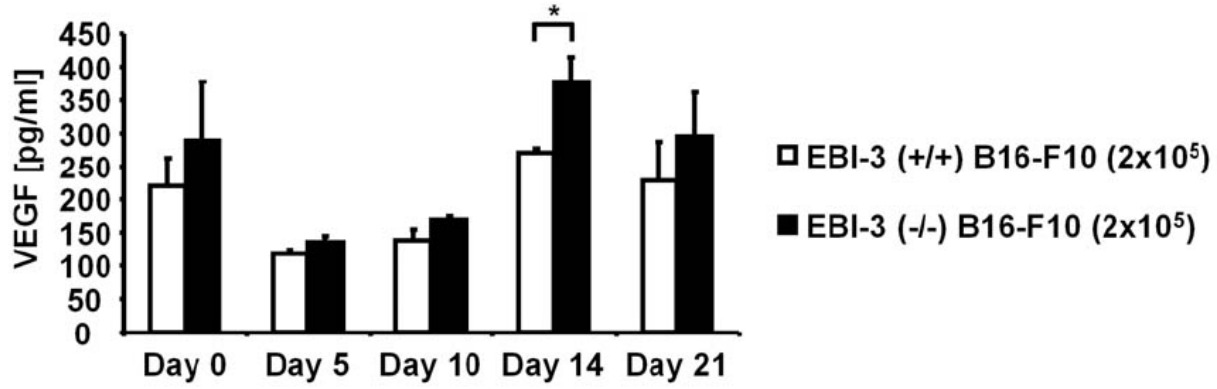

Figure 28: VEGF production in lung tissue of EBI-3 deficient mice. Proteins were isolated of lung tissue from EBI-3 deficient and B6 wild-type mice. From each sample 700 µg of total lung protein were used for VEGF detection by ELISA. VEGF production was only found to be significantly altered on day 14 after tumor cell injection when VEGF was upregulated in EBI-3 deficient lung proteins.

To confirm the results obtained by ELISA, I used the total lung proteins for Western Blot analysis. The detection of VEGF was quantified versus the ubiquitously expressed β-Actin as displayed in Figure 29. Although the Western Blot exposes a decrease of VEGF in EBI-3 deficient lungs 10 days after tumor cell injection, the change was not confirmed by ELISA and therefore considered as irrelevant.

Taken together, the investigation for VEGF expression in the lungs of B16-F10 injected B6 wild-type and EBI-3 deficient mice did not show any differences that could explain the slower development of melanotic colonies in the lungs of EBI-3 deficient mice.

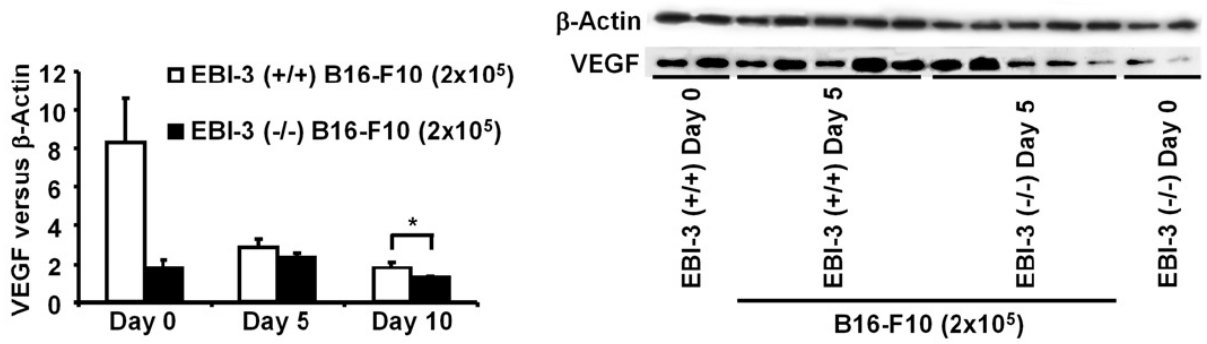

Figure 29: Western Blot from total lung protein stained for VEGF expression. Proteins were isolated of lung tissue from EBI-3 deficient and B6 wild-type mice. Western blot analysis from the isolated total lung proteins was performed for VEGF and quantified versus β-Actin which demonstrated only small differences in expression of VEGF in EBI-3 (-/-) mice compared to B6 wild-type mice.

4.2.2 Expression of VEGF Receptor in the lungs of B16-F10 injected mice

Although, expression of VEGF in the lungs of the mice used in this B16-F10 model remained constant, another factor is involved in the process of neovascularization. To be able to create a new vascular system, VEGF has to bind to its receptor. The family of VEGF receptors includes its major member VEGFR-2 (Flk-1)[64]. If Flk-1 is down-regulated in EBI-3 deficient lungs the expressed VEGF lacks its binding partner and cannot function.

Examination of Flk-1 on histological lung sections from naïve and tumor bearing EBI-3 deficient and B6 wild-type mice was performed with a fluorochrome-labeled anti-Flk-1 antibody. The expression of Flk-1 was then analyzed with a fluorescence microscope connected to a camera and found to be equally expressed on cells of EBI-3 deficient and B6 wild-type lung tissue (Figure 30).

Thus, neither VEGF nor its receptor Flk-1 seem to be involved in the slower growth of B16-F10 induced melanoma colonies in the lungs of EBI-3 deficient mice.

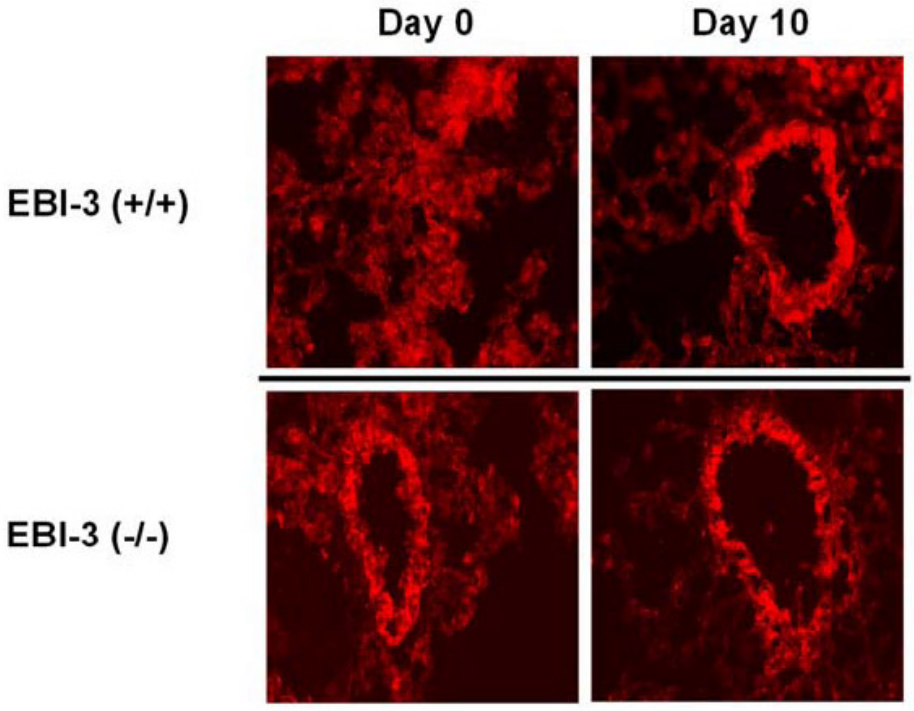

Figure 30: Immunohistochemical staining with anti-Flk-1 (anti-VEGFR-2) antibody on naïve and tumor bearing lung tissue. Representative histological sections across lungs of wild-type (upper images) and EBI-3 (-/-) mice (lower images) are displayed after staining with fluorochrome labeled anti-Flk-1 antibody. Sections were taken at the indicated time-points before and after tumor cell injection. Quantification with the fluorescence microscope revealed by 40x magnification that the expression of Flk-1 in lung tissue does neither depend on EBI-3 nor on injection of B16-F10 cells.

4.3 Analysis of EBI-3 deficient Dendritic Cells in the murine model of B16-F10 induced lung melanoma

EBI-3 is highly expressed on activated dendritic cells and the lack of this protein leads to an altered immune response especially regarding the $CD4^+$ T cells, which generally improved inflammatory diseases. In addition, recent studies showed that EBI-3 deficient dendritic cells were able to reduce allergic asthma in a murine model when these cells were transferred into recipient wild-type mice[65]. This knowledge led to the postulation that the EBI-3 deficient dendritic cells in the model of B16-F10 induced metastatic melanoma should be a subject for further characterization with the aim to identify a dendritic cell population that can be used as a possible anti-tumor vaccine.

4.3.1 Plasmacytoid Dendritic Cells of B16-F10 melanoma bearing EBI-3 deficient mice

The first dendritic cell population I investigated was the plasmacytoid DCs (pDC) which are characterized by TLR7 and TLR9 expression and IFN-α production upon stimulation with many enveloped viruses. The cells are known to express the murine dendritic cell marker CD11c and the marker PDCA-1 that is specific for pDCs but expression of MHC class II molecules is extremely low. pDCs are responsive to IL-3 but not to GM-CSF and can induce T cells to produce either IFN-γ or IL-4 depending on the environmental conditions[66-68].

FACS analysis was performed by generating total lung cell suspensions of lungs from naïve and B16-F10 melanoma bearing EBI-3 deficient and B6 wild-type mice. These cell suspensions were then immuno-stained for the pDC markers. Co-expression of both markers on one cell was increased in the lungs of EBI-3 (-/-) mice bearing tumor five days after the intravenous injection of B16-F10 compared to B6 wild-type littermates (Figure 31). At day 10 a significant increase in the expression of pDCs markers ($CD11c^+PDCA\text{-}1^+$) was found in the draining lymph nodes of EBI-3 (-/-) mice (Figure 31, lower left graph).

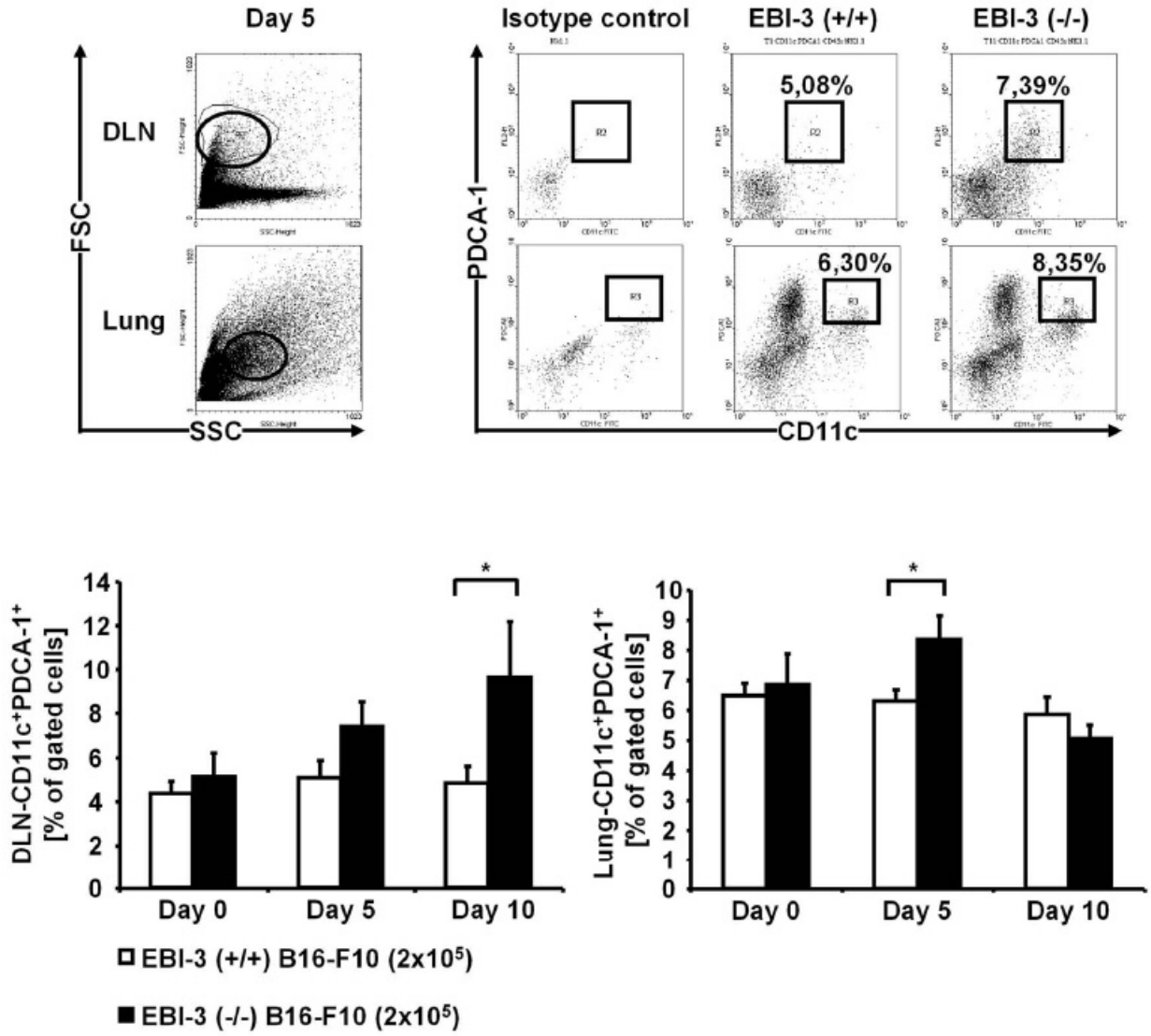

Figure 31: Increased number of plasmacytoid Dendritic Cells in local draining lymph nodes and lungs of EBI-3 deficient mice. Cell suspension of thoracic DLN and lungs of EBI-3 (-/-) and B6 wild-type mice were immuno-stained for the indicated markers and analyzed by FACS. pDCs defined as $CD11c^+PDCA^+$ cells were upregulated in DLN (upper panels) and lungs (lower panels) of EBI-3 deficient mice 5 days after tumor cell injection.

4.3.2 Interferon-γ producing Killer Dendritic Cells of B16-F10 melanoma bearing EBI-3 deficient mice

Interferon-γ producing killer dendritic cells (IK-DCs) are a novel subset of DCs with cross-priming functions that has been recently described to express markers related to those of plasmacytoid DCs and NK cells. It has been suggested that this cell population

might function as a tumor scavenger by producing high amounts of IFN-γ and inducing TNF-related apoptosis-inducing ligand (TRAIL) dependent killing upon contact with tumor cells[69-71]. Like conventional dendritic cells, IK-DCs also have the capacity to present antigen after activation of Toll like receptor (TLR)-9 and may be involved in tumor antigen cross presentation to T cells[72, 73].

In order to test whether IK-DCs might play a role in controlling lung metastasis in the B16-F10 model with EBI-3 deficient mice, I analyzed IK-DCs in the local draining lymph nodes (DLN) as well as in the lungs of B6 wild-type and EBI-3 deficient mice. This was performed before, five, and ten days after intravenous injection of B16-F10 cells. IK-DCs are characterized by markers for plasmacytoid dendritic cells like B220 (CD45R) and the natural killer (NK) cell marker NK1.1 in addition to CD11c expression. FACS analysis of total lung cell suspensions revealed that the number of $CD11c^+B220^+NK1.1^+$ cells represents around 50% of lung $CD11c^+$ cells in both untreated and tumor bearing EBI-3 (-/-) mice (Figure 32 right graph). At day 5, but not at day 10, after melanoma cell injection, IK-DCs were found to be increased in the DLNs and lungs of EBI-3 deficient mice as presented in Figure 32. Therefore, IK-DCs represent the majority of the CD11c cells populating the lungs of EBI-3 (-/-) mice.

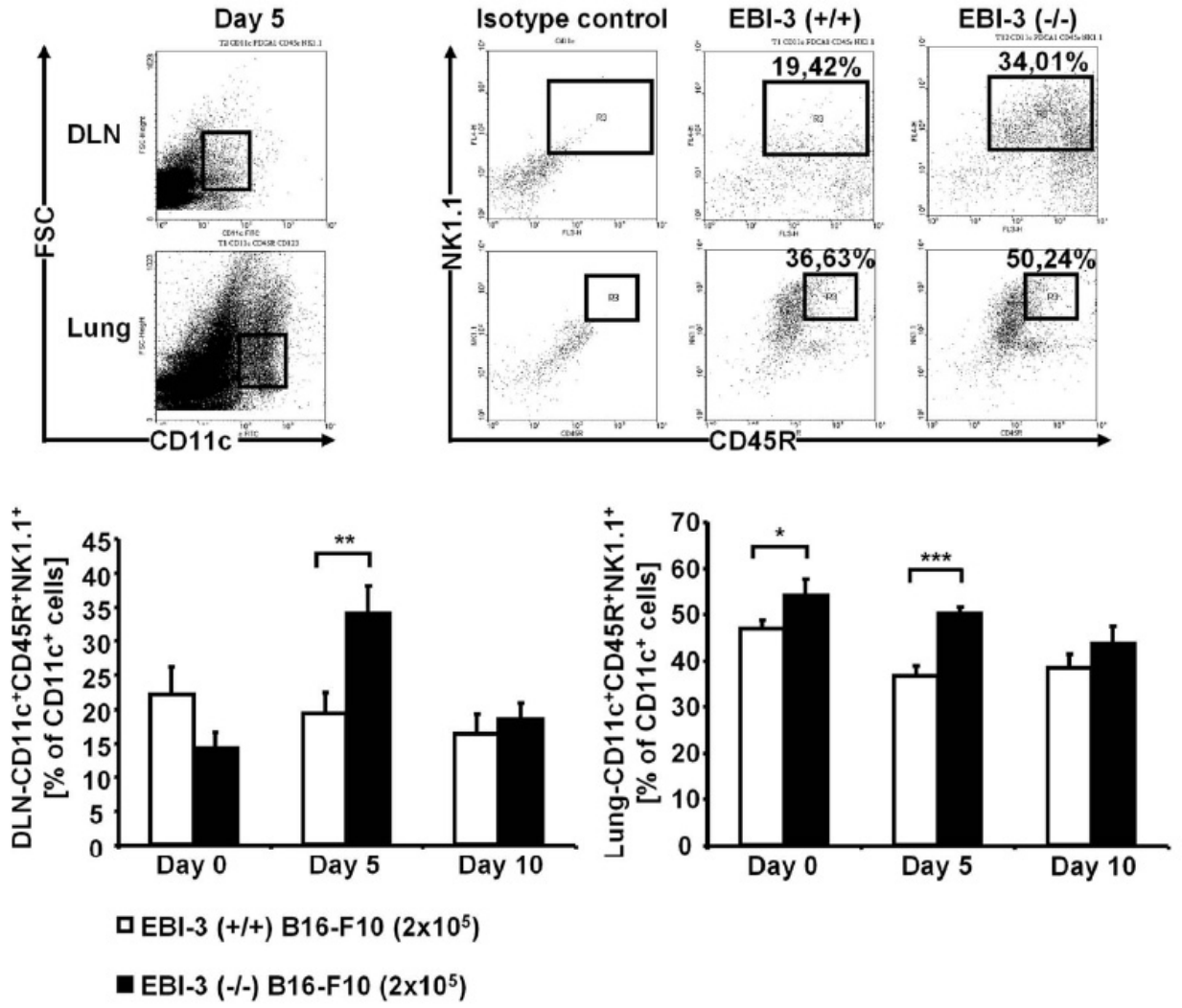

Figure 32: Increased number of IK-DCs in local draining lymph nodes and lungs of EBI-3 deficient mice. Cell suspension of thoracic DLN and lungs of EBI-3 (-/-) and B6 wild-type mice were immuno-stained for the indicated markers and analyzed by FACS. The IK-DC population defined as $CD11c^+CD45R^+NK1.1^+$ cells was upregulated in the lungs and draining lymph nodes of EBI-3 (-/-) mice 5 days after tumor cell injection.

Taieb et al. as well as Chan and colleagues closely investigated the phenotype of IK-DCs and described several additional cell surface molecules that are expressed on IK-DC although most of them to a lesser extent[69, 70]. I used isolated $CD11c^+$ lung cells for detection of Fas ligand (FasL) and the IL-2 receptor β-chain (CD122) on IK-DC by FACS analysis. Figure 33 illustrates that expression of FasL as well as CD122 on IK-DCs was slightly increased on EBI-3 deficient lung cells at day 5 after tumor cell injection compared to the expression of these markers on B6 wild-type cells. The

upregulated expression was detected at the same time point when the classical IK-DCs were increased in the EBI-3 deficient lungs.

Thus, the IK-DCs of the EBI-3 deficient mice exhibit all characteristics described for this cell population and its many astonishing functions.

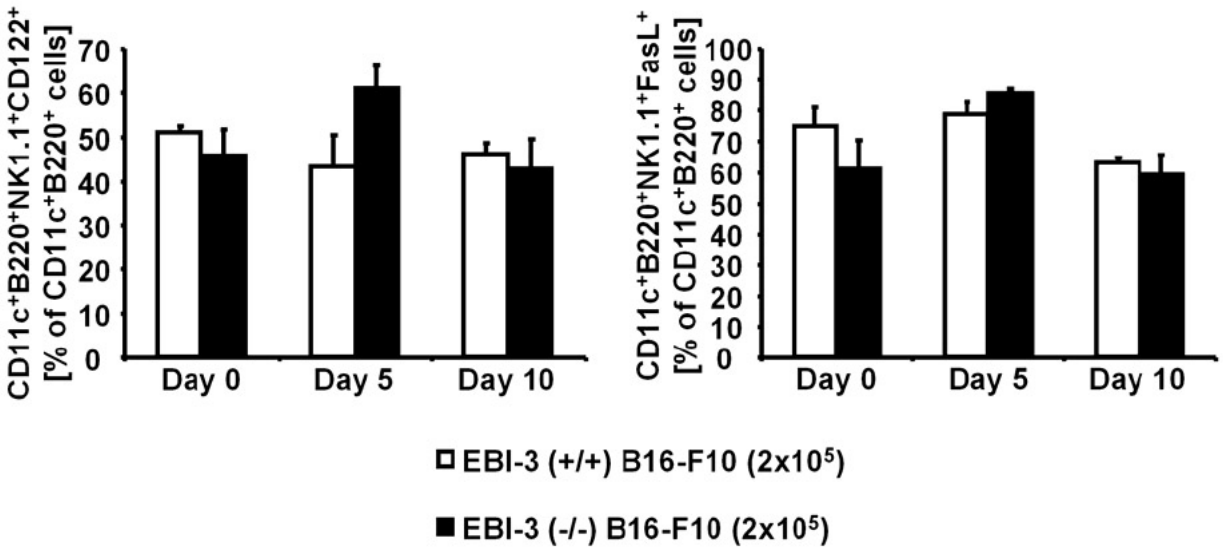

Figure 33: Expression of additional markers described for IK-DCs. Cell suspensions of lungs of EBI-3 (-/-) and B6 wild-type mice were purified for $CD11c^+$ cells by magnetic bead separation and immuno-stained for the indicated markers and analyzed by FACS. Expression of CD122 (left graph) and FasL (right graph) on IK-DC positive cells is slightly but not significantly upregulated 5 days after tumor cell injection.

IFN-γ is a cytokine whose production relates to Th1 immune responses against pathogens and tumors. IFN-γ production was initially associated with cells of lymphoid origin, particular natural killer cells and T cells[56, 74]. However, it is now clear that myeloid cells like dendritic cells and macrophages are also capable to produce this cytokine. Specifically, the novel subset of DCs, the above described IK-DCs, has been recently described to secrete IFN-γ as an initiating step of an anti-tumor response.

Relating to these published findings, I next analyzed IFN-γ production of isolated $CD11c^+$ cells. Naïve and B16-F10 injected lung $CD11c^+$ cells from B6 wild-type and EBI-3 deficient mice were used for 24h culture with LPS after overnight culture. An ELISA assay for IFN-γ demonstrated that the cells isolated from the lungs of tumor bearing EBI-3 deficient mice 5 days after the injection of B16-F10 melanoma cells released significantly higher amounts of IFN-γ compared to the $CD11c^+$ cells isolated

from the wild-type littermates (Figure 34, upper left graph). This observation is consistent with the enlarged amount of IK-DCs found in the lungs of EBI-3 deficient mice at the same time point after tumor cell injection when the IFN-γ production was upregulated. Likewise, the right graph in Figure 34 shows $CD11c^+$ splenocytes derived from EBI-3 deficient mice on day 3, after tumor cell injection, that released increased amounts of IFN-γ upon 24h challenge with LPS and CpG compared to the same cell population obtained from B6 wild-type littermates. This finding contributes to the high number of IK-DCs found in the lungs of B16-F10 induced melanoma bearing EBI-3 deficient mice. Although the isolated $CD11c^+$ lung cell populations showed a purity of over 90%, I tried to confirm this finding in vivo.

In the next step I used $CD11c^+$ lung cells purified from naïve and tumor bearing EBI-3 deficient and B6 wild-type mice for intracellular FACS analysis of IFN-γ production by IK-DCs. The isolated dendritic cells were stained with the cell surface markers CD45R and NK1.1 followed by intracellular staining for IFN-γ. The results of this FACS analysis are displayed in the lower graph of Figure 34 and confirm the discovery of the importance of the increased amount of IK-DC in the lungs of EBI-3 deficient mice injected with B16-F10 cells 5 days before. Even though the intracellular IFN-γ production was decreased in naïve EBI-3 deficient mice, the cytokine was produced to a significantly higher extent compared to the B6 wild-type mice 5 days after tumor cell injection, which is consistent with the increased number of IK-DCs in the EBI-3 deficient mice.

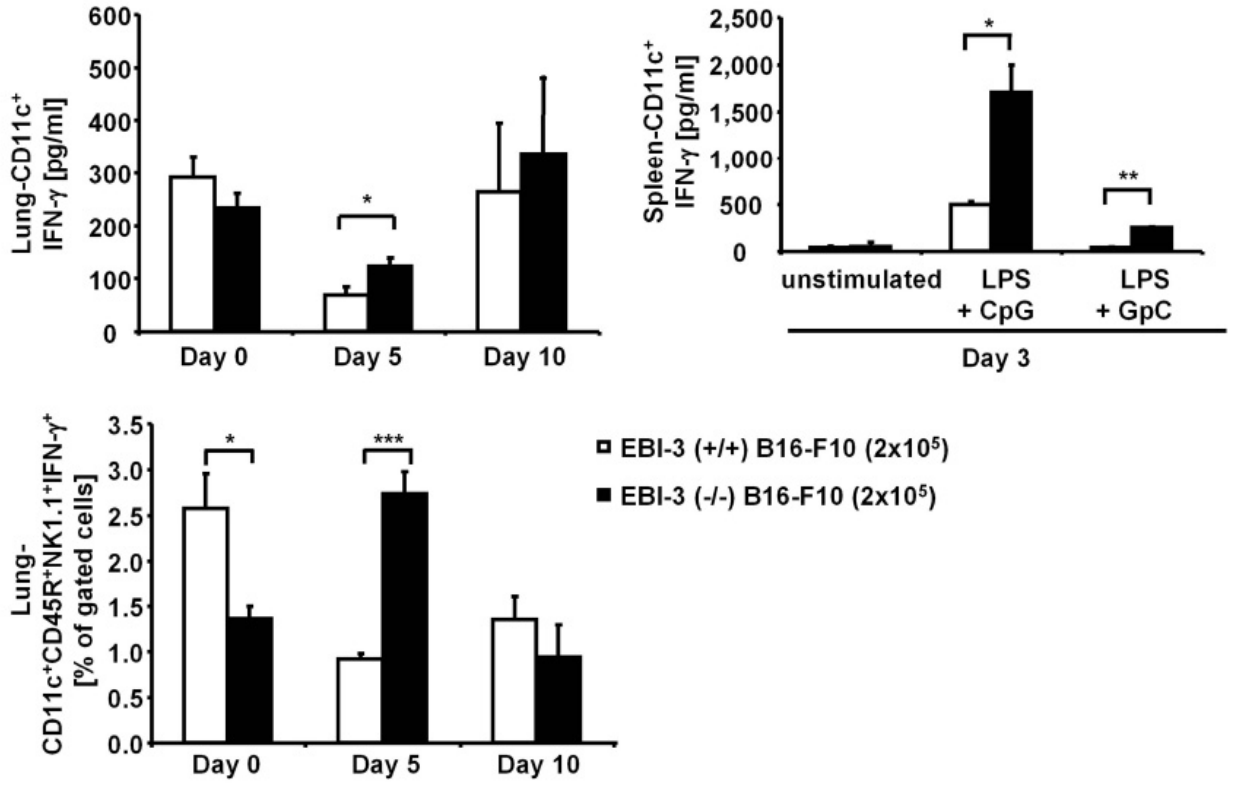

Figure 34: IFN-γ production of CD11c$^+$ cells and IK-DCs. Cell suspensions of lungs and spleens of EBI-3 (-/-) and B6 wild-type mice were purified for CD11c$^+$ cells by magnetic bead separation. (upper left graph) The CD11c$^+$ lung cells were cultured with LPS for 24h and supernatants were taken for cytokine analysis by ELISA. Supernatants of lung CD11c$^+$ cells from EBI-3 (-/-) mice released increased amounts of IFN-γ 5 days after tumor cell injection compared to supernatants from wild-type littermates. (right panel) CD11c$^+$ splenocytes derived from EBI-3 (-/-) mice that were injected with B16-F10 cells three days before released increased amounts of IFN-γ compared to those isolated from the wild-type littermates upon 24h LPS and CpG stimulation. (lower graph) CD11c$^+$ lung cells from EBI-3 (-/-) and wild-type mice were immuno-stained for intracellular FACS analysis. On day 5 after tumor cell injection EBI-3 (-/-) lung cells expressing the markers for IK-DCs produced higher amounts of IFN-γ compared to the wild-type littermates.

Natural killer cells were originally identified because of their capability to lyse tumor cells in vitro without previous immune sensitization. NK cells have attracted the attention of many scientists, and are a very well studied cell population with regard to their origin, receptor repertoire, differentiation and effector functions. NK cells represent a unique subset of lymphocytes that is able to bridge innate and adaptive immunity[75]. NKT cells define a subset of T cells that share some characteristics with NK cells and in

addition express a semi-invariant T cell receptor that is restricted to the binding of CD1d proteins[76].

In contrast to the IK-DC population, the NK and NKT cells, which are the two cell populations that in addition to IK-DCs express NK1.1 on their cell surface, are decreased in the lungs of EBI-3 deficient mice at any investigated time point. NK cells were characterized by expression of NK1.1 but not CD3ε while NKT cells co-express NK1.1 and the MHC class I-like molecule CD1d. Figure 35 shows the number of NK and NKT cells in EBI-3 deficient lungs compared to the expression of the same markers on B6 wild-type lung cells. The major defect in NK and NKT cells is consistent with the finding from Nieuwenhuis and suggests that these cell types are not having an impact on the increased cytokine production and ameliorated anti-tumor response detected in the EBI-3 deficient mice[56].

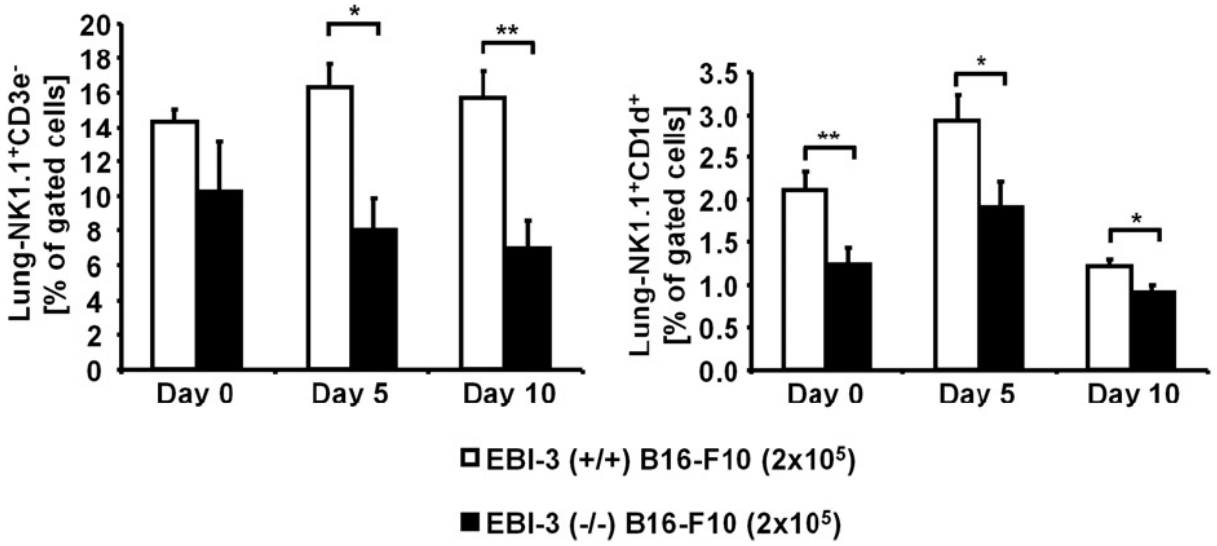

Figure 35: Decreased lung NK and NKT cells in melanoma bearing EBI-3 (-/-) mice. Cell suspensions of lungs of EBI-3 (-/-) and B6 wild-type mice were stained for the indicated markers and examined by FACS analysis. The $NK1.1^{+}CD3\varepsilon^{-}$ as well as the $NK1.1^{+}CD1d^{+}$ cell populations in the lungs of EBI-3 (-/-) mice were down-regulated at all indicated time points.

4.3.3 Conventional Dendritic Cells of B16-F10 melanoma bearing EBI-3 deficient mice

It is commonly believed that antigen trapping and presentation are primary tasks of DCs[66]. Recently, Heath et al. [77] proposed a cellular cascade of antigen recognition,

uptake, transport, and presentation involving at least two different DC subsets for the priming of $CD8^+$ T cells in peripheral lymph nodes. According to this model, $CD8\alpha^-$ DCs transport antigen into T cell areas of DLNs, where $CD8\alpha^+$ DCs are localized. The $CD8\alpha^+$DCs are known for their efficient uptake of apoptotic cells and are believed to present reprocessed antigen from $CD8\alpha^-$ DCs to $CD8^+$ T cells via crosspresentation[78, 79].

Since $CD8\alpha^+CD11c^+$ DCs seem to be the cell population that is able to present antigen to $CD8^+$ T cells in a way that enables the $CD8^+$ T cells to induce an effective immune response, I analyzed this subset of DCs in the lungs and local draining lymph nodes of B6 wild-type and EBI-3 deficient mice bearing melanoma. FACS analysis of total lung cell suspension revealed a significant increase in this DC subset in the lungs of EBI-3 deficient mice at day 10 after B16-F10 cell injection (Figure 36, lower panel of dot plots). Throughout tumor development the same cell population remained indifferent in the DLNs of B6 wild-type and EBI-3 deficient mice (Figure 36, left graph). This finding suggests that conventional DCs of EBI-3 deficient mice maturate and increase at a later time point of the disease when the pDCs and IK-DCs of these mice are no longer able to accomplish their T cell priming function.

Up to now I have evaluated three different subpopulations of dendritic cells in the lungs and DLNs of the EBI-3 deficient mice. All of these cell populations were found to be upregulated in the lungs of the gene-targeted mice at a certain time point of the disease. This leads to the hypothesis that the total number of $CD11c^+$ cells might be increased in the absence of EBI-3. Surprisingly, compared to the $CD11c^+$ cells of B6 wild-type mice the number of $CD11c^+$ cells in the EBI-3 deficient lungs was the same at all investigated time points. Thus, the increased number of certain DC populations during tumor development must be due to antigen recognition and following DC differentiation.

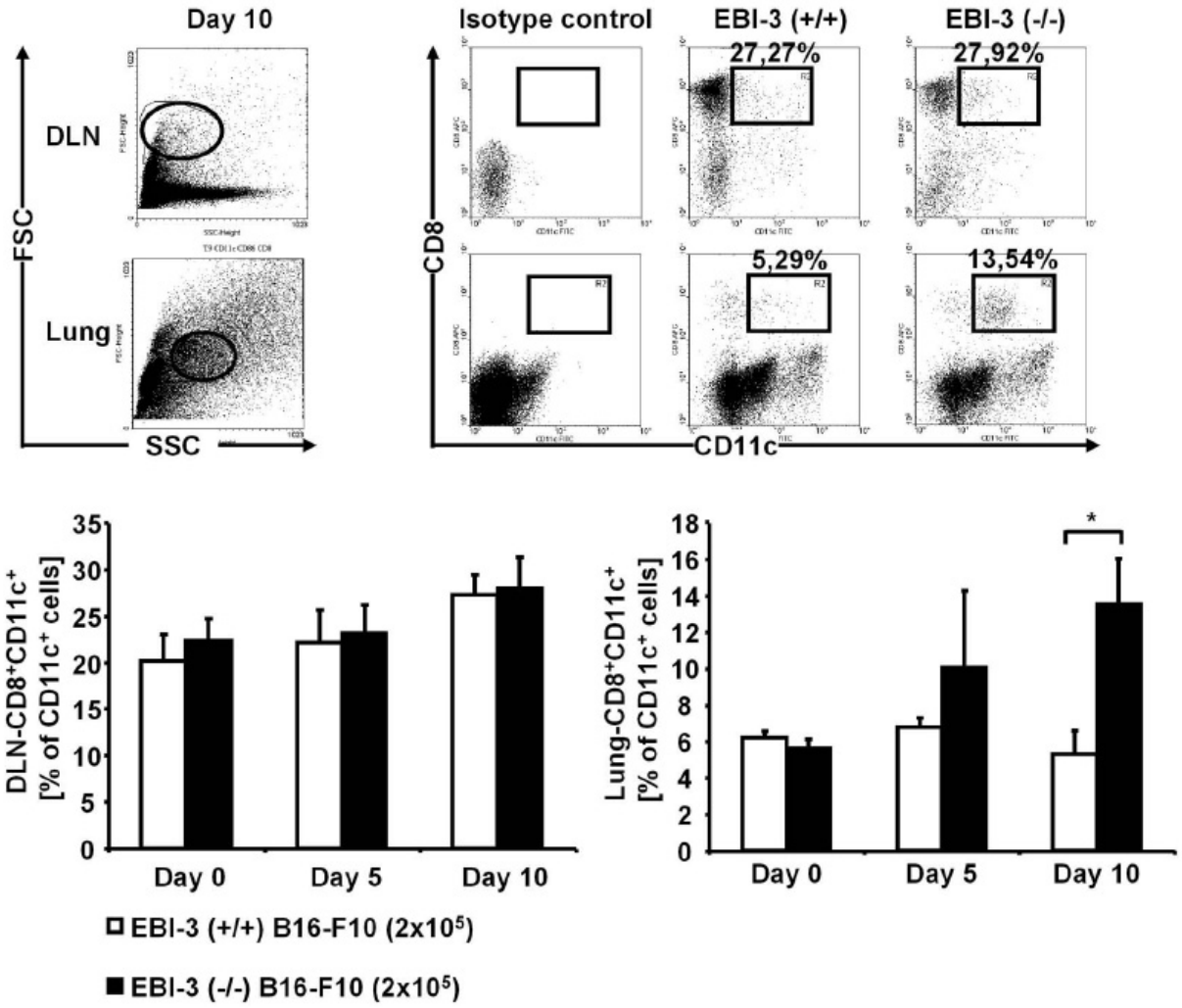

Figure 36: Increased lung conventional dendritic cells in melanoma bearing EBI-3 (-/-) mice at later stages of the disease. Cell suspensions of DLN and lungs of EBI-3 (-/-) and B6 wild-type mice were stained for the indicated markers and analyzed by FACS analysis. The $CD11c^+CD8^+$ population in the DLN did not show any differences between B6 wild-type and EBI-3 (-/-) mice (upper panel) but this cell population was increased in the lungs of EBI-3 (-/-) mice at day 10 after tumor cell injection.

Mature conventional DCs have to express MHC molecules as well as co-stimulatory molecules in order to be fully functional. MHC molecules are able to present processed antigen on the surface of the dendritic cells. $CD4^+$ T cell are able to recognize antigen presented by MHC class II molecules while $CD8^+$ T cells can bind to MHC class I molecules on dendritic cells. Both, $CD4^+$ and $CD8^+$ T cells need to be activated for an effective anti-tumor immune response.

I investigated markers of lung DC maturation by FACS analysis at different time points during the development of the B16-F10 induced lung melanoma. Figure 37

shows that compared to B6 wild-type mice $CD11c^+$ lung cells expressing CD8 and MHC class I molecule were found to be significantly increased in the lungs of EBI-3 deficient mice at day 10 after tumor cell injection.

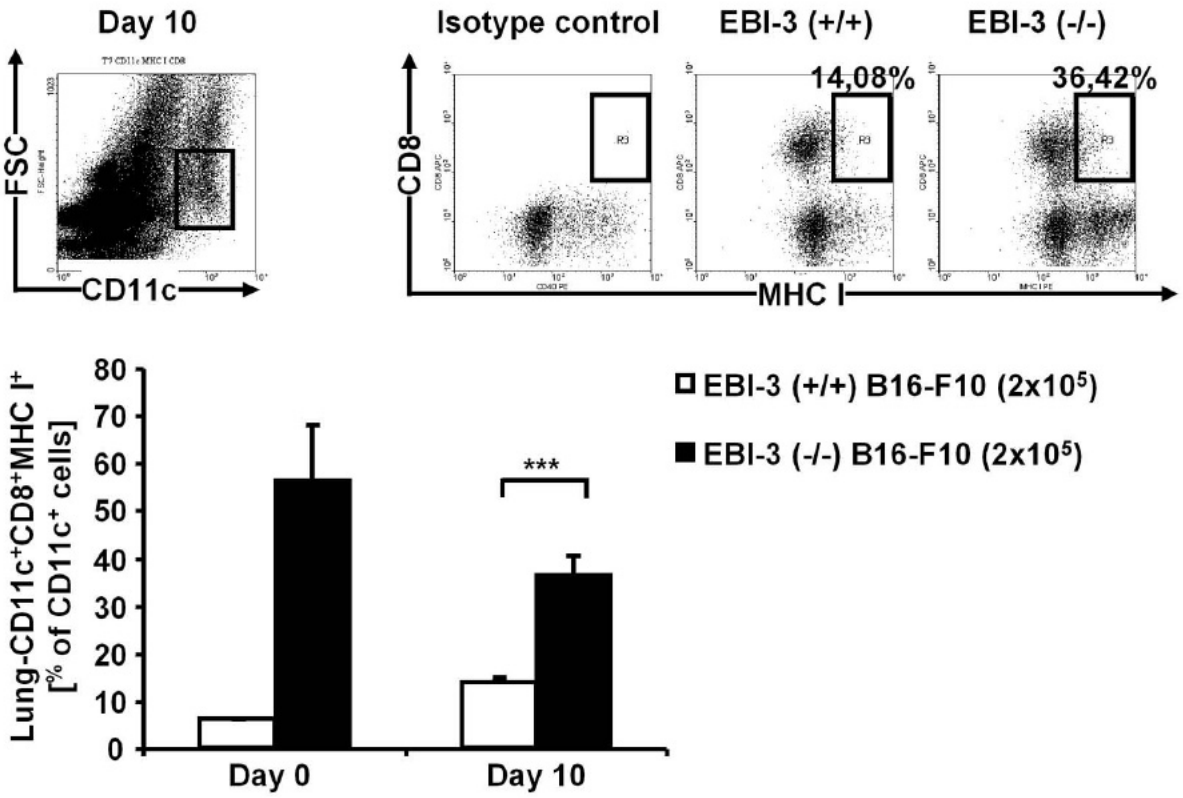

Figure 37: Expression of MHC class I molecule on CD11c+ lung cells. Cell suspensions of lungs of EBI-3 (-/-) and B6 wild-type mice were stained for the indicated markers and analyzed by FACS analysis. The expression of MHC class I molecules on $CD11c^+CD8^+$ cells was found to be elevated in EBI-3 deficient lungs.

In addition, the expression of MHC class II molecules was also measured on the same cell population in both types of naïve and tumor bearing mice. MHC class II molecules were found to be expressed at a significantly higher rate on $CD11c^+$ lung cells obtained from tumor bearing EBI-3 deficient mice compared to $CD11c^+$ cells from B6 wild-type littermates (Figure 38).

The outcome of the investigation concerning MHC molecules clearly indicates that conventional lung dendritic cells of EBI-3 deficient mice are more mature than this cell type of B6 wild-type mice.

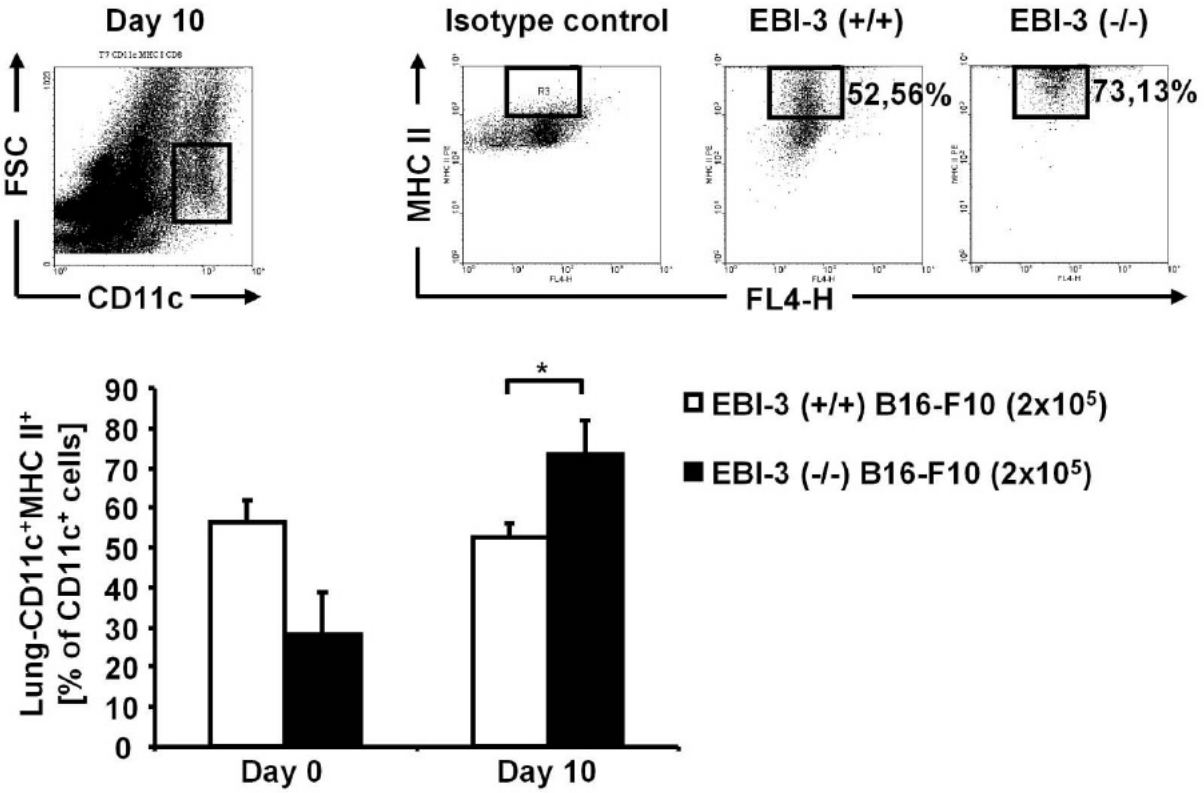

Figure 38: Expression of MHC class II molecule on CD11c$^+$ lung cells. Cell suspensions of lungs of EBI-3 (-/-) and B6 wild-type mice were stained for the indicated markers and analyzed by FACS analysis. Expression of MHC II molecules on CD11c$^+$ cells was found to be elevated in EBI-3 deficient lungs 10 days after tumor cell injection.

Antigen presentation is one major task of CD11c$^+$CD8$^+$ dendritic cells. But in order to really function and be able to bind to T cells, DCs have to express co-stimulatory molecules whose binding partners are found on T cells. The most important family of co-stimulatory molecules is the class of B7 molecules. Expression of B7-1 (CD80) and B7-2 (CD86) are important factors for the physical interaction of dendritic cells with T cells in the lymph nodes. In addition, all mature B cells, DCs and several other cell types, express CD40. This molecule binds to CD40 ligand on activated T cells and the interaction induces humoral immune responses as well as cell-mediated responses including the T cell dependent development of memory B cells[80].

FACS analysis of total lung cell suspensions from EBI-3 deficient and B6 wild-type mice shed light on the expression of the CD80 molecule on CD11c$^+$ lung cells revealing that the expression of CD80 was very high but did not differ when the two types of mice were compared (Figure 39).

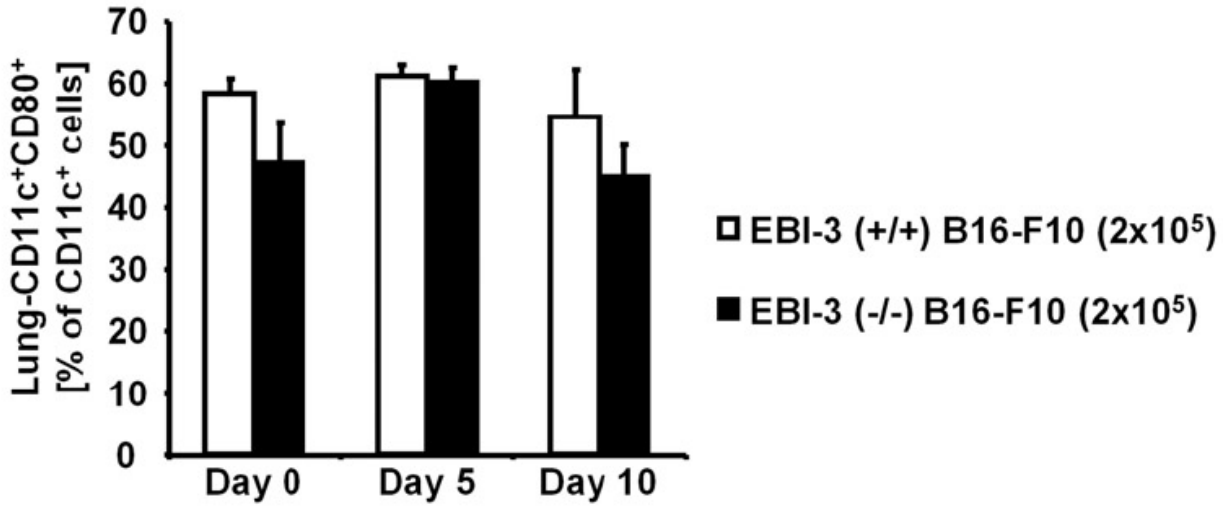

Figure 39: Expression of CD80 on CD11c$^+$ lung cells. Cell suspensions of lungs of EBI-3 (-/-) and B6 wild-type mice were stained for the indicated markers and analyzed by FACS analysis. Expression of the co-stimulatory molecule CD80 on CD11c$^+$ cells was measured by FACS and found to be equally expressed in EBI-3 deficient and B6 wild-type lungs before and after tumor cell injection.

In Figure 40 the further examination of the factors that contribute to an effective DC-T cell interaction are displayed. It was found that the expression of CD86 as well as CD40 on lung CD11c$^+$ cells did not alter during tumor development. In addition, the comparison between EBI-3 deficient and B6 wild-type mice concerning the expression of these molecules did not show any differences.

Taken together, the expression of co-stimulatory molecules on CD11c$^+$ lung cells is very high and therefore enabling these cells to interact with T cells. But neither the lack of EBI-3 nor the changes in the immune system during B16-F10 induce tumor development influence the expression of the co-stimulatory molecules in the lungs of the considered animals.

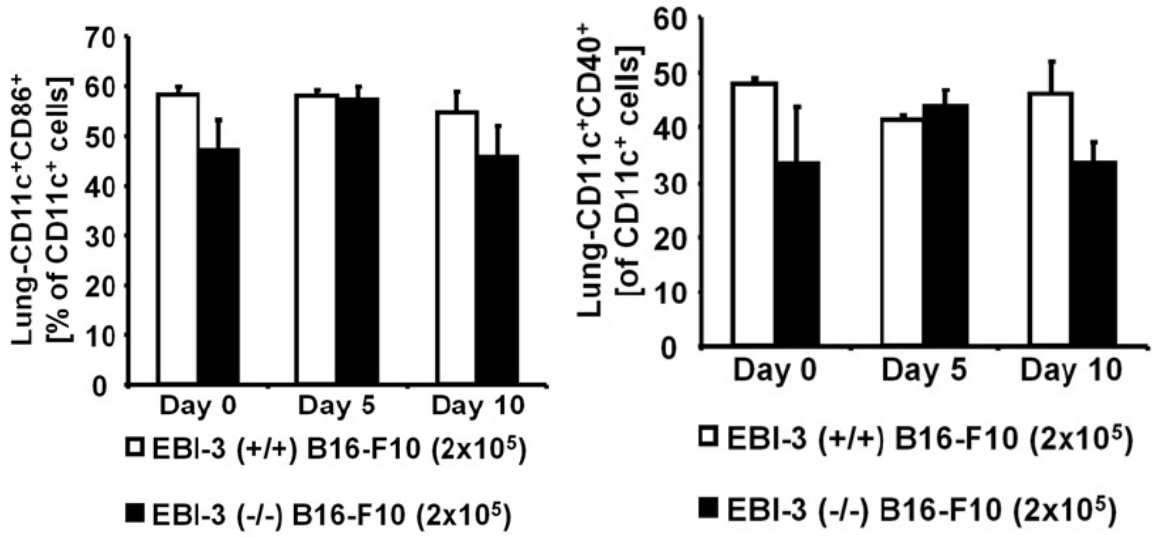

Figure 40: Expression of CD86 and CD40 on CD11c$^+$ lung cells. Cell suspensions of lungs of EBI-3 (-/-) and B6 wild-type mice were stained for the indicated markers and analyzed by FACS analysis. Expression of the co-stimulatory molecule CD86 (left graph) and CD40 (right graph) on CD11c$^+$ lung cells was found to be equally expressed in EBI-3 deficient and B6 wild-type lungs before and after tumor cell injection.

Many characteristics of conventional DCs have been described in the model of B16-F10 lung melanoma. In addition, mature DCs secrete large amounts of IL-12 to control the Th cell fate and this cytokine in combination with NK cells favors strong cytolytic activity against various tumor cells and immature DCs.

To complete the studies on DCs, I analyzed the secretion of the IL-12p70 and the IL-12p40 subunit. The BALF was obtained from naïve and tumor bearing EBI-3 deficient and B6 wild-type mice and the supernatants were taken for an IL-12p70 ELISA assay. The results are shown in the left graph of Figure 41 and present a significant boost of IL-12p70 secretion from the lungs of EBI-3 deficient mice compared to the B6 wild-type littermates at day 10 after tumor cell injection. The monomeric IL-12p40 subunit was measured in 24h supernatants of in vitro cultured CD11c$^+$ lung cells, which were obtained as usual. Like the IL-12p70 production, the secretion of IL-12p40 was found to be significantly increased from EBI-3 deficient CD11c$^+$ lung cells at day 10 after tumor cell injection (Figure 41, right graph).

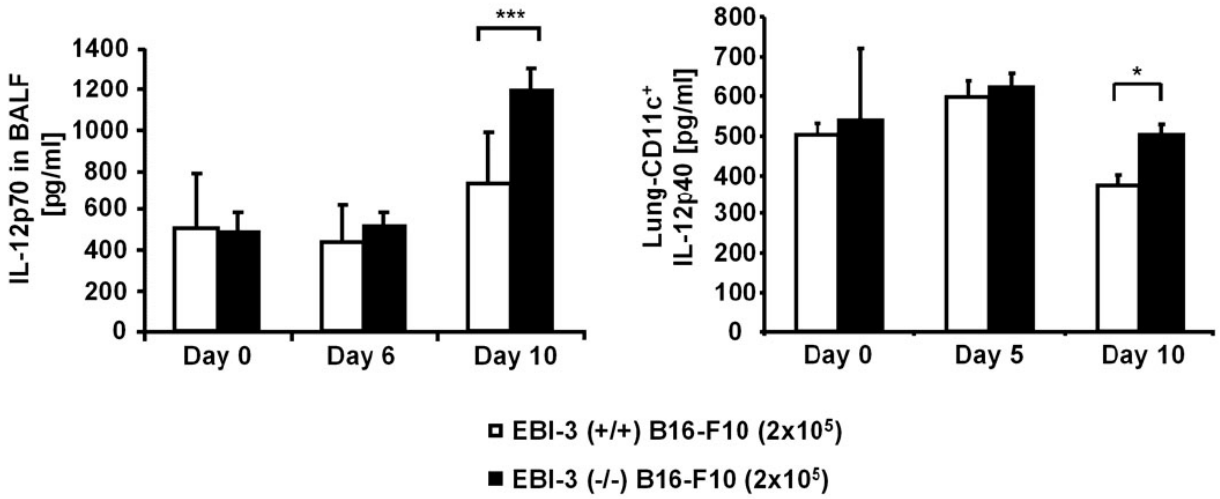

Figure 41: IL-12 production in BALF and in 24h supernatants of CD11c$^+$ cell culture. (left graph) IL-12p70 levels in the supernatants of the BALF was measured by ELISA and found to be elevated in EBI-3 (-/-) mice at day 10 after intravenous injection of B16-F10 cells. (right graph) Cell suspensions of lungs of EBI-3 (-/-) and B6 wild-type were purified for CD11c$^+$ cells by magnetic bead separation. The CD11c$^+$ lung cells were cultured with LPS for 24h and supernatants were taken for cytokine analysis by ELISA. 10 days after tumor cell injection IL-12p40 was elevated in the supernatants of CD11c$^+$ cells compared to cells from wild-type littermates.

4.3.4 Adoptive transfer of in vivo primed EBI-3 deficient CD11c$^+$ cells

Many clinical trials applying immunological substances as anti-tumor treatment have used the transfer of efficiently primed DCs as vaccine for the tumor-bearing patient. Several trials held promise considering the response of the patients. One major problem remains: the selection of the correct time point of treatment, the correct type of DC, the most efficient antigen and the best working antigen-priming method[27, 81].

The results on EBI-3 deficient DCs in the model of B16-F10 induced metastatic melanoma are very promising. The lack of EBI-3 seems to induce maturation of several types of DCs and in addition be able to present antigen in a more effective way than the wild-type DCs do. These findings led me to design a transfer experiment using CD11c$^+$ lung cells from EBI-3 deficient and B6 wild-type mice that were injected with 2x10^5 B16-F10 cells 5 days before CD11c cell isolation. 5x10^5 purified CD11c$^+$ lung cells were co-injected with 2x10^5 B16-F10 cells into naïve B6 wild-type recipient mice. A third group of B6 wild-type mice received 2x10^5 B16-F10 cells without additional treatment in order to function as controls. 14 days after the treatment with antigen primed CD11c$^+$ cells the

recipient mice were sacrificed and the development of melanotic lung metastases was monitored.

Figure 42 displays representative lungs of the transfer experiment, showing that the expected tumor protection of the B6 wild-type mice that received primed $CD11c^+$ cells from EBI-3 deficient lungs failed. A variety of reasons for the malfunction of the experiment are possible. The chosen time point for CD11c cell isolation might be surprising meaning that the $CD11c^+$ cells were not yet efficiently primed. Eventually, the number of transferred cells was too low or the EBI-3 deficient $CD11c^+$ cells do not have the capability to interact with wild-type T cells. Still, the fact that EBI-3 deficient mice are protected from B16-F10 induced lung metastases of melanoma remains. It is therefore necessary to keep investigating the differences between B6 wild-type and EBI-3 deficient lung cells to uncover the mechanism used by the EBI-3 deficient immune system.

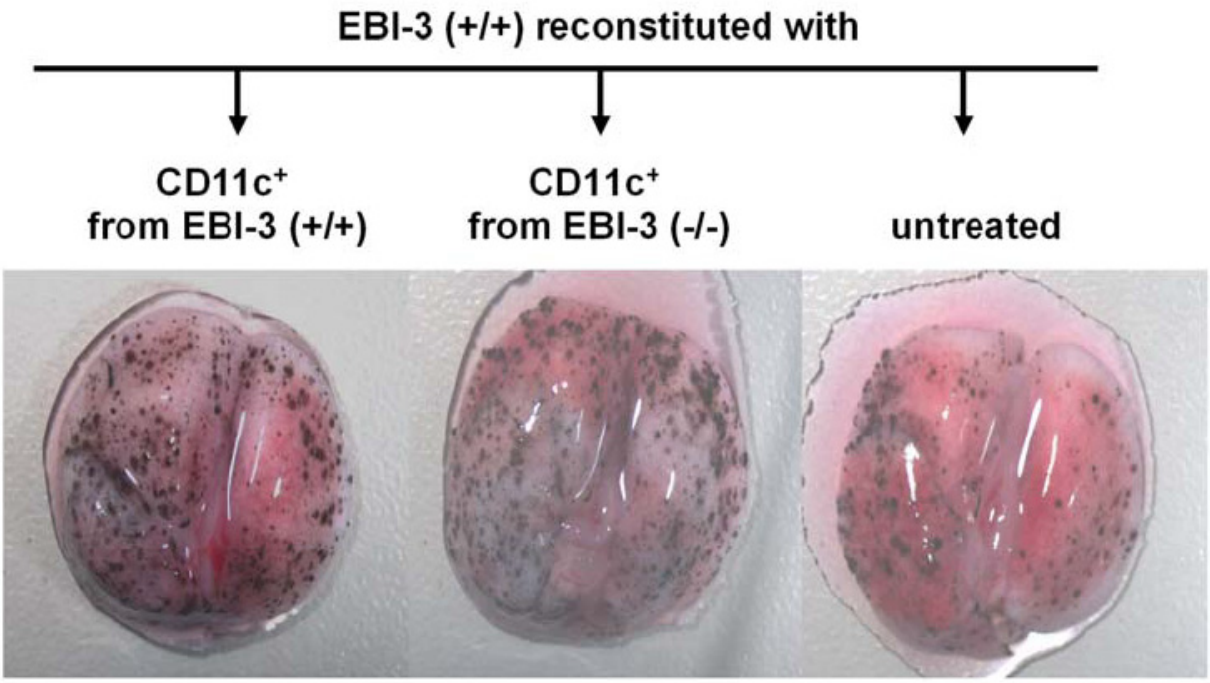

Figure 42: Adoptive transfer of in vivo primed $CD11c^+$ cells. $CD11c^+$ cells of EBI-3 deficient and B6 wild-type mice were in vivo primed by injection of $2x10^5$ B16-F10 cells. $5x10^5$ tumor antigen primed $CD11c^+$ lung cells of both EBI-3 (+/+) (left lung) and EBI-3 (-/-) (middle lung) mice were isolated by magnetic bead separation and together with $2x10^5$ B16-F10 cells intravenously transferred into B6 wild-type mice. Untreated tumor bearing control received $2x10^5$ B16-F10 cells (right lung).

4.4 Analysis of EBI-3 deficient T cells in the murine model of B16-F10 induced lung melanoma

T cells are of lymphoid origin and represent the major factor of the cell mediated anti-tumor immune response. It is therefore very likely that the reduced growth of melanotic colonies in the lungs of EBI-3 deficient mice is due to a mechanism induced by tumor-antigen primed T cells. As described in the introduction and was shown in many studies, the best anti-tumor effect was achieved when $CD4^+$ and $CD8^+$ T cells were simultaneously involved in the immune response[82].

4.4.1 Activation status of EBI-3 deficient T cells

T cells have to encounter the same antigenic structures as the APC that is going to present the processed antigen to the T cell. Thus, it is necessary that T cells are activated in order to become a primed T cell and fulfill their effector functions as T helper or cytotoxic T cell.

Consequently, I analyzed the activation status of $CD4^+$ as well as $CD8^+$ T cells in the EBI-3 deficient mice in the model of B16-F10 induced melanoma. The expression of the adhesion molecule CD44 was first described by Robert Dalchau in 1980 and is now known to be upregulated on antigen-activated T lymphocytes[83]. Total lung cell suspensions of naïve and B16-F10 cell injected B6 wild-type and EBI-3 deficient mice were immuno-stained for FACS analysis. Ten days after tumor cell injection the expression of CD44 on $CD4^+$ lung T cells was found to be significantly upregulated in the EBI-3 deficient mice compared to the B6 wild-type littermates. In the DLNs the same cell population was steadily expressed without showing differences between the EBI-3 deficient and the B6 wild-type mice. Results of both activated lung- and DLN cells are displayed in Figure 43.

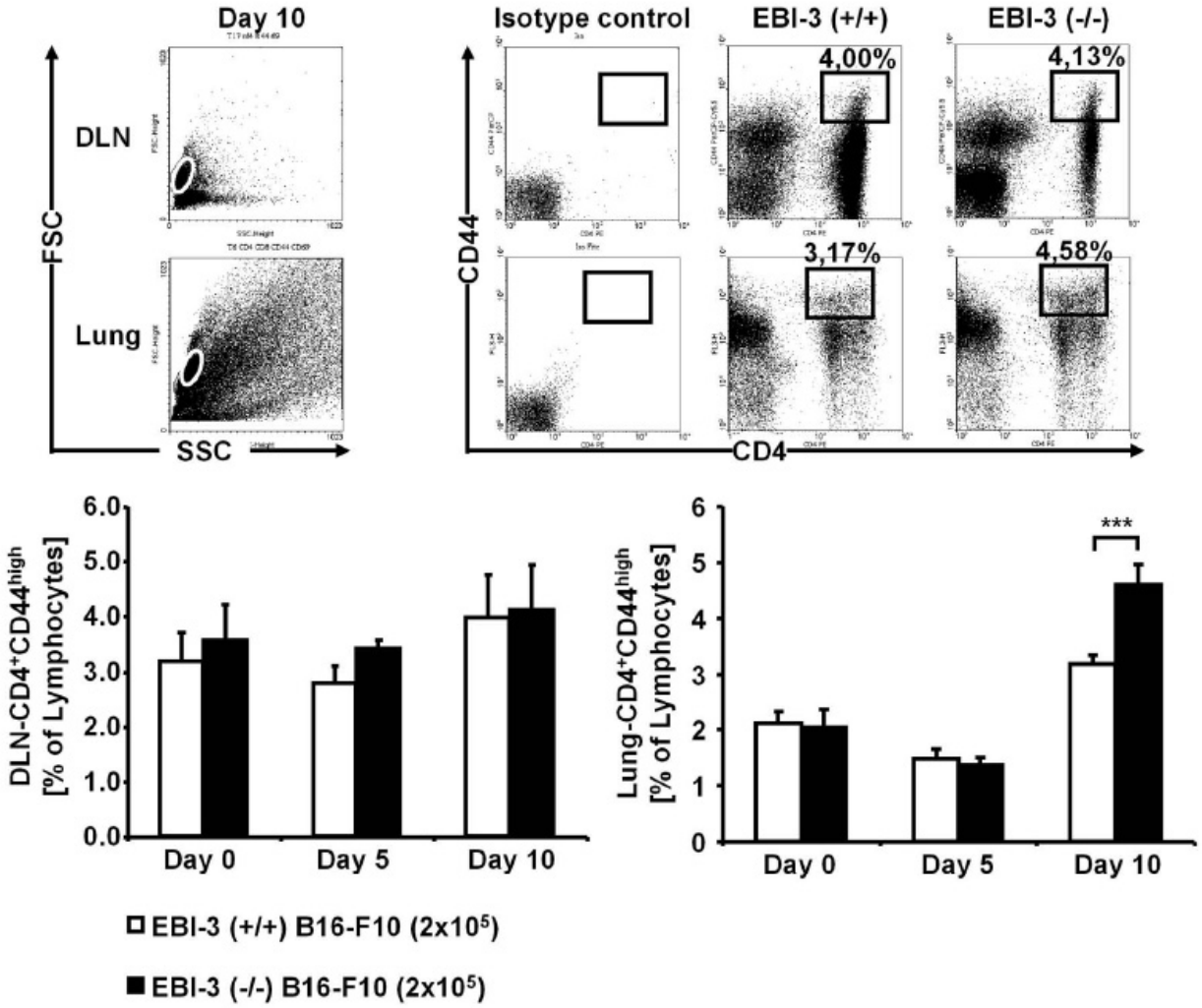

Figure 43: Expression of the activation marker CD44 on $CD4^+$ T cells in local draining lymph nodes and lungs of EBI-3 deficient mice. Cell suspensions of DLN and lungs of EBI-3 (-/-) and B6 wild-type mice were stained for the indicated markers and analyzed by FACS analysis. The $CD4^+CD44^{high}$ population in the DLN did not show any differences between B6 wild-type and EBI-3 (-/-) mice (upper panel) while the lung population was significantly increased in EBI-3 (-/-) mice on day 10 after tumor cell injection (lower panel).

CD69 is a membrane receptor expressed on lymphocytes. Its expression on these cells is restricted to the sites of active immune responses in vivo at a very early time point after activation of the cells[84]. This allows the use of CD69 as a T cell marker for early activation. When examining the co-expression of CD44 and CD69 on $CD4^+$ T cells of EBI-3 deficient and B6 wild-type lungs the results resembled the one obtained above. Figure 44 displays that before and five days after tumor cell injection

the expression of both activation molecules remained unchanged in the lungs and DLNs of EBI-3 deficient and B6 wild-type $CD4^+$ T cells. Surprisingly, at day 10 after B16-F10 injection, the population of the $CD4^+CD44^+CD69^+$ T cells was significantly decreased in the DLNs of the EBI-3 deficient mice, while at the same time point the number of activated $CD4^+$ T cells was found to be severely increased in the EBI-3 deficient lungs. This indicates a possible migration of activated T helper cell from the DLNs to the lung.

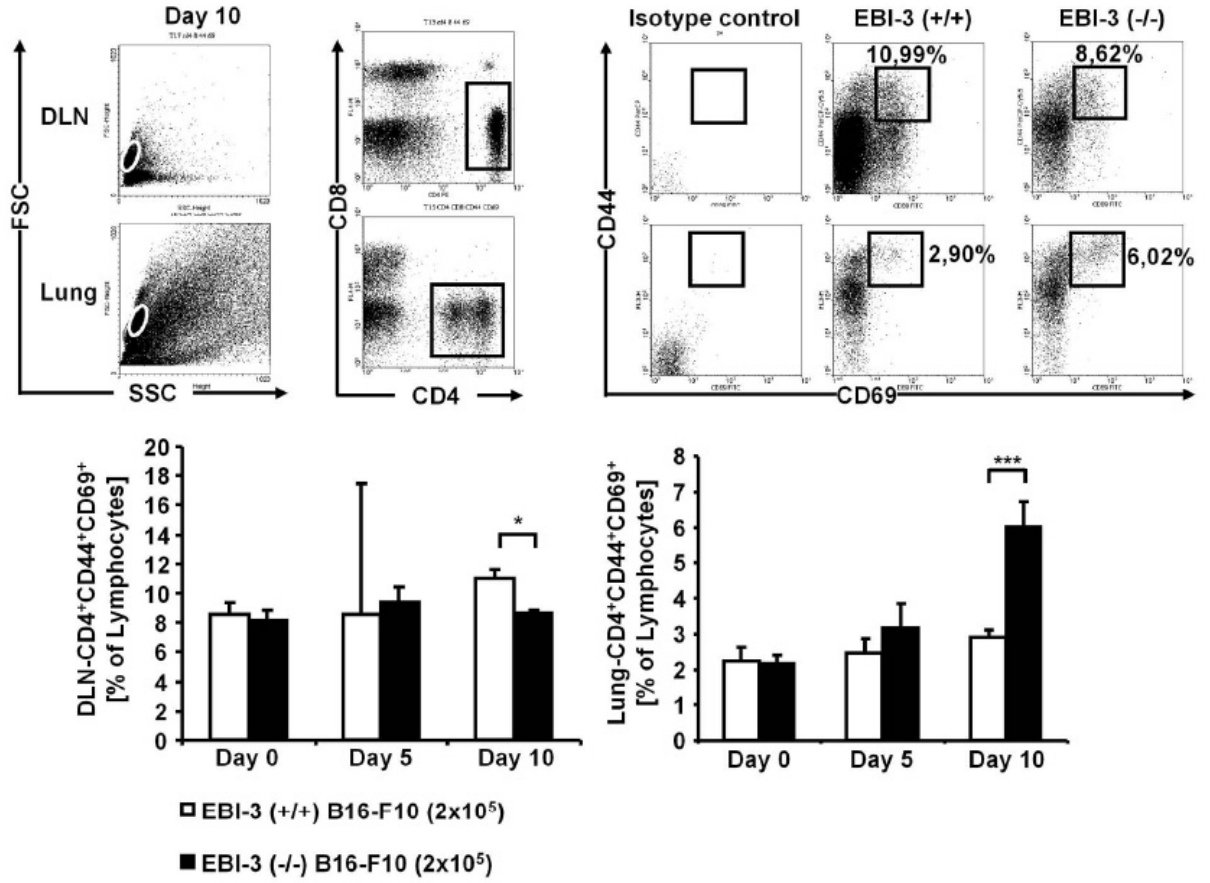

Figure 44: Expression of the CD69 molecule on activated $CD4^+$ T cells in local draining lymph nodes and lungs of EBI-3 deficient mice. Cell suspensions of DLN and lungs of EBI-3 (-/-) and B6 wild-type mice were stained for the indicated markers and analyzed by FACS analysis. The $CD4^+CD44^+CD69^+$ population was found to be decreased in the DLN of EBI-3 (-/-) mice 10 days after B16-F10 cell injection (upper panel) while that cell population was increased in EBI-3 (-/-) lungs at the same time point (lower panel).

The same markers were analyzed on $CD8^+$ T cells. Similar to the findings on $CD4^+$ T cells, the expression of the adhesion marker CD44 was increased in the lungs of EBI-3 deficient mice bearing melanoma at day 10. In contrast to the $CD4^+$ T cells, the

activated $CD8^+$ T cells were additionally increased in EBI-3 deficient DLNs at day 10 after tumor cell injection (Figure 45).

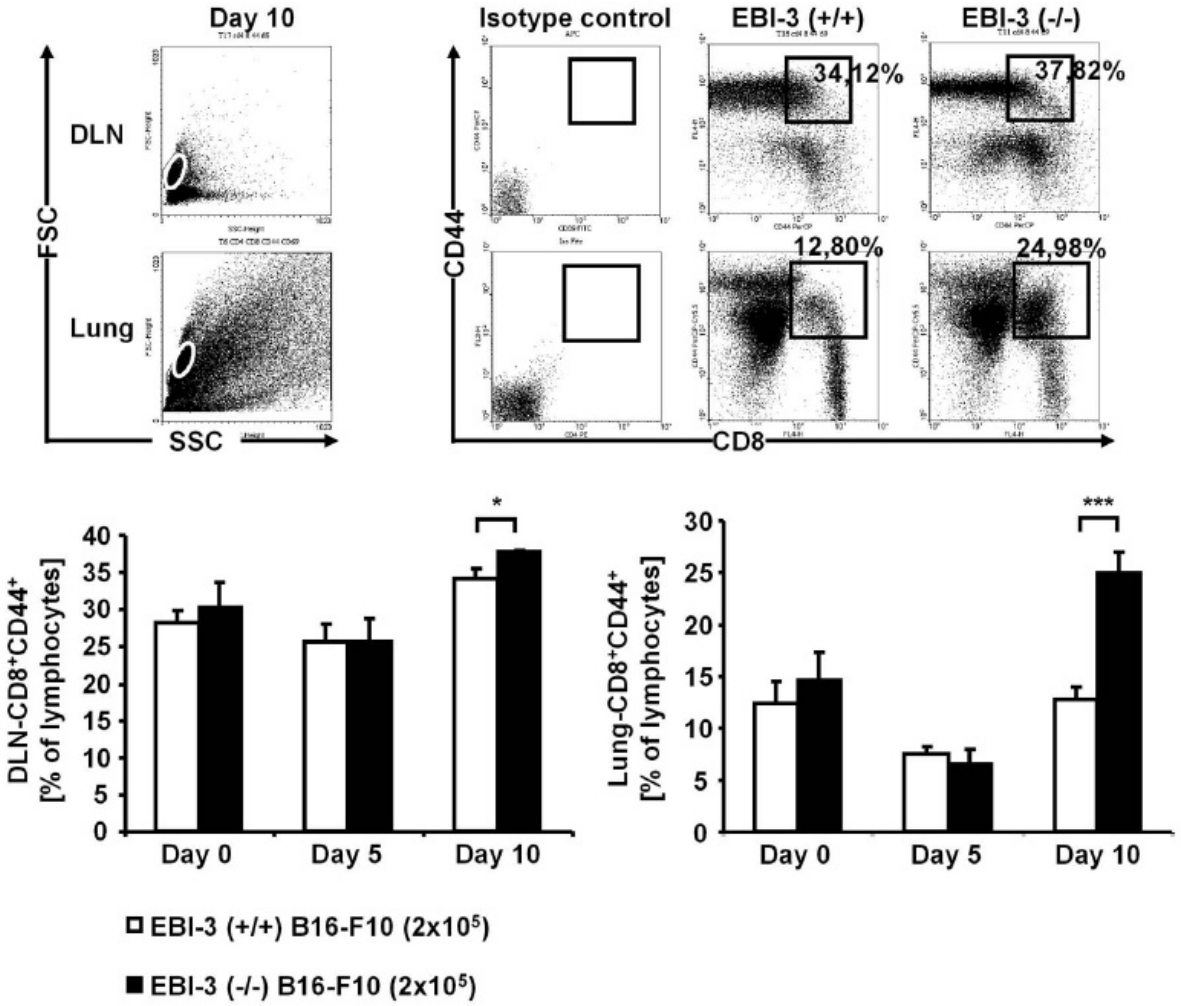

Figure 45: Expression of the activation marker CD44 on $CD8^+$ T cells in local draining lymph nodes and lungs of EBI-3 deficient mice. Cell suspensions of DLN and lungs of EBI-3 (-/-) and B6 wild-type mice were stained for the indicated markers and analyzed by FACS analysis. At day 10 after tumor cell injection the number of activated $CD8^+CD44^+$ T cells in DLN (upper panel) and lungs (lower panel) was increased in EBI-3 (-/-) mice.

4.4.2 Migration capacity of activated EBI-3 deficient T cells

Activated T cells circulate in the blood stream or the lymphoid system. In order to perform their specific function in the immune defense the T cells have to enter the infected tissue. The integrin $\alpha 4\beta 1$, which is also known as VLA-4 or CD49d, is one of

the adhesion molecules expressed on T cells that can bind to its partner VCAM-1 on endothelial cells. The interaction of both molecules starts the process that allows the emigration of T cells from the blood stream into tissue. Expression of CD49d on T cells is often upregulated upon antigen priming and cytokine secretion and is necessary for the T cell to reach its destination[85].

The migration capability of activated $CD4^+$ T ($CD4^+CD44^+CD49d^+$ cells) cells was found to be increased in the lungs of the EBI-3 deficient mice compared to their wild-type littermates at day 10 after B16-F10 melanoma cell injection (Figure 46). A similar phenomenon was observed in the activated $CD8^+$ T cells of the EBI-3 deficient lungs. The number of $CD8^+CD44^+CD49d^+$ T cells was significantly increased in the lungs of EBI-3 deficient mice starting from day 5 after tumor cell injection (Figure 47).

These results indicate that the EBI-3 deficient lung T cells are more capable of entering the lung tissue via CD49d interaction than the T cells from B6 wild-type mice. However, the total number of $CD4^+$ T cells as well as $CD8^+$ T cells was found to be the same in the lungs of EBI-3 deficient and B6 wild-type tumor bearing lungs. Only the number of activated cells increases during tumor development.

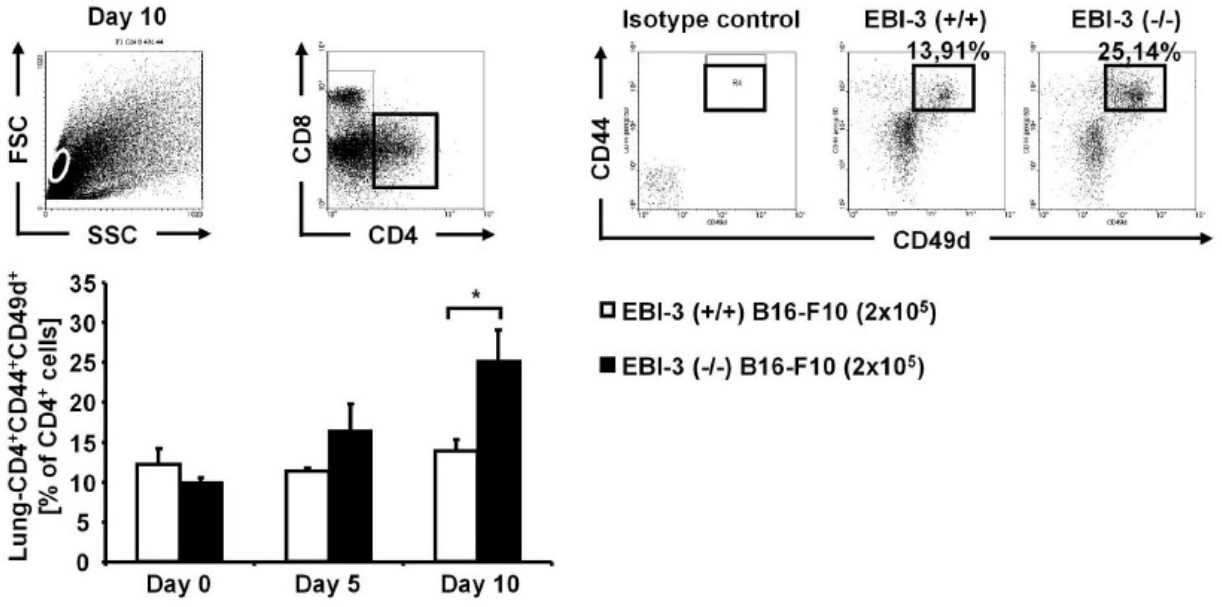

Figure 46: Expression of the migration marker VLA-4 on activated $CD4^+$ lung T cells of EBI-3 deficient mice. Cell suspensions of lungs of EBI-3 (-/-) and B6 wild-type mice were stained for the indicated markers and analyzed by FACS analysis. VLA-4 (CD49d) was found to be significantly increased on activated EBI-3 (-/-) $CD4^+$ T cells 10 days after B16-F10 cell injection.

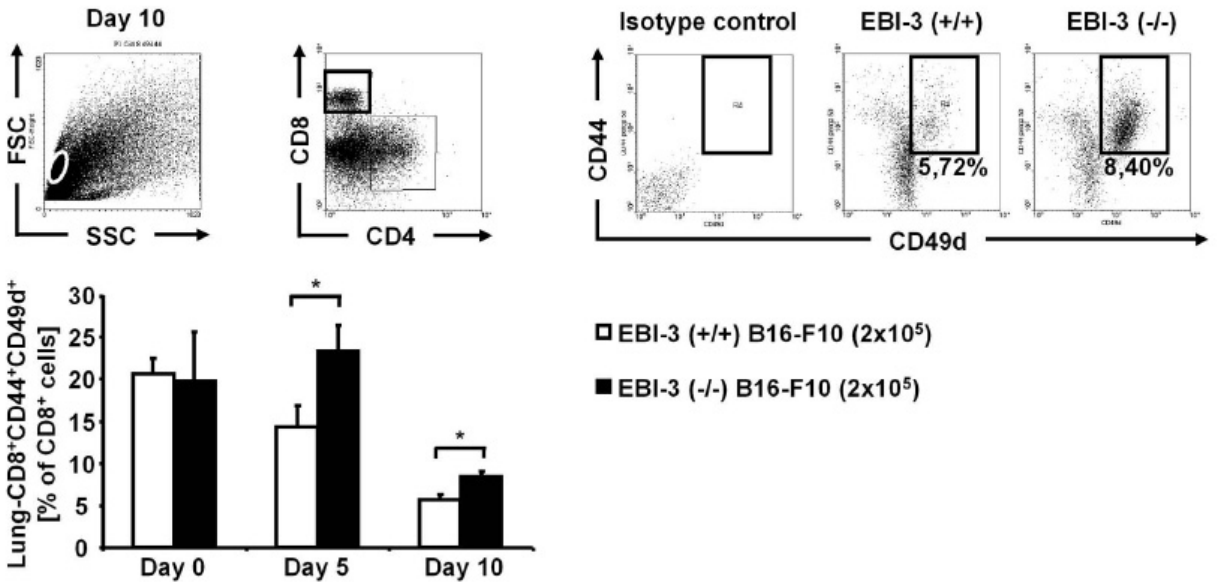

Figure 47: Expression of the migration marker VLA-4 on activated CD8$^+$ lung T cells of EBI-3 deficient mice. Cell suspensions of DLN and lungs of EBI-3 (-/-) and B6 wild-type mice were stained for the indicated markers and analyzed by FACS analysis. After B16-F10 cell injection VLA-4 (CD49d) was found to be significantly increased on activated EBI-3 (-/-) CD8$^+$ T cells compared to the VLA-4 expression on the same cell population in wild-type littermates.

4.4.3 VCAM-1 on EBI-3 deficient lung endothelial cells

VCAM-1 belongs to the family of CAMs that is involved in cell migration through endothelial barriers. The molecule is expressed on endothelial cells and becomes upregulated by inflammatory cytokine production in order to allow anti-inflammatory immune cells to migrate through the endothelium. In addition, many tumors are capable of increasing the VCAM-1 expression on endothelial cells for their own purpose, namely metastasizing to the organ[85]. Cells that want to enter tissue have to interact with VCAM-1. The binding partner CD49d, that is also called VLA-4, was found to be highly expressed on activated EBI-3 deficient lung CD4$^+$ and CD8$^+$ T cells. There is great interest to learn about the expression of VCAM-1 on lung endothelial cells in the model of B16-F10 induced metastatic melanoma.

FACS analysis with total lung cell suspensions of naïve and tumor bearing EBI-3 deficient and B6 wild-type mice unexpectedly displayed a decrease of VCAM-1 (CD106) on EBI-3 deficient endothelial cells which where characterized by the CD31 molecule

(Figure 48). The negative regulation of EBI-3 deficient VCAM-1 expression was greatest on day 5 after tumor cell injection.

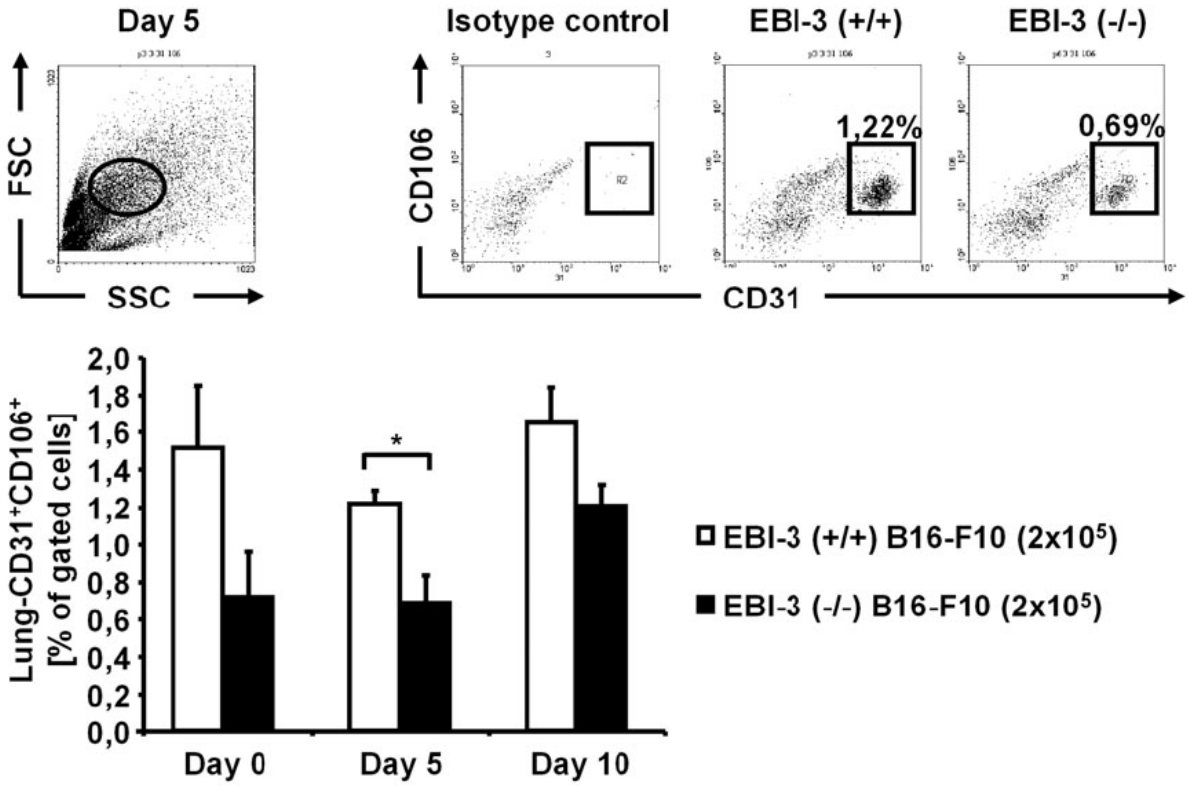

Figure 48: VCAM-1 expression on endothelial lung cells of EBI-3 deficient mice. Cell suspensions of lungs of EBI-3 (-/-) and B6 wild-type mice were stained for the indicated markers and examined by FACS analysis. Hereby, endothelial cells were characterized by the expression of the CD31 molecule on their cell surface. On all indicated time points the number VCAM-1 (CD106) expressing endothelial cells was decreased in EBI-3 (-/-) mice although the difference to the wild-type mice was significant only for day 5 after tumor cell injection.

Further investigation for the expression of VCAM-1 was performed by an ELISA specific for murine VCAM-1. Total lung cell suspensions of naïve and tumor cell injected EBI-3 deficient and B6 wild-type mice were cultured for 24h with mouse anti-CD3 antibody and anti-CD28 antibody. The supernatants of this culture were used for the above described assay. Similar to the results obtained by FACS analysis, the ELISA demonstrated a significant down-regulation in VCAM-1 production in total lung cells from EBI-3 deficient mice with increasing differences during melanoma development if compared to the B6 wild-type littermates (Figure 49).

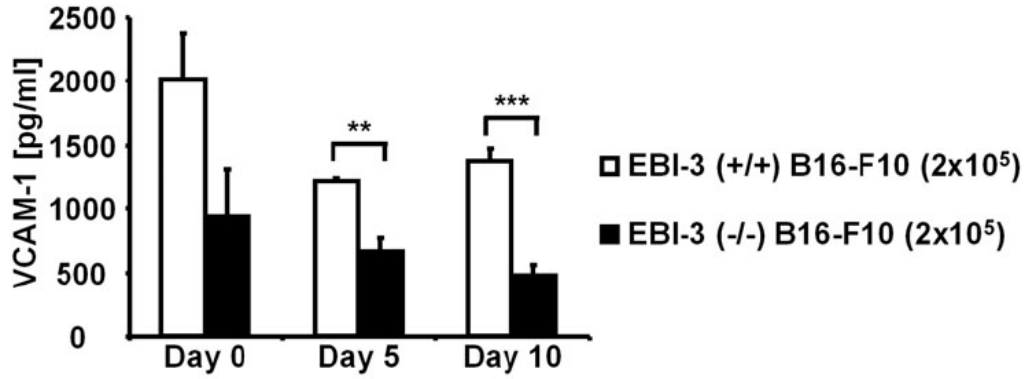

Figure 49: VCAM-1 production from supernatants of 24h culture of total lung cells. Cell suspensions of lungs of EBI-3 (-/-) and B6 wild-type mice were cultured with anti-CD3 and anti-CD28 antibody for 24h. The supernatants were taken for cytokine analysis by ELISA. On all indicated time points VCAM-1 was elevated in the supernatants of total lung cells compared to cells from wild-type littermates.

Since the total lung cells used in the experiment were cultured with T cell stimulating adjuvants, the question occurred whether the VCAM-1 secretion was influenced by the in vitro conditions. To complete the studies on VCAM-1 secretion in the lung, I designed an experiment in which the BALF was taken from healthy and B16-F10 melanoma bearing mice. Afterwards, the lungs were removed for lung cell isolation. The total lung cell suspensions were now cultured with LPS for 24h and the supernatants from this culture, as well as from the BALF, were used in the ELISA. Amazingly, the outcome was quite different from the two previous experiments. Although I found a small decrease of VCAM-1 secretion in naïve EBI-3 deficient mice as well as in the same mice that were intravenously injected with B16-F10 5 days before, the picture changed on day 10 after tumor cell injection. At that time point in both the BALF and the LPS-stimulated cell culture, the VCAM-1 secretion was increased in EBI-3 deficient mice compared to the B6 wild-type littermates, as demonstrated in Figure 50.

Taken together, the results of VCAM-1 studies are confusing. However, since the FACS measurement was performed immediately following cell isolation without additional treatment it resembles an in vivo situation. In addition, the down-regulation of VCAM-1 has already been published for EBI-3 deficient mice in an inflammatory model of allergic asthma[65].

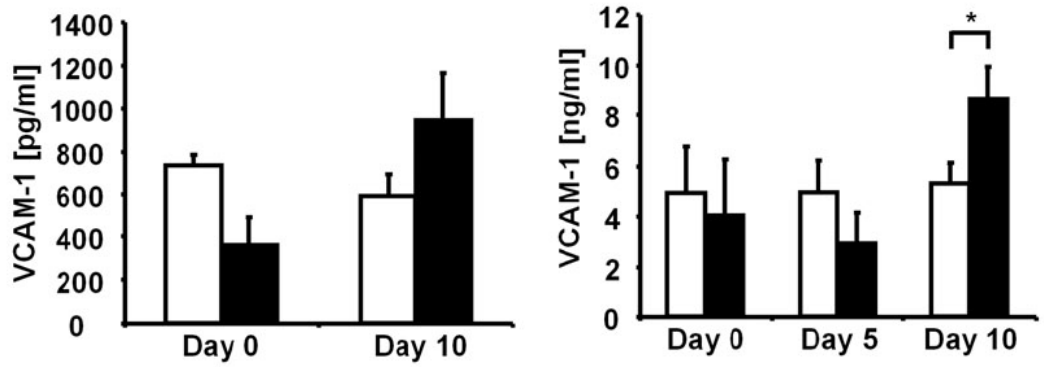

Figure 50: VCAM-1 production from supernatants of 24h culture of total lung cells and from BALF. (left graph) Cell suspensions of lungs of EBI-3 (-/-) and B6 wild-type mice were cultured with LPS for 24h and supernatants were taken for cytokine analysis by ELISA. 10 days after tumor cell injection VCAM-1 was elevated in the supernatants of the total lung cells compared to cells from wild-type littermates while in the supernatants of untreated mice the amount of VCAM-1 was decreased in EBI-3 (-/-) cells. (right graph) The BALF was taken from EBI-3 deficient and B6 wild-type mice and the supernatants of the BALF were taken for cytokine analysis by ELISA. Secretion of VCAM-1 was found to be slightly down-regulated in EBI-3 (-/-) mice compared to their wild-type littermates at day 0 and 5 after tumor cell injection. In contrast, 10 days after tumor cell injection the amount of VCAM-1 in EBI-3 deficient lung cells was increased compared to the VCAM-1 detected in B6 wild-type lung cells.

4.4.4 Analysis of EBI-3 deficient T regulatory cells in the murine model of B16-F10 induced lung melanoma

The positive and negative selection in the thymus is not able to eliminate all naïve self reactive T cells. Therefore the immune system provides several additional mechanisms that inhibit autoimmune reactions in the host. T regulatory cells have long been described as one major sentinel in the eradication of upcoming autoimmune reactions. This cell type has the capability to negatively regulate T cell differentiation and proliferation. Upon stimulation with TGF-β naïve $CD4^+$ T cells are induced to differentiate into T regulatory cells that express CD25 on their cell surface in addition to CD4 and produce Forkhead box protein 3 (Foxp3) intracellularly[86, 87].

One problem in initiating an appropriate anti-tumor immune response is the fact that tumor tissue is a mutated product of self-tissue and therefore very likely to cause an autoimmune response by increasing the population of T regulatory cells. In most clinical trials an effective anti-tumor response almost always correlates with an increase of autoimmunity[81]. For that reason, the examination of changes in the population of T

regulatory cells in the model of B16-F10 induced metastatic melanoma, are of great interest.

A first overview of the situation was gained by FACS analysis of total lung cell suspensions from EBI-3 deficient and B6 wild-type mice at various time points during tumor development. The staining with anti-CD4 and anti-CD25 antibodies revealed that the T regulatory cell population was relatively small and remained at a constant level during tumor development. Figure 51 also shows that there are no differences between EBI-3 deficient and B6 wild-type mice except for day 10.

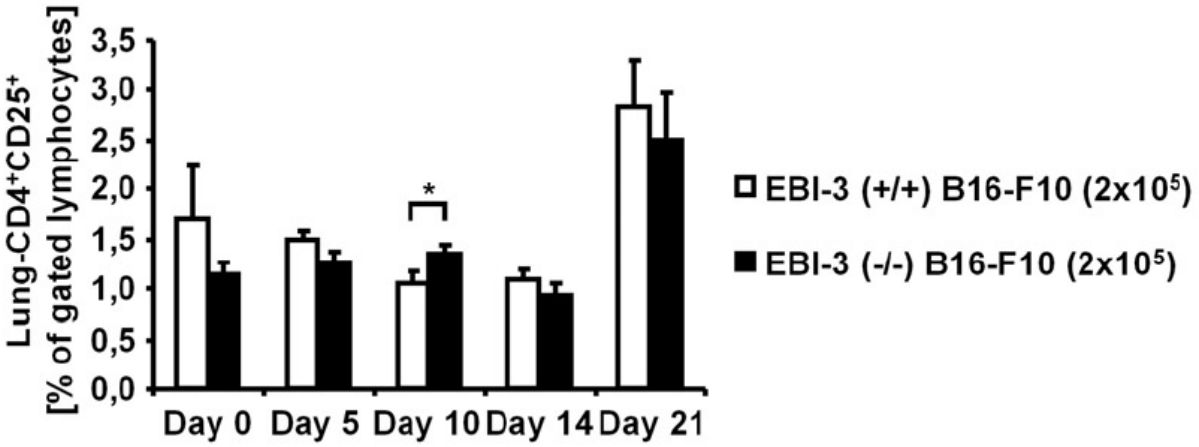

Figure 51: Expression of the IL-2 receptor α-chain (CD25) on $CD4^+$ lung T cells from EBI-3 deficient mice. Cell suspensions of lungs of EBI-3 (-/-) and B6 wild-type mice were stained for the indicated markers and analyzed by FACS analysis. At day 10 after tumor cell injection the number of activated $CD4^+CD25^+$ T cells in the lungs was increased in EBI-3 (-/-) mice while at all other indicated time points the CD25 molecule was equally expressed on the $CD4^+$ lung T cells of both types of mice.

Furthermore, the additional staining for intracellular expression of Foxp3 confirmed the small but constant number of T regulatory cells that is displayed in Figure 52. These results suggest that T regulatory cells do not have an impact on the tumor development in EBI-3 deficient and B6 wild-type mice in the model of metastatic lung melanoma.

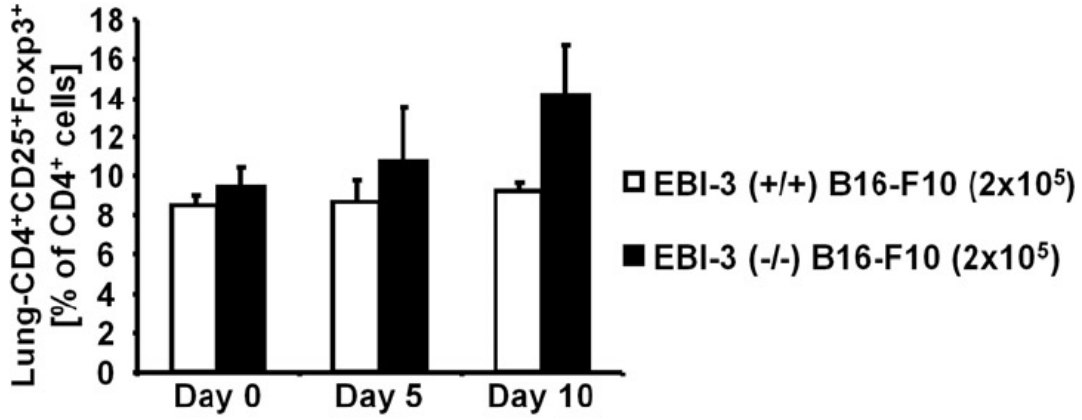

Figure 52: Expression of the IL-2 receptor α-chain (CD25) and Foxp3 on $CD4^+$ lung T cells from EBI-3 deficient mice. Cell suspensions of lungs of EBI-3 (-/-) and B6 wild-type mice were stained for the indicated markers and examined by intracellular FACS analysis. The marker for T regulatory cells ($CD4^+CD25^+Foxp3^+$) remained equally expressed in both types of mice at all indicated time points.

The T regulatory cell-inducing factor is the secretion of TFG-β in the presence of naïve $CD4^+$ T cells. The existence of this cytokine was measured in the BALF obtained from mice in my model of B16-F10 induced melanoma. An ELISA gave evidence for the constant levels of T regulatory cells since the secretion of TGF-β was found to be low and steady in all investigated groups of mice (Figure 53).

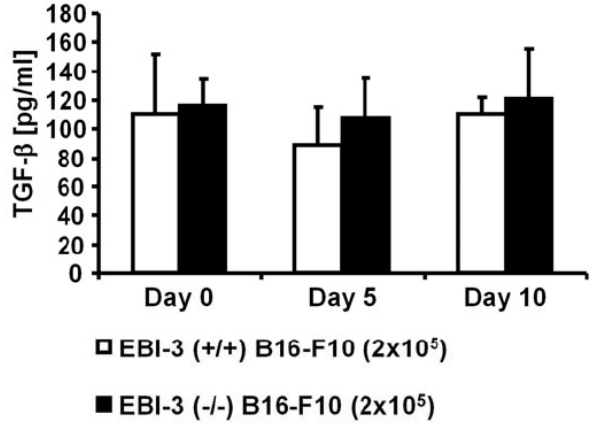

Figure 53: TGF-β secretion in the supernatants of BALF from EBI-3 deficient mice. The BALF was taken from EBI-3 deficient and B6 wild-type mice and the supernatants of the BALF were taken for cytokine analysis by ELISA. TGF-β was found to be equally expressed in the BALF of EBI-3 (-/-) and B6 wild-type mice before and after tumor cell injection.

IL-10 is a multifunctional cytokine that is able to suppress inflammatory responses as well as the activation and effector function of T cells. Many cell populations secrete this cytokine, among them myeloid DCs[88].

IL-10 secretion was determined in supernatants of isolated lung $CD11c^+$ cells after 24h culture with LPS. The cytokine was found to be slightly decreased in all groups of EBI-3 deficient mice compared to the B6 wild-type littermates. At day 5 after tumor cell injection, the differences in IL-10 production were considered significant.

Other publications report an increase of IL-10 secretion from this cell type of EBI-3 deficient mice compared to B6 wild-type littermates although the stimulating conditions were different. Hausding et al. demonstrated that after allergen challenge the IL-10 production in EBI-3 deficient lung $CD11c^+$ cells is increased[65].

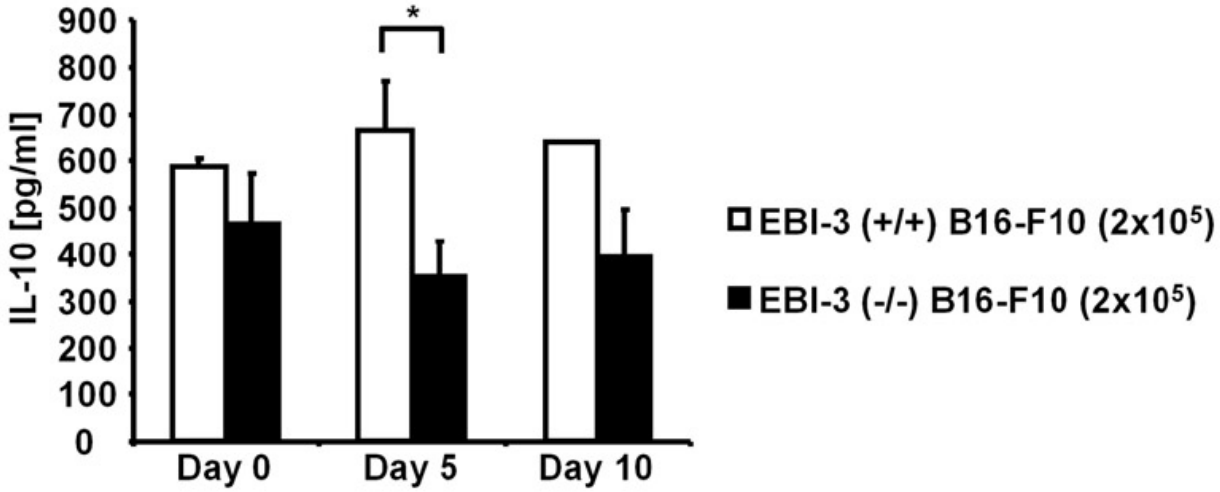

Figure 54: IL-10 production in supernatants of 24h $CD11c^+$ cell culture from EBI-3 deficient mice. Cell suspensions of lungs of EBI-3 (-/-) and B6 wild-type were purified for $CD11c^+$ cells by magnetic bead separation. The $CD11c^+$ lung cells were cultured with LPS for 24h and supernatants were taken for cytokine analysis by ELISA. 5 days after tumor cell injection IL-10 was decreased in the supernatants of $CD11c^+$ cells compared to cells from wild-type littermates.

Another cell population that has been connected with the capability of acting as T regulatory cells is the $CD8^+CD122^+$ population. CD122 is the IL-2 receptor β-chain and when expressed in $CD8^+$ T cells known to down-regulate IFN-γ production and proliferation[89]. IFN-γ secretion by activated T cells is crucial for the induction of an anti-tumor immune response. Increased numbers of activated $CD4^+$ and $CD8^+$ T cells have already been found in B16-F10 lung melanoma bearing EBI-3 deficient lungs.

These findings are very promising to uncover the mechanism by which the EBI-3 deficient immune system is induced to fight tumor development. In contrast, an increased population of $CD8^+CD122^+$ T cells would indicate a suppression of IFN-γ.

FACS analysis of total lung cell suspensions showed a decrease of CD122 expression on $CD8^+$ T cell in the lungs of EBI-3 deficient mice 5 days after tumor cell injection (Figure 55). This discovery gives hope to an increased IFN-γ production by the $CD8^+CD122^-$ cell population.

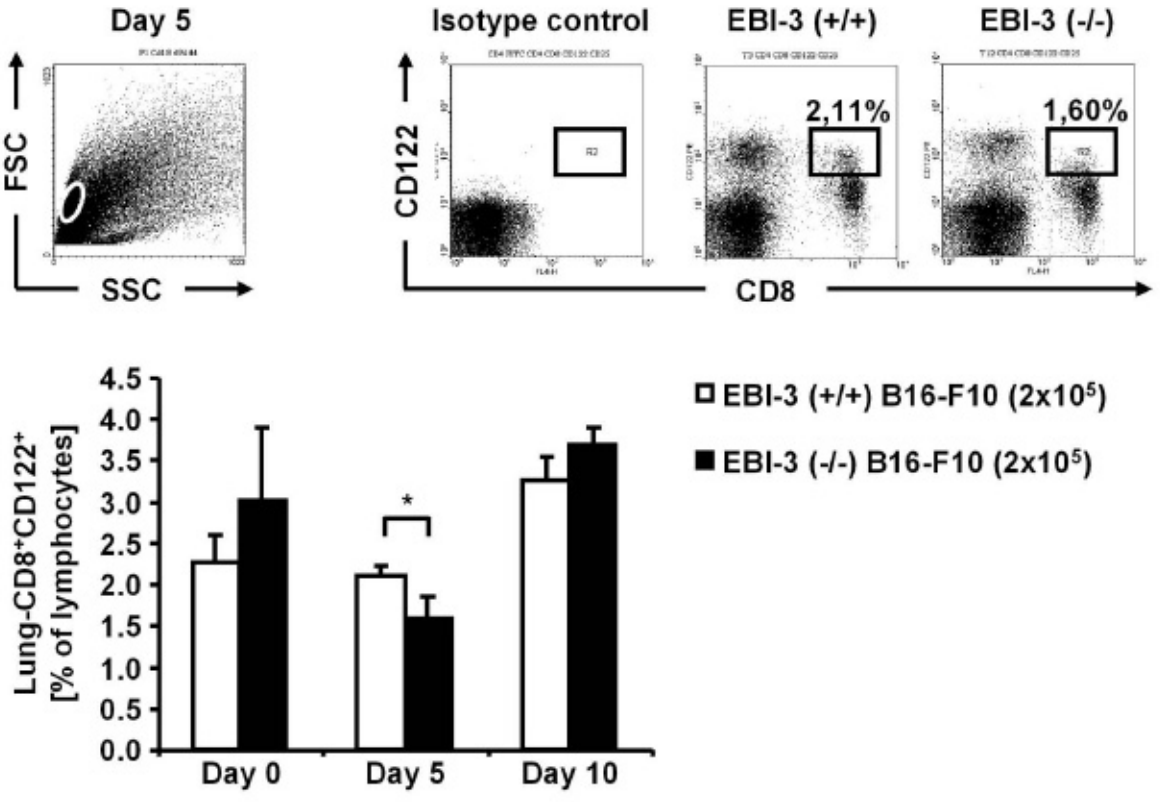

Figure 55: Expression of the IL-2 receptor β-chain (CD122) on $CD8^+$ lung T cells of EBI-3 deficient mice. Cell suspensions of lungs of EBI-3 (-/-) and B6 wild-type mice were stained for the indicated markers and analyzed by FACS analysis. Lung $CD8^+CD122^+$ T cells were down-regulated in EBI-3 (-/-) mice 5 days after i.v. injection of the B16-F10 cell line.

4.4.5 Cytokine production from EBI-3 deficient CD8$^+$ T cells in the murine model of B16-F10 induced lung melanoma

T cells secrete numerous cytokines, some of which are involved in anti-tumor immune responses and will be investigated in the following section.

IFN-γ has already been described in this thesis as a strong stimulator of potent Th1 cell responses. I therefore analyzed the amount of this cytokine produced by CD8$^+$ T cells from naïve and B16-F10 cell injected EBI-3 deficient and B6 wild-type lungs after 24h stimulation with anti-CD3 antibody. The ELISA measurement brought to light that at day 5 after tumor cell injection, when the CD8$^+$CD122$^+$ cell population was decreased in EBI-3 deficient mice, a significant increase of IFN-γ in the same lungs was observed (Figure 56).

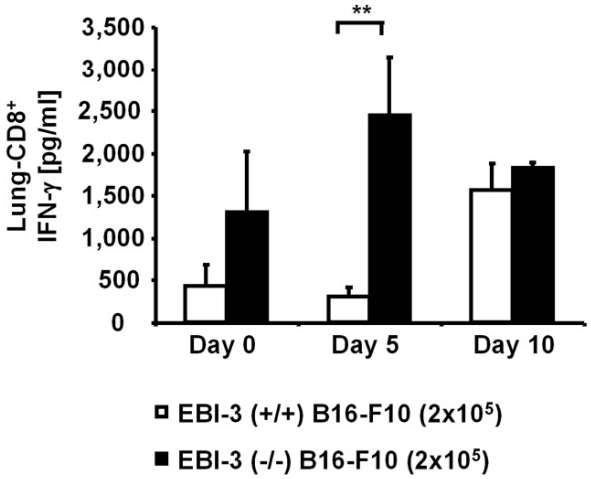

Figure 56: IFN-γ production in 24h supernatants of CD8$^+$ T cell culture from EBI-3 deficient mice. Cell suspensions of lungs of EBI-3 (-/-) and B6 wild-type mice were purified for CD8$^+$ cells by magnetic bead separation and cultured with anti-CD3 antibody for 24h. Expression of IFN-γ was measured by ELISA and found to be increased in EBI-3 (-/-) mice at day 5 after tumor cell injection.

Intracellular FACS staining was used to confirm this situation in vivo. The intracellular production of IFN-γ in CD8$^+$ T cells was found to be equal in the lungs of EBI-3 deficient and B6 wild-type mice at day 5 after tumor cell injection, but was significantly upregulated in EBI-3 deficient lung CD8$^+$ T cells at the following time point of investigation (Figure 57).

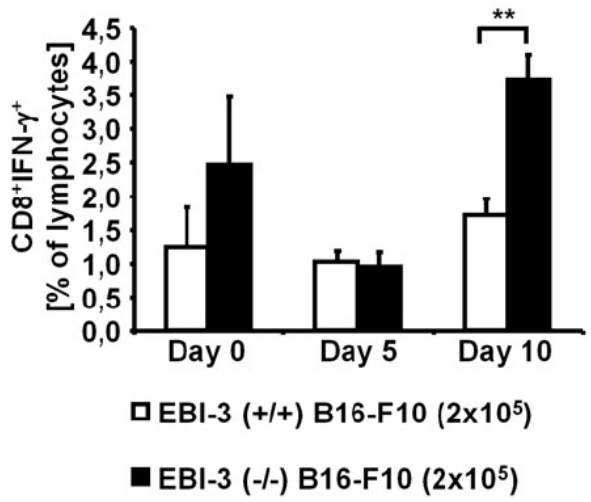

Figure 57: Intracellular IFN-γ production in CD8$^+$ T cells from EBI-3 deficient mice. Cell suspensions of lungs from EBI-3 (-/-) and B6 wild-type mice were immuno-stained for intracellular FACS analysis. On day 10 after tumor cell injection EBI-3 (-/-) lung cells produced higher amounts of IFN-γ compared to the wild-type littermates.

4.4.6 Analysis of the Th2 immune response in EBI-3 deficient CD4$^+$ T cells in the murine model of B16-F10 induced lung melanoma

Nieuwenhuis and colleagues generated the EBI-3 deficient mice and found in their initial experiments that the lack of EBI-3 leads to a defect in the production of Th2 cytokines like IL-4, IL-5 and IL-13 while the immune system of these mice favors Th1 immune responses[56].

Total lung proteins from naïve and B16-F10 cell injected EBI-3 deficient and B6 wild-type mice were used for Western Blot analysis. The incubation of the protein containing membrane with an antibody against the Th2 transcription factor GATA-3 confirmed the previous finding regarding the defective Th2 immune response. While in naïve EBI-3 deficient mice, compared to B6 wild-type littermates, the difference in GATA-3 expression remained small, a significant decrease was found in the EBI-3 deficient lung proteins at day 10 after melanoma cell injection (left panel of Figure 58).

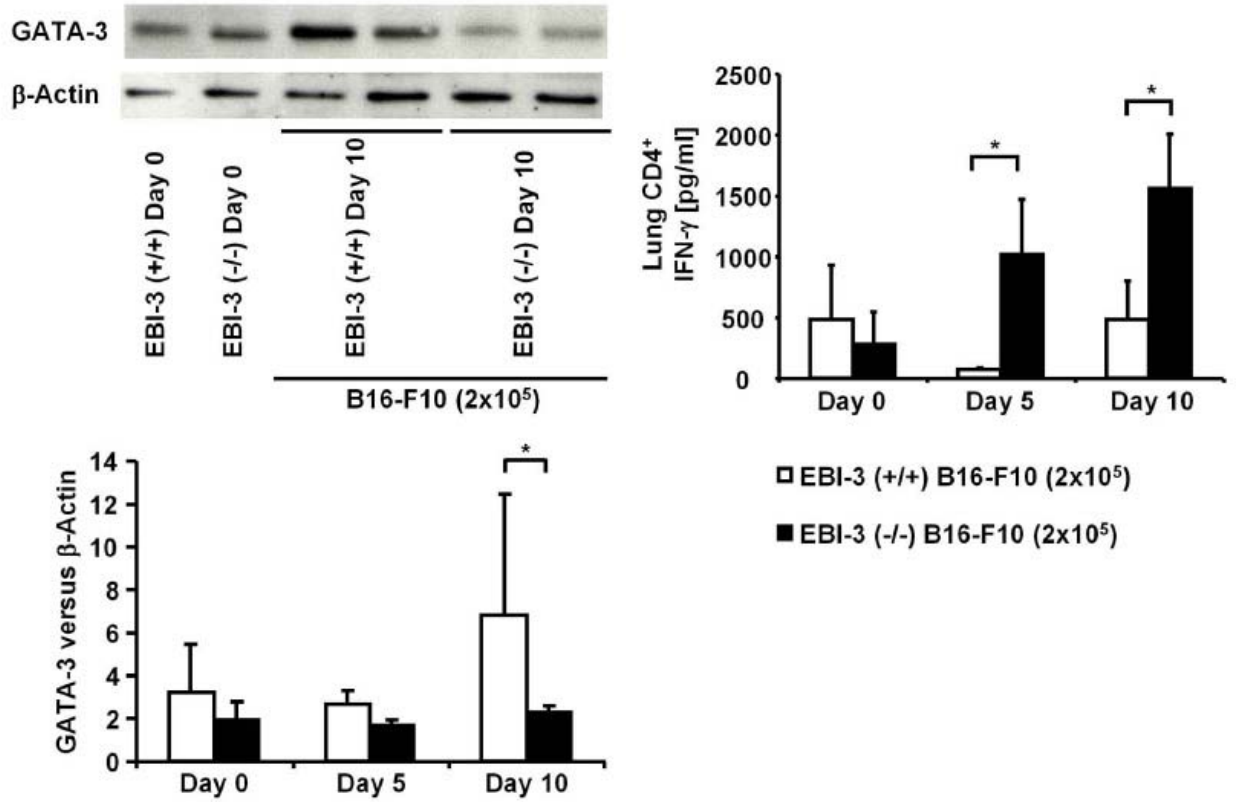

Figure 58: Defective Th2 immune response in EBI-3 deficient lungs. (left panel) Proteins were isolated from lung tissue of EBI-3 deficient and B6 wild-type mice. Western blot analysis from the isolated total lung proteins was performed for GATA-3 and quantified versus β-Actin and showed a decrease of the Th2 signature transcription factor GATA-3 in EBI-3 (-/-) mice 10 days after tumor cell injection. (right graph) Cell suspensions of lungs from EBI-3 (-/-) and B6 wild-type mice were purified for $CD4^+$ cells by magnetic bead separation and cultured for 24h with anti-CD3 antibody. Expression of IFN-γ was measured by ELISA and found to be increased in EBI-3 (-/-) mice after tumor cell injection.

In contrast to the failing Th2 immune response, the Th1 response has often been reported to be strong in EBI-3 deficient mice with inflammatory diseases[56, 57, 65].

I now focused on the IFN-γ secretion from $CD4^+$ T cells and therefore performed an ELISA detecting IFN-γ in supernatants of $CD4^+$ T cell culture that was stimulated for 24h with anti-CD3 antibody. The $CD4^+$ T cells were obtained from naïve and B16-F10 melanoma bearing EBI-3 deficient and B6 wild-type mice. The right panel of Figure 58 displays the significantly increased IFN-γ production in EBI-3 deficient $CD4^+$ lung T cells, compared to B6 wild-type lung cells after tumor cell injection. Similar results were achieved when staining total lung cell suspensions of both types of mice for intracellular FACS analysis directed against the production of IFN-γ in $CD4^+$ cells. Even though the

increase in IFN-γ production from EBI-3 deficient $CD4^+$ T cells compared to the amount of IFN-γ detected in wild-type $CD4^+$ T cells remained insignificant, the graph in Figure 59 still confirms a small upregulation of Th1 like immune responses in tumor bearing EBI-3 deficient lungs.

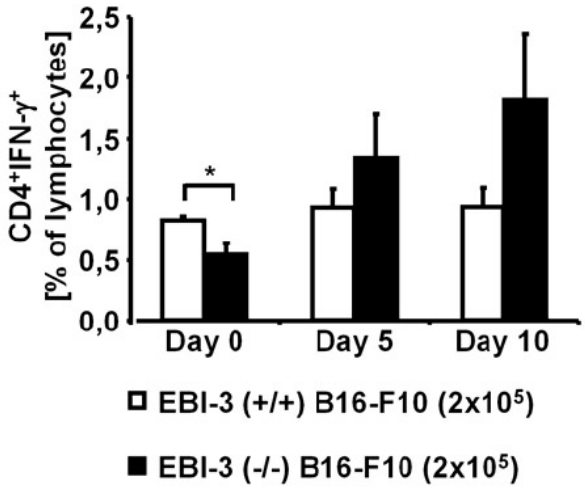

Figure 59: Intracellular IFN-γ production in $CD4^+$ T cells from EBI-3 deficient mice. Cell suspensions of lungs from EBI-3 (-/-) and B6 wild-type mice were immuno-stained for intracellular FACS analysis. After tumor cell injection EBI-3 (-/-) lung cells produced insignificantly higher amounts of IFN-γ compared to the wild-type littermates.

Interleukin-17 secretion has recently gained a lot of attention among the scientific audience, provoking intense studies in the newly identified subclass of $CD4^+$ T cells, namely the Th17 cells. Naïve $CD4^+$ T cells under the combined influence of IL-6 and TGF-β differentiate into Th17 cells then producing IL-17 among other cytokines and initiating inflammation and autoimmunity. IL-27 is believed to inhibit the development of Th17 cells when present during early CD4 cell activation[90]. The lack of EBI-3, which in consequence leads to the lack of functional IL-27, should therefore direct a pro-Th17 environment with enlarged IL-17 secretion from $CD4^+$ T cells.

$CD4^+$ lung T cells from naïve and B16-F10 melanoma cell injected EBI-3 deficient and B6 wild-type mice were cultured as described above and analyzed for IL-17 secretion by ELISA. Only at day 10 after tumor cell injection, the EBI-3 deficient $CD4^+$ T cells caused an augmented production of IL-17 compared to the amount of cytokine found in B6 wild-type mice (Figure 60).

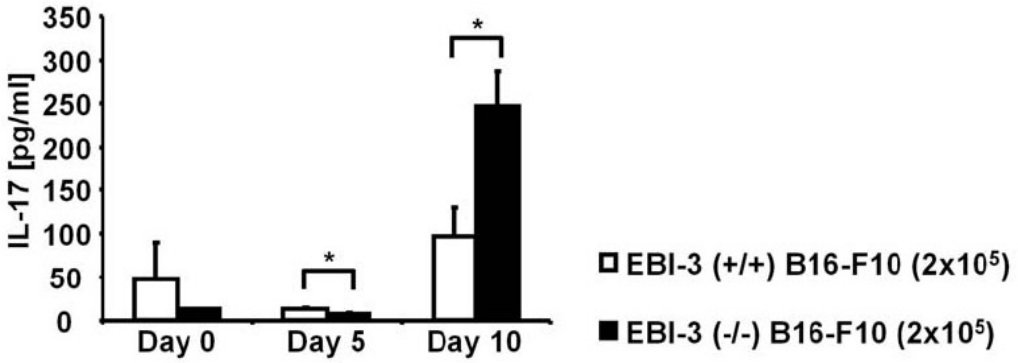

Figure 60: IL-17 production in 24h supernatants of CD4$^+$ T cell culture. Cell suspensions of lungs from EBI-3 (-/-) and B6 wild-type were purified for CD4$^+$ cells by magnetic bead separation. The CD4$^+$ lung cells were cultured with anti-CD3 antibody for 24h and supernatants were taken for cytokine analysis by ELISA. 10 days after tumor cell injection IL-17 was elevated in the supernatants of CD4$^+$ cells compared to cells from wild-type littermates.

4.5 Apoptosis induced by EBI-3 deficient T cells in the murine model of B16-F10 induced lung melanoma

Apoptosis is the progress of programmed cell death, usually initiated by antigen-primed and activated CD8$^+$ T cells. Many different mechanisms for apoptosis have been reported, all of which end in the destruction of the target cells. Major impact is thought to have the tumor necrosis factor-α (TNF-α) which can be secreted from some types of B cells, while its expression from T cells is especially high[91, 92].

The levels of TNF-α were investigated in supernatants from CD4$^+$ T cells obtained from mice in my model of B16-F10 induced lung tumor. Compared to B6 wild-type CD4$^+$ T cells the performed ELISA revealed a dramatic increase of TNF-α production from EBI-3 deficient CD4$^+$ T cells after these mice have been injected with melanoma cells (Figure 61).

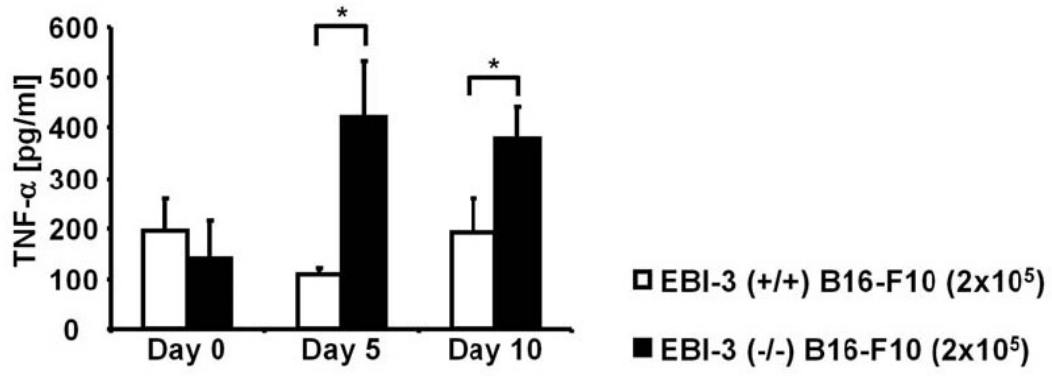

Figure 61: TNF-α production in 24h supernatants of CD4$^+$ T cell culture. Cell suspensions of lungs from EBI-3 (-/-) and B6 wild-type mice were purified for CD4$^+$ cells by magnetic bead separation and cultured for 24h with anti-CD3 antibody. Expression of TNF-α was measured by ELISA and found to be increased in EBI-3 (-/-) mice after tumor cell injection.

Since CD4$^+$ T cells are also called T helper cells which implies that the functions of this cell population is mainly to support the many tasks of CD8$^+$ T cells, I depicted in Figure 62 a simplified diagram of two important mechanisms of apoptosis induced by CD8$^+$ T cells.

Upon T cell receptor stimulation, a complex signaling cascade is induced intracellularly, which in turn activates nuclear factor of activated T cells (NFAT) in the nucleus causing transcription of nuclear factor-kappa B (NFκB). This process is followed by expression of FasL on the surface of the T cell. FasL can then bind to its partner Fas, which is expressed on many tumor cells as well as on T cells. The FasL-Fas interaction finalizes in apoptosis of the Fas-expressing cell by intracellular activation of Fas associated protein with death domain (FADD) and several apoptosis-inducing caspases that are downstream of FADD.

A similar mechanism is induced if the T cell secretes TNF-α and this cytokines binds to its receptor, the TNFR, on the target cell[91].

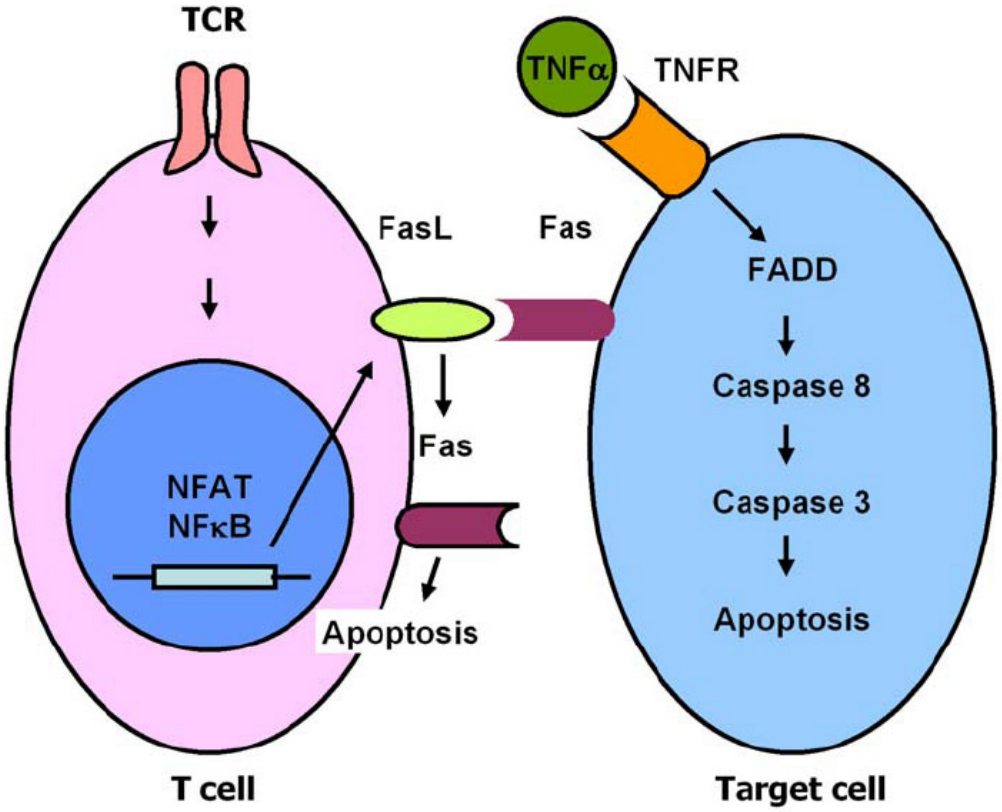

Figure 62: Mechanism of apoptosis induced by $CD8^+$ T cells via secretion of TNF-α or expression of FasL.

4.5.1 In vivo apoptosis of B16-F10 melanoma cells in EBI-3 deficient mice

Considering the increased TNF-α secretion from $CD4^+$ T cells, I then asked the question whether injected B16-F10 cells were not able to develop lung melanoma in EBI-3 deficient lungs because of increased in situ apoptosis of the tumor cells once they reached the lung. Consistent with this hypothesis, the B16-F10 melanoma cell apoptosis was found to be increased in total lung cell suspensions received from 10 day melanoma bearing EBI-3 deficient mice, compared to those obtained from B6 wild-type littermates. The apoptosis measurement was performed by FACS analysis after staining the lung cells with Annexin V and PI. Double positive cells were considered as apoptotic and quantification of this experiment is shown in Figure 63.

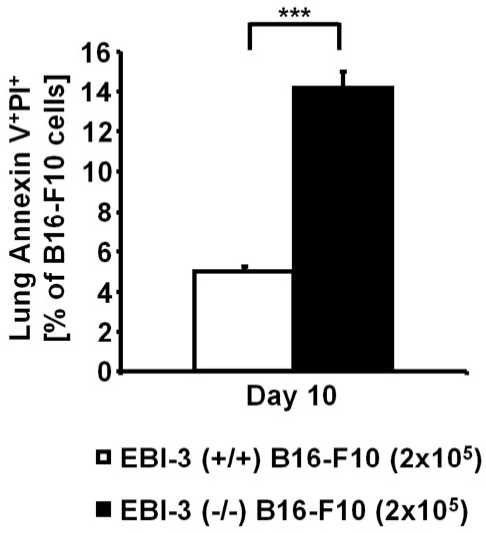

Figure 63: Apoptosis of B16-F10 cells in vivo. Cell suspensions of tumor bearing lungs from EBI-3 (-/-) and B6 wild-type mice were stained for the indicated markers and examined by FACS analysis. Annexin V and PI showed increased apoptosis of B16-F10 cells in EBI-3 (-/-) lungs 10 days after i.v. injection of the melanoma cell line.

The clone of the B16-F10 cell line I used was also analyzed for the expression of several other markers. FACS measurement of in vitro cultured melanoma cells gave answers to the question whether EBI-3 deficient T cells will be able to induce melanoma cell apoptosis, since in this case the melanoma cells have to express the corresponding ligands.

Fas as well as TNFR II (CD120b) was found to be expressed at moderate levels indicating T cell induced apoptosis as one possible mechanism by which the EBI-3 deficient mice fight the development of B16-F10 melanoma cell induced lung metastases. In addition, the expression of MHC molecules on B16-F10 cells was extremely high, demonstrating that the tumor cell clone does not belong to the many available B16-F10 clones that are low immunogenic.

4.5.2 FasL induced apoptosis in EBI-3 deficient mice

The following experiments were set to define several mechanisms of apoptosis in the EBI-3 deficient murine model of lung melanoma. At first I evaluated the expression of FasL on $CD8^+$ T cells obtained from naïve and B16-F10 cell injected EBI-3 deficient and

B6 wild-type lungs. FACS measurement showed a striking increase of FasL expression on EBI-3 deficient $CD8^+$ T cells compared to B6 wild-type cells after the injection of B16-F10 melanoma cells.

With Fas expressed on the tumor cells and FasL found increased on the $CD8^+$ T cells of EBI-3 deficient lungs, the reduced growth of melanotic colonies in the lungs of EBI-3 deficient mice might be a result of FasL induced apoptosis.

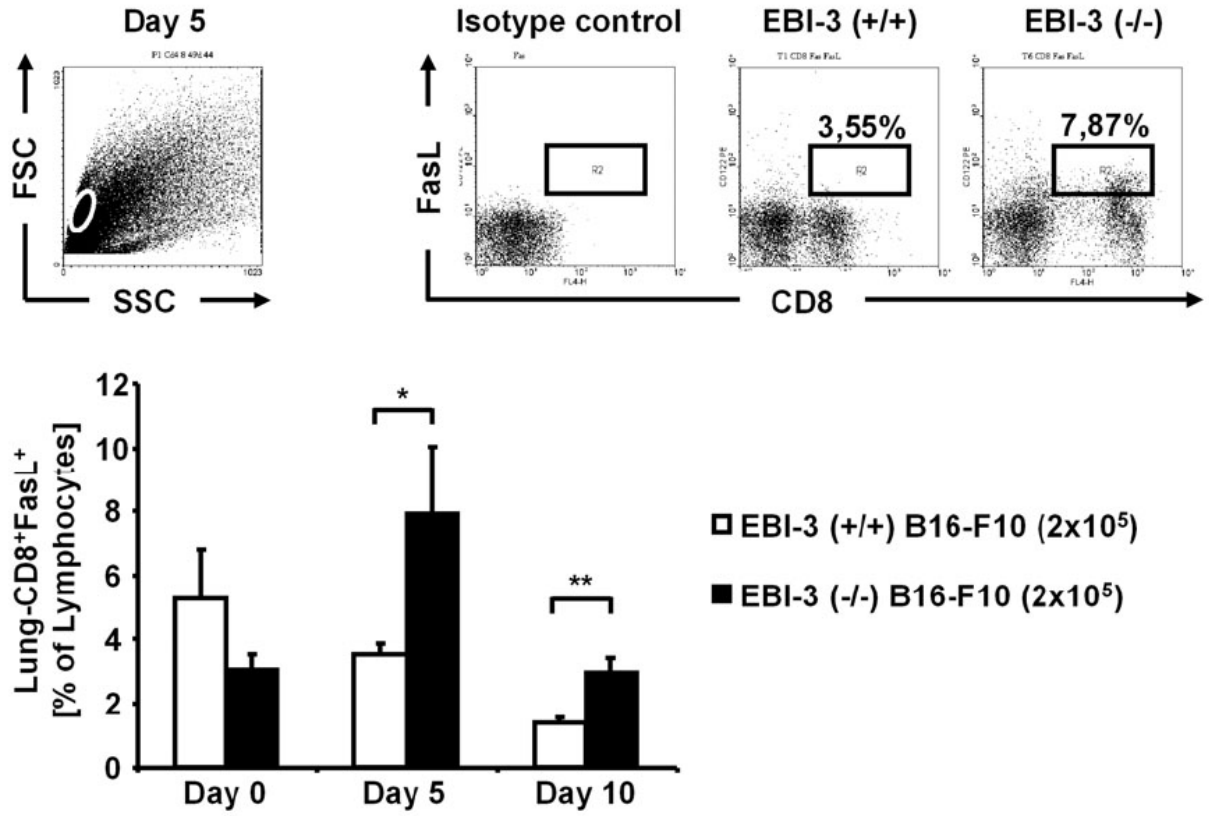

Figure 64: Expression of FasL on $CD8^+$ cells in EBI-3 deficient mice. Cell suspensions of lungs from EBI-3 (-/-) and B6 wild-type mice were stained for the indicated markers and examined by FACS analysis. The expression of the apoptosis inducing molecule FasL was found to be increased on EBI-3 (-/-) $CD8^+$ cells after B16-F10 cell injection.

4.5.3 TNF-dependent apoptosis in EBI-3 deficient mice

These findings of increased TNF-α secretion from $CD4^+$ T cells and TNFR expression on B16-F10 cells indicated an increased tumor cell killing capability in the cellular component isolated from the lungs of EBI-3 deficient mice compared to the B6 wild-type littermates. The levels of TNF-α secreted from the $CD8^+$ T cells in this model still needed to be investigated.

An ELISA performed with 24h supernatants of isolated lung $CD8^+$ T cells from naïve and tumor bearing EBI-3 deficient and B6 wild-type mice confirmed the assumption. Detection of TNF-α showed an impressive increase of this cytokine in EBI-3 deficient lung $CD8^+$ T cells compared to the cytokine level in B6 wild-type lungs (Figure 65, upper graph).

Another TNF family member is TRAIL, which stands for TNF related apoptosis inducing ligand. It can bind to the death receptors DR4 and DR5 which belong to the family of TNFRs as well[93]. Therefore it can signal through the TNFR cascade and is of interest as tumor cell apoptosis inducing factor. Total lung proteins from naïve and B16-F10 injected EBI-3 deficient and B6 wild-type mice were used for Western Blot analysis. Just like TNF-α, TRAIL was also found to be upregulated in EBI-3 deficient lungs compared to wild-type littermates after tumor cell injection (Figure 65, middle panel).

The performed experiments still fail to answer the question if the increased tumor cell apoptosis detected in the lungs of EBI-3 deficient mice is due to FasL or TNF signaling. Neutralization of TNF-α with increasing concentrations of an anti-TNF-α antibody was then performed in cell co-culture experiments in which $CD8^+$ T cells were isolated from the lungs of EBI-3 deficient mice at different time points after i.v. injection of B16-F10 and co-cultured with B16-F10 cells. As shown in the lower panel of Figure 65, apoptosis of B16-F10 cells, which was detected in the culture without anti-TNF-α antibodies, could be best neutralized with anti-TNF-α antibodies in a dose-dependent manner, when $CD8^+$ T cells were isolated 5 days after tumor cell injection and co-cultured with B16-F10 melanoma cells in a 1:1 ratio.

The same experiment was performed using an anti-Fas antibody. A Fas-dependent reduction of the tumor cell apoptosis was not detected indicating that in contrast to TNF-α, the increased expression of FasL on EBI-3 deficient $CD8^+$ T cells does not function in direct melanoma cell killing.

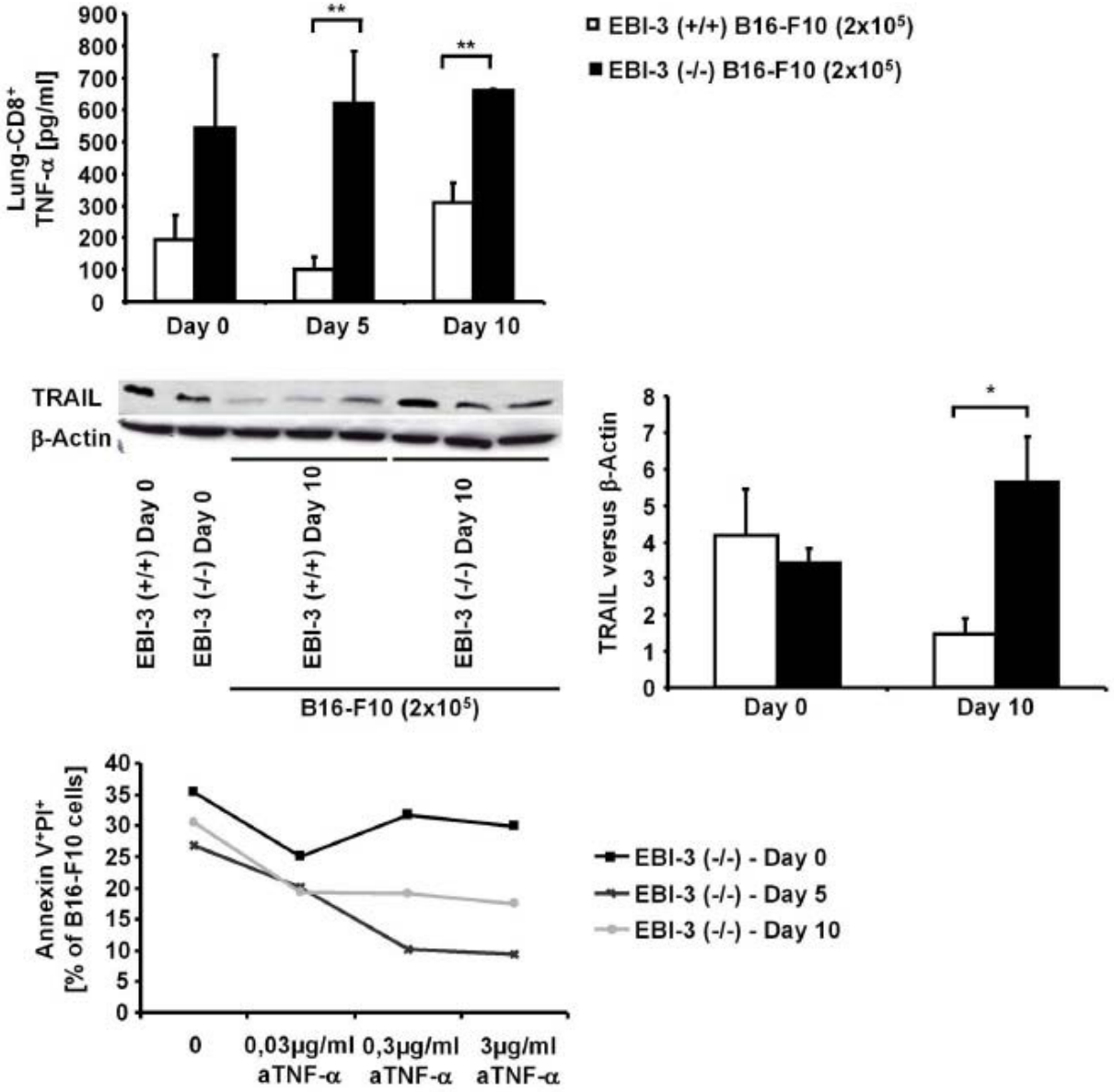

Figure 65: TNF dependent apoptosis. (upper graph) Cell suspensions of lungs from EBI-3 deficient and B6 wild-type mice were purified for $CD8^+$ cells by magnetic bead separation. The $CD8^+$ cells were cultured for 24h with anti-CD3 antibody and supernatants were taken for cytokine analysis. TNF-α production was measured by ELISA and found to be increased in EBI-3 (-/-) mice. (middle panel) Proteins of lung tissue were isolated from EBI-3 deficient and B6 wild-type mice. Western blot analysis from the isolated total lung proteins was performed for the pro-apoptotic protein TRAIL and quantified versus β-Actin. TRAIL expression was increased in EBI-3 (-/-) lungs compared to wild-type littermates 10 days after tumor cell injection. (lower panel) Cell suspensions of lungs from EBI-3 deficient mice were purified for $CD8^+$ cells by magnetic bead separation. The $CD8^+$ cells were co-cultured for 24h with anti-CD3 antibody, increasing concentrations of anti-TNF-α antibody and a constant number of B16-F10 melanoma

cells. FACS staining for Annexin V and PI revealed the TNF-α dependent apoptosis induced by in vivo primed EBI-3 deficient $CD8^+$ cells.

4.5.4 Anti-apoptotic proteins involved in tumor cell apoptosis in EBI-3 deficient mice

The Bcl-2 family consists of anti-apoptotic and pro-apoptotic proteins that influence apoptosis. Bcl-xL, Mcl-1, Bcl-w, A-1 and Bcl-2 itself are antagonists of apoptosis. The diminished release of Bcl-xL and Bcl-2 can help the immune system to inhibit tumor growth[94].

To detect the levels of Bcl-xL in the murine model of B16-F10 induced lung melanoma, I took lungs from naïve and tumor cell injected EBI-3 deficient and B6 wild-type mice and froze the tissue in “optimal cutting temperature” (OCT) compound in order to perform histological sections of lung tissue. After pretreatment, the sections were incubated in a first step with anti-CD8 antibody and linked to streptavidin-cy3 fluorochrome that emits green light when using a fluorescence microscope. A second incubation was performed with anti-Bcl-xL antibody that was labeled with streptavidin-cy2 fluorochrome that emits red light when observing the sections with a fluorescence microscope.

As displayed in Figure 66 the expression of Bcl-xL was very low in all samples and did not alter during tumor development. Neither was a difference found when sections from EBI-3 deficient and B6 wild-type mice were compared under various magnifications.

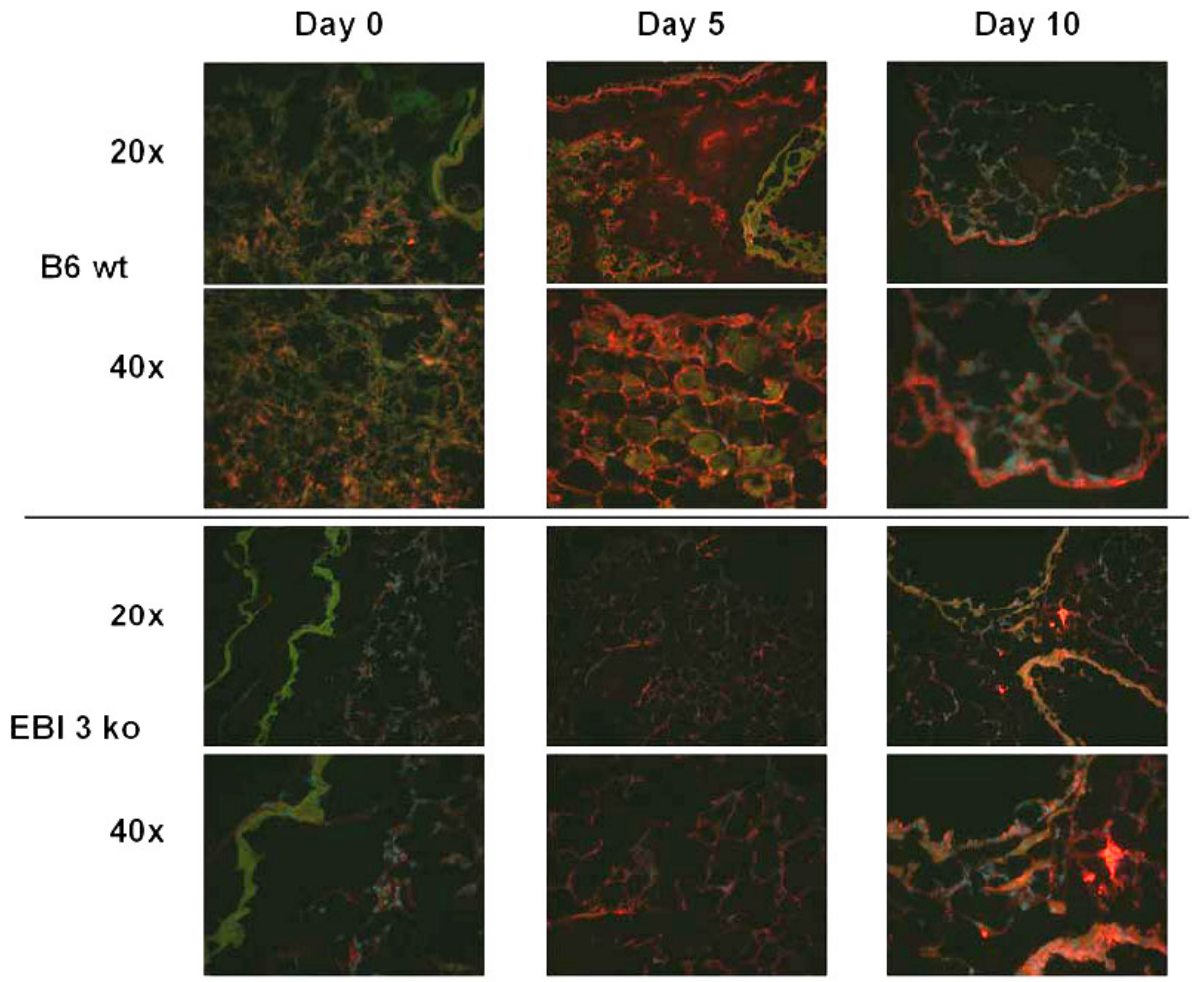

Figure 66: Immunohistochemical staining with anti-CD8 and anti-Bcl-xL antibody on naïve and tumor bearing lung tissue. Representative histological sections across lungs of wild-type (upper images) and EBI-3 (-/-) mice (lower images) are displayed after staining with anti-CD8 antibody and conjugated to streptavidin-cy2. A second staining with anti-Bcl-xL was performed on the same sections followed by streptavidin-cy3 labeling. Sections were taken at the indicated time-points before and after tumor cell injection. Quantification with the fluorescence microscope revealed that the expression of Bcl-xL on $CD8^+$ lung cells does neither depend on EBI-3 nor on injection of B16-F10 cells.

A Western Blot analysis was performed using a Bcl-2 antibody on a membrane containing total lung proteins of naïve and tumor bearing EBI-3 deficient and B6 wild-type mice. The upper panel of Figure 67 demonstrates the bands received from samples of naïve and tumor cell injected mice 5 days earlier. The lower graph of the same figure displays the quantification of Bcl-2 versus β-Actin. Both graphs reveal that the expression of Bcl-2 does neither change during tumor development nor between EBI-3 deficient and B6 wild-type mice.

This suggests that anti-apoptotic proteins do not influence the reduced tumor development observed in EBI-3 deficient mice.

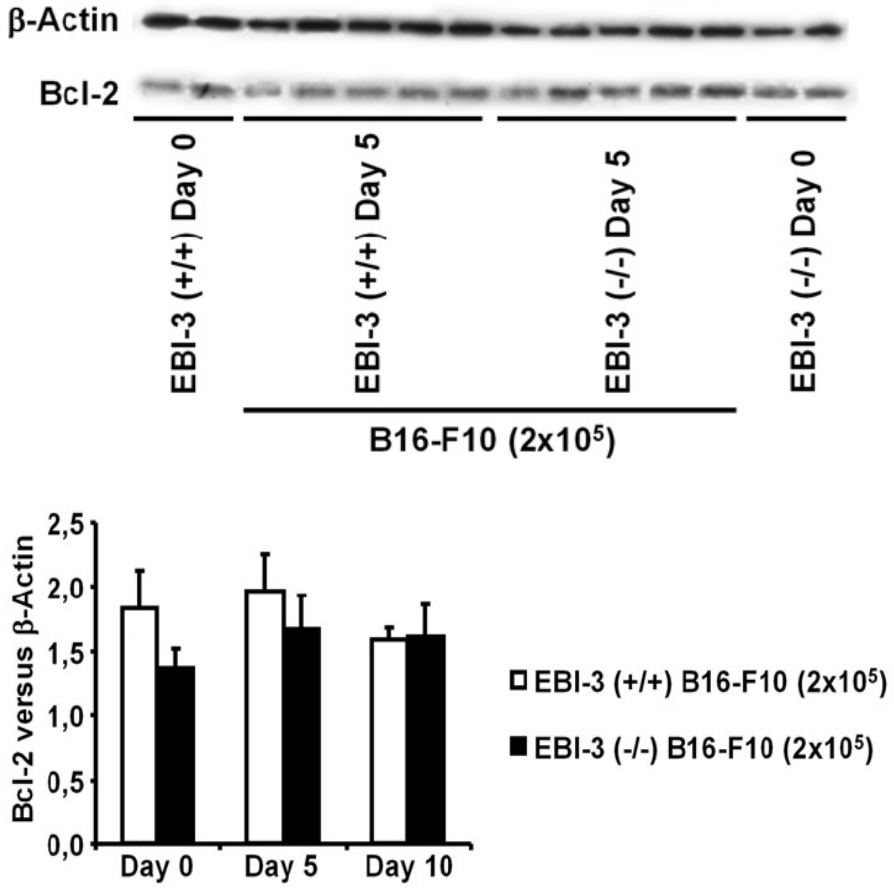

Figure 67: Western Blot of total lung proteins stained for Bcl-2. Proteins of lung tissue were isolated from EBI-3 deficient and B6 wild-type mice. Western blot analysis from the isolated total lung proteins was performed for the anti-apoptotic protein Bcl-2 and quantified versus β-Actin. Bcl-2 expression did not vary during tumor development in EBI-3 (-/-) and B6 wild-type mice.

4.6 Adoptive transfer of in vivo primed EBI-3 deficient $CD8^+$ T cells

4.6.1 In vivo Transfer of $CD8^+$ T cells into tumor bearing recipient mice

To directly prove the in vivo relationship between lung tumor size and the apoptotic function of $CD8^+$ T cells from the EBI-3 deficient tumor bearing lungs, I designed an adoptive transfer experiment.

$CD8^+$ T cells were isolated from the lungs of EBI-3 deficient and B6 wild-type mice 5 days after B16-F10 melanoma cell injection when the pDC and IK-DC numbers were increased in EBI-3 deficient mice compared to their wild-type littermates. These

$CD8^+$ T cells were then intravenously co-injected with B16-F10 cells into naïve B6 wild-type recipient mice. A third group of B6 wild-type mice was injected with B16-F10 cells only and served as control for the later comparison of melanoma development in $CD8^+$ T cell treated and untreated mice. The lungs of these mice were removed at day 10 and 14 after the adoptive T cell transfer and lung melanoma development was monitored.

As shown in Figure 68, growth of lung metastasis in the B6 wild-type mice could be exceptionally reduced when the mice were reconstituted intravenously with $CD8^+$ T cells isolated from EBI-3 deficient mice that had been injected with the B16-F10 melanoma cells five days earlier. In contrast, the reconstitution of B6 wild-type mice with antigen-primed wild-type $CD8^+$ T cells did not improve the anti-tumor immune response.

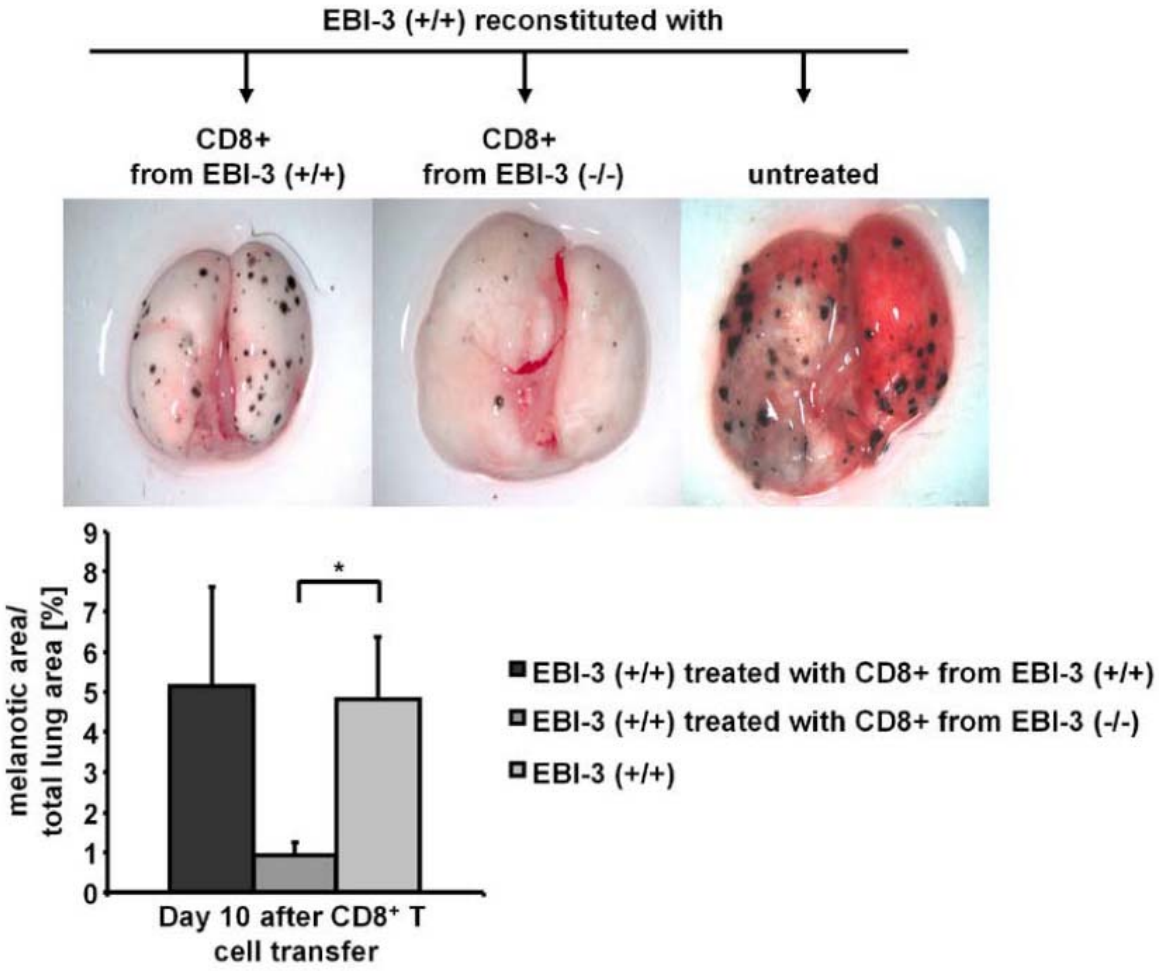

Figure 68: Adoptive transfer of in vivo primed $CD8^+$ T cells. $CD8^+$ T cells of EBI-3 deficient and B6 wild-type mice were in vivo primed by injection of $2x10^5$ B16-F10 cells. $5x10^5$ tumor antigen primed $CD8^+$ lung T cells of both EBI-3 (+/+) (left lung) and EBI-3 (-/-) (middle lung) mice were isolated by magnetic

bead separation and together with $2x10^5$ B16-F10 cells intravenously transferred into B6 wild-type mice. Untreated tumor bearing control received $2x10^5$ B16-F10 cells (right lung). Quantification analysis 10 days after the cell transfer showed significantly reduced melanoma growth in the lungs of mice treated with tumor antigen primed $CD8^+$ T cells of EBI-3 (-/-) lungs (graph).

4.6.2 Analysis of the immune response in recipient mice after $CD8^+$ T cell transfer

After the successful T cell transfer it remained to survey the effect of the $CD8^+$ T cell transfer on the immune system of the B6 wild-type recipient mice.

FACS analyzes of total lung cell suspensions of all recipient mice and controls revealed that the number of activated $CD8^+$ T cells was significantly increased in the recipients of EBI-3 deficient antigen-primed $CD8^+$ lung T cells compared to the control group (Figure 69).

This finding was accompanied by increased levels of TNF-α secretion in the BALF of mice reconstituted with activated EBI-3 deficient $CD8^+$ lung T cells (Figure 70).

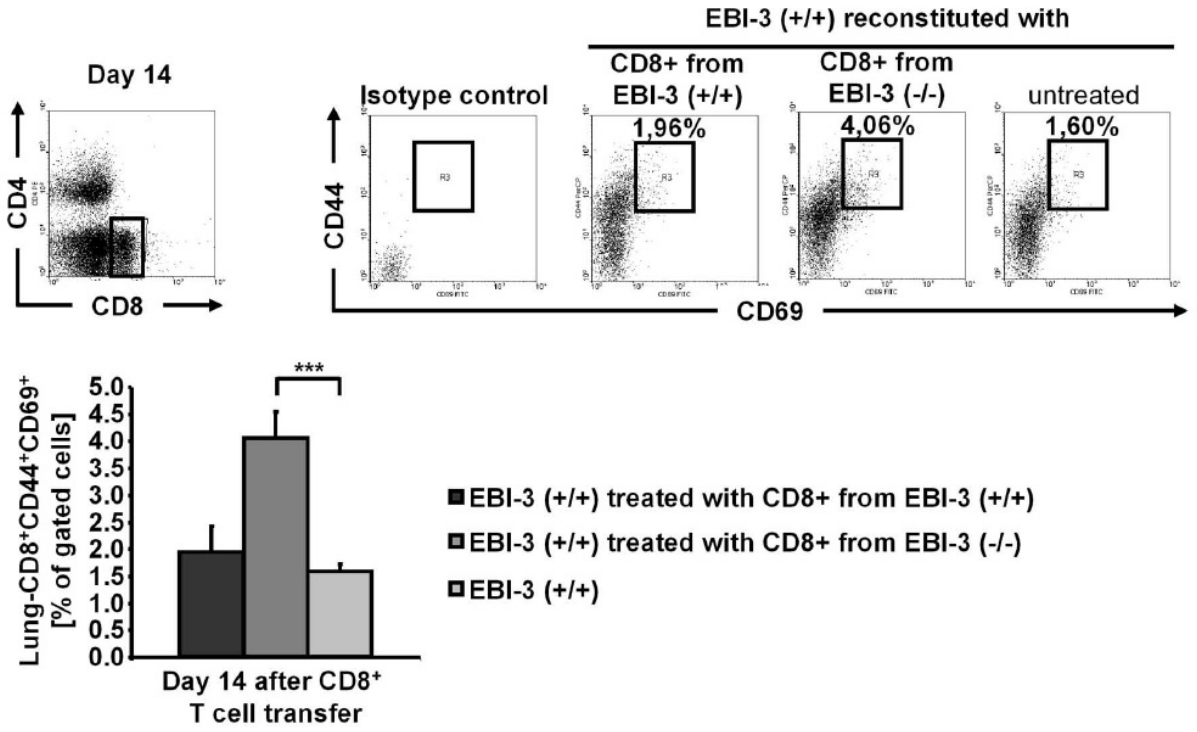

Figure 69: Expression of activation marker on $CD8^+$ T cells of recipient mice. Staining of total lung cell suspensions for $CD8^+$, $CD44^+$ and $CD69^+$ was followed by FACS analysis. An increased number of activated $CD8^+$ T cells was observed in recipients of EBI-3 (-/-) $CD8^+$ T cells.

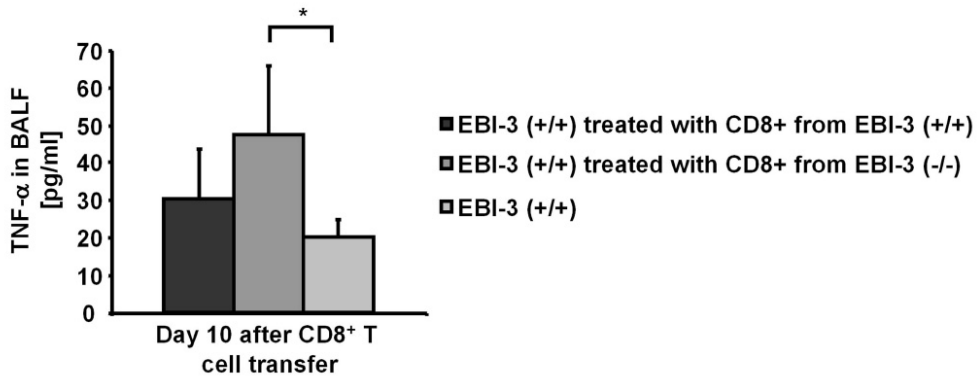

Figure 70: TNF-α production in BALF of recipient mice. The BALF was obtained from recipient mice in the $CD8^+$ T cell transfer experiment and supernatants were taken for cytokine analysis. The levels of TNF-α in the BALF were measured by ELISA and found to be elevated in the recipients of EBI-3 (-/-) $CD8^+$ T cells.

Taken together, the two most important factors in fighting the B16-F10 induced melanoma seemed to be the extraordinary activation of $CD8^+$ T cells which results in high secretion of TNF-α. This transfer experiment demonstrated that the immune response in recipient mice of antigen-primed EBI-3 deficient $CD8^+$ lung T cells resembles the immune response that was observed in EBI-3 deficient lung melanoma bearing mice in this thesis. Therefore, targeting EBI-3 in metastatic melanoma is a promising approach in anti-tumor therapy.

5 Discussion

5.1 Discussion of results

The innate and adaptive immune system is permanently challenged by entering pathogens and transformed cells that have to be eliminated by the many mechanisms of the immune system. In order to maintain a nearly total defense of external pathogens, but tolerate self-antigens, it is necessary to distinguish between self and non-self. Transformed cells originate from self-tissue and are therefore privileged to escape the recognition of the immune surveillance. In addition, most cancers developed several mechanisms to evade the immune system, allowing the cancers to grow and spread without being targeted by the host's immune defense, as well as many therapeutic approaches.

This thesis describes the role of EBI-3, a subunit of the IL-27, in the development of lung metastases of melanoma. The main focus of the work was monitoring the development of artificially induced lung metastases of melanoma in EBI-3 deficient mice and to decipher the immune mechanisms that contribute to the observed changes.

The tumor model I used to induce the metastatic disease was selected for its ability to form only pulmonary tumor nodules, while being very aggressive and allowing short experimental designs. Another advantage of the chosen murine B16-F10 melanoma cell line is the widespread and well-published use of this cell line in various models of cutaneous and metastatic melanoma. By injecting the melanoma cells intravenously, the process of developing metastases was mimicked. It is a commonly accepted mechanism that metastatic tumor growth is initiated by the spread of tumor cells through the bloodstream where cells circulate until they can adhere to the vascular endothelium and enter new tissue. An unfortunate consequence of the criteria used in this model is the fact that it lacks a primary tumor while metastatic growth is artificially induced, which might alter the natural immune response in recipient mice. Figure 24 displays the development of the lung metastases in both EBI-3 deficient and B6 wild-type mice, clearly indicating a protection of the gene targeted knockouts from metastatic tumor growth. Quantification of metastatic colonies was performed by calculating the surface of the lung that is covered with tumor compared to the tumor free area. This method is unable to define the tumor mass exactly since it only relates to the two-

dimensional area and disregards the fact that metastatic colonies show a three-dimensional growth. Lung histology shown in Figure 25 partially compensates for the quantification method showing that until a very late time point in tumor development, the inner lung tissue remains tumor free and metastatic growth is concentrated on the pleura of the lung. Additionally, the survival curve (Figure 26) confirms the finding that EBI-3 deficient mice are significantly protected from lung metastases of melanoma, leading to a prolonged survival of the EBI-3 deficient mice and indicating the EBI-3 gene as a promising target for the development of effective immunological anti-tumor therapies.

To assure that EBI-3 deficient mice used in the experiments do lack the EBI-3 gene, offspring were permanently genotyped.

Although this work shows for the first time that EBI-3 deficient mice are significantly protected from metastatic melanoma, other groups have already worked on the role of IL-27 and EBI-3 in cancer. Hisada et al. as well as Chiyo and colleagues established a model of murine C26 colon carcinomas overexpressing IL-27 that were capable to clear the tumor by enhanced effector function of $CD8^+$ T cells via T-bet and IFN-γ production but not via STAT4[95, 96]. A study was published by Salcedo creating murine tumor cells to overexpress IL-27. Reduced tumor mass and reduced metastases were found in the recipient mice whose tumors were heavily infiltrated by $CD8^+$ T cells[97]. Furthermore, Shimizu et al. transduced B16-F10 cells to express IL-27 and found reduced tumor mass in mice inoculated with these cells compared to recipients of the naïve B16-F10 cell line. The group was also able to show suppressed tumor-induced neovascularization and production of the antiangiogenic chemokines IP-10 and MIG[98]. Similar results were published by Oniki and colleagues that also transduced B16-F10 cells to overexpress IL-27 and detected that the IL-27 dependent anti-tumor response involved NK cells but not IFN-γ, while the tumor killing could be improved by additional treatment with IL-18 and IL-12[99]. Taken together, the five studies suggest a protective role of IL-27 in tumor development, which is in contrast to my finding in EBI-3 deficient mice that in consequence also lack IL-27 and should therefore contribute to a fastened tumor growth. However none of the above-mentioned investigators used endogenous IL-27 and are therefore not able to predict its role in vivo. A different research study from Larousserie et al. found EBI-3 expression upregulated in several

human T cell lymphomas compared to normal activated T cells, while a significant detection of p28 or IL-27 could not be identified. This leads Larousserie to propose a role for EBI-3, independently from p28, in the regulation of anti-tumor immune responses[100].

According to Shimizu, neoangiogenesis is regulated by IL-27 which also indicates a change of VEGF and VEGF receptor expression in EBI-3 deficient mice upon tumor cell injection[98]. I analyzed VEGF expression in total lung tissue by Western Blot and ELISA, as well as the expression of the VEGF receptor-2 Flk-1 (Figure 27 - Figure 30). Both factors were neither affected by the lack of EBI-3 nor by the developing tumor metastases. Similar to Shimizu, I found that the B16-F10 induced melanoma colonies are vascularized (data not shown) and Kim proved the capability of VEGF antagonists to reduce B16-F10 induced metastases[101]. These results suggest the blockade of VEGF or its receptor as an adjuvant in addition to the lack of EBI-3 in anti-cancer treatment. Thus the combined blockade of VEGF and EBI-3 might be a promising treatment for patients of metastatic melanoma.

The fact that EBI-3 is highly expressed by dendritic cells and that changes in the antigen presenting ability of these DCs are described in literature[65], contributed to my interest in different subsets of EBI-3 deficient dendritic cells in the model of murine metastatic melanoma. Plasmacytoid dendritic cells and their impact in cancer are well described. Colonna reviews the finding that immature DCs and pDCs infiltrate solid tumors but lack the ability to activate T cells although constantly presenting tumor antigen and thus inducing T regulatory cells that inhibit immunity[102]. This DC subset is usually activated by viral antigens that stimulate the toll like receptors 7 and 9 and secrete large amounts of TNF-α and IFN-α. I characterized the pDCs by FACS analysis and found their number unchanged in the DLNs of naïve and B16-F10 melanoma bearing EBI-3 deficient and B6 wild-type mice. The picture observed in the lungs is somewhat different since pDCs were increased in 5 days tumor bearing EBI-3 deficient mice compared to the wild-type littermates (Figure 31). However, in my experiments the secretion of TNF-α from $CD11c^+$ cells remained unchanged and IFN-α was not detectable although the cell culture was stimulated with LPS prior to cytokine analysis. Although pDCs are poor antigen presenting cells and might induce tolerogenic T cells, their activation still contributes to an anti-tumor response since IFN-α has the potency to

induce tumor killing and is already in clinical use[103]. The fact that pDCs are upregulated in tumor bearing EBI-3 deficient lungs but are not fully functional might be due to different reasons. The activation of pDCs is highest by viral antigens but this cell type is hardly stimulated upon bacterial infection. The B16-F10 cell line is neither of bacterial nor of viral origin and in addition was often described to be low immunogenic, meaning that its potential to present antigen is diminished owing to low expression of MHC molecules. The last argument could be disproved in this thesis because the B16-F10 clone I used expressed extremely high amounts of MHC molecules, indicating that the cell line is capable of inducing efficient cell dependent immune responses. It is therefore more likely that the low levels of IFN-α secretion from $CD11c^+$ cells are due to the culturing conditions. First of all, pDCs were not isolated from the lungs of the mice but the population of total $CD11c^+$ lung cells. Keeping in mind that pDCs represent only 6% of total lung dendritic cells and that cultivation with LPS imitated bacterial antigen, leads to the conclusion that the amount of pDCs in the $CD11c^+$ cell culture was too low in addition to inappropriate stimulating conditions in culture.

IK-DCs have recently been the focus of many immunological studies. These cells are a subset of DCs that in addition express NK cell markers and were found to secrete IFN-γ[69, 70]. In addition to this surprising combination of cell surface markers, IK-DCs were also shown to exhibit multiple functions in immunosurveillance and can link adaptive and innate immunity. The activation of IK-DCs results in the secretion of IFN-γ and subsequent expression of TRAIL, which initiates tumor killing after attracting tumor cells via the NK-type receptor. Finally, the activated IK-DC can become DC-like and express MHC molecules which enable the cells to present antigen[72]. In this thesis the IK-DC of EBI-3 deficient mice are characterized for the first time and exhibit all markers described for this cell type. More interestingly, the IK-DCs are upregulated at day 5 after B16-F10 cell injection in the DLN and lungs of EBI-3 deficient mice compared to the B6 wild-type littermates (Figure 32). The expression of additional markers like FasL and CD122 were also found to be expressed although to a lesser extent (Figure 33). IFN-γ secretion was revealed to be increased from isolated EBI-3 deficient $CD11c^+$ lung cells at day 5 after tumor cell injection, and was confirmed by intracellular FACS analysis for this cytokine (Figure 34). Taieb et al. evidenced cell-mediated cytotoxicity through NK receptors of IK-DCs that caused TRAIL dependent killing of B16-F10 tumors. In

addition, Chaudhry et al. demonstrated that IL-18 and CpG contribute to IFN-γ production from IK-DCs. Later, they successfully used a transfer of activated IK-DCs into IFN-γ deficient mice to reduce B16-F10 induced lung metastases[104]. Taken together the findings of these studies and the fact that EBI-3 deficient IK-DCs become upregulated and secrete more IFN-γ upon intravenous injection of B16-F10 cells, suggest that EBI-3 deficient IK-DCs might be a strong inducer of the anti-tumor immune response observed in the EBI-3 deficient mice.

In contrast to these promising findings is the often raised objection that NK cells are potent IFN-γ producing cells and cell isolation procedures never reveal 100% pure cell fractions, consequently IFN-γ found in $CD11c^+$ cell culture might be a result of impurities of NK cells in the culture and not secreted from DC subsets. The publication of Chaudhry and colleagues proves that under several conditions IK-DCs produce significantly more IFN-γ than NK cells[104]. In addition, the NK cells as well as NKT cells in naïve and tumor bearing EBI-3 deficient mice are dramatically reduced in number and function, compared to these cell populations of B6 wild-type mice, as shown in my work (Figure 35) as well as publicized by Nieuwenhuis et al. for the NKT cells[56].

To finalize the studies on dendritic cells, I analyzed the conventional DCs expressing CD11c and CD8. These cells are the classical antigen presenting cells expressing high amounts of MHC molecules as well as co-stimulatory molecules on their cell surface and secrete IL-12[73]. As displayed in Figure 36 - Figure 40, the EBI-3 deficient lung dendritic cells were more activated and mature at day 10 after intravenous tumor cell injection, compared to the wild-type lung DCs. The increase in CD8 expression on EBI-3 deficient $CD11c^+$ cells might also be an explanation for the elevated IFN-γ secretion from the EBI-3 deficient lung DCs. In addition, $CD11c^+$ cells isolated from EBI-3 deficient lungs secreted higher levels of both IL-12p40 and IL-12p70 at day 10 after B16-F10 cell injection as well (Figure 41). Similar results were achieved by Hausding et al. who analyzed the EBI-3 deficient DCs in a murine model of allergic asthma[65].

Both, the enlarged number of functional IK-DCs in EBI-3 deficient tumor bearing mice as well as the higher number of activated and mature conventional EBI-3 deficient DCs, suggest the use of these cells for cell transfer experiments in order to reduce

tumor growth in wild-type mice. Which is the most suited subset of dendritic cells for a successful tumor treatment was the question that arose. I chose a design where $CD11c^+$ lung cells were isolated from EBI-3 deficient and B6 wild-type mice at day 5 after intravenous injection of B16-F10 cells. At that time point these cells were primed with B16-F10 tumor antigen, and 50% of the EBI-3 deficient lung $CD11c^+$ cells expressed IK-DC markers and were able to secrete high amounts of IFN-γ. The isolated $CD11c^+$ cells were then co-injected with B16-F10 cells into B6 wild-type mice and the development of lung metastases was monitored. As shown in Figure 42 the attempt to reduce tumor growth in B6 wild-type recipients failed completely. There are several considerations for possible reasons for the disappointment. Possibly the number of $CD11c^+$ cells transferred into each recipient mouse was too low, although a number that resembled the amount of $CD11c^+$ cells present in one murine lung was chosen. It is as well possible that the tumor killing capacities of the high quantity of IK-DCs, which were included in the transferred cell population, were not strong enough to fight the metastases developing in wild-type mice. Very likely, the strong anti-tumor function of the IK-DC, demonstrated in the study published by Taieb using immunodeficient recipient mice, is not fully transferable to wild-type recipients. Chaudhry, who used immune-competent IFN-γ deficient recipient mice, initiated efforts to activate the isolated IK-DCs prior to injection. In conclusion, the $CD11c^+$ cell transfer I used lacked a pure IK-DC population that might need supplementary in vitro activation in addition to the in vivo priming with tumor cells. Another possibility improving the anti-tumor response by DC transfer is the design of an experiment isolating $CD11c^+$ cells from the lungs of EBI-3 deficient mice at day 10 after antigen presentation in vivo when the conventional DCs display the phenotype of activated and mature APCs.

IL-27 is an early product of antigen presenting cells and is known to influence Th1 differentiation of naïve $CD4^+$ T cells. Furthermore, the early work of Nieuwenhuis and colleagues with EBI-3 deficient mice displayed a defect in the Th2 development of these mice. Several models revealed that IL-27, as well as the lack of the IL-27 receptor, leads to increased activation and IFN-γ production of $CD8^+$ T cells[95, 105]. Both, the work on IL-27 and studies with EBI-3 deficient mice indicate that the two molecules are strongly involved in T cell responses. My project was aimed at identifying the differences between EBI-3 deficient $CD4^+$ and $CD8^+$ T cells in metastatic cancer as

well as evaluating their impact for a possible anti-tumor treatment. Figure 43 - Figure 45 display the activation status of $CD4^+$ and $CD8^+$ T cells which is increased in the lungs of EBI-3 deficient mice 10 days after the intravenous injection of B16-F10 cells. These results are consistent with the observation that conventional EBI-3 deficient lung DCs are increased and more mature compared to the wild-type cells at that time point. It also indicates that the EBI-3 deficient T cells were activated by antigen presentation of conventional DCs and that the activated T cells are involved in the anti-tumor response seen in the lungs of EBI-3 deficient mice.

In order to fight the developing metastases, the T cells have to be recruited from circulating through the blood and lymphatic system to migrate into the affected tissue. Usually, cytokines that are produced upon infection act as danger signals causing an upregulation of several surface markers on T cells and endothelial cells that in combination allow the T cells to enter the affected tissue. The cell surface integrin $\alpha_4\beta_1$ (VLA-4) is expressed on T cells and can upon binding to its partner VCAM-1 on the vascular endothelium cause the T cell to emigrate from the blood stream into tissue. Matching the activation status of tumor bearing EBI-3 deficient lung T cells, $CD4^+$ and $CD8^+$ T cells of EBI-3 deficient mice showed a significant upregulation of the surface expression of VLA-4 after tumor cell injection. However the results concerning its binding partner VCAM-1 are somewhat confusing as summarized in Figure 46 - Figure 50. FACS analysis revealed a decrease of VCAM-1 expression on endothelial EBI-3 deficient lung cells, which was also confirmed by an ELISA, performed with 24h supernatants of total lung cell culture. Astonishingly, further ELISAs using supernatants of the BALF and total lung cell culture that was stimulated with LPS exhibited increased VCAM-1 expression from EBI-3 deficient lung cells. To decipher the reason for these outcomes, I analyzed literature and found that Hausding et al. was able to demonstrate that VCAM-1 expression on EBI-3 deficient lung endothelial cells is decreased in a murine model of allergic airway disease[65]. Furthermore, the stimulating function of LPS on the VCAM-1 expression on endothelial cells and airway smooth muscle cells has been published[106]. In addition to the in vitro situation that was altered by LPS stimulation, all ELISAs mirror the VCAM-1 secretion of total lung cells. For the evaluation of the T cells` migration capacity only the VCAM-1 expression on vascular endothelial cells is of interest. Therefore, the FACS analysis performed with freshly

isolated lung cells stained for endothelial cells reveals the picture closest to reality. But accepting the FACS and thus the diminished VCAM-1 expression on EBI-3 deficient endothelial cells questions the high number of activated T cells expressing VLA-4 in the lungs of EBI-3 deficient mice. Conversely, the low VCAM-1 expression could contribute to the retarded melanoma growth observed in the EBI-3 deficient lungs since most tumor cells express high levels of VLA-4 and use the same route to enter tissue as the T cells. This statement could not be clarified because the B16-F10 cell line was not checked for VLA-4 expression.

Except for the blockade of the newly portrayed Th17 cell development, IL-27 was not yet described to influence the development of T regulatory cell subsets[54]. Administering anti-tumor immune-therapeutics usually increases the T regulatory cell population which in turn diminishes the effect of the therapy[29, 81]. Analysis of T regulatory cells in my model of B16-F10 induced lung melanoma confirmed the assumption that the lack of EBI-3 does not influence the number of T regulatory cells present in naïve and tumor bearing mice (Figure 51 - Figure 54). Cytokines like TGF-β and IL-10, which are both known to contribute to increased Treg populations were also found unchanged or in the case of IL-10 even down-regulated in EBI-3 deficient DCs. In this thesis the Tregs of EBI-3 deficient lungs are investigated for the first time, but IL-10 expression from DC supernatants were already published by Hausding and found to be increased in his model of inflammatory airway disease. This finding indicates that IL-10 is involved in many mechanisms as published and is differently regulated in inflammation and cancer[88, 107]. Anti-tumor therapies including the blockade of EBI-3 might therefore be a possibility to avoid unnecessary increase of T regulatory cells during T effector cell expansion in the patient.

In addition to $CD4^+$ T regulatory cells, a subset of $CD8^+$ T cells was recently shown to have similar functions in suppressing the CD8 effector response[89]. These cells are characterized by the expression of the IL-2 receptor β chain, called CD122, and regulate T cell responses via suppression of IFN-γ. Consistent with the elevated numbers of activated EBI-3 deficient $CD8^+$ T cells in tumor bearing lungs, I found the CD8 population expressing CD122 down-regulated at day 5 after B16-F10 cell injection which would contribute to a high secretion of IFN-γ (Figure 55). Intracellular FACS (Figure 57) and additional ELISA (Figure 56) demonstrated for the first time that EBI-3

deficient $CD8^+$ T cells are capable of secreting large amounts of this cytokine after activation by antigen presenting cells. This phenomenon was already published for $CD4^+$ T cells of these gene targeted mice in an inflammatory model of colitis [56] which I was able to confirm for the EBI-3 deficient $CD4^+$ T cells in the murine model of metastatic melanoma (as shown in Figure 59). Beyond that, the colitis model as well as the inflammatory mouse model used by Hausding, depicted a defect in the EBI-3 deficient $CD4^+$ T cells concerning the Th2 development of these cells[56, 65]. The increased IFN-γ production from activated $CD4^+$ T cells and the decrease in the expression of the Th2 transcription factor GATA-3 which I detected, confirm the inability of EBI-3 deficient $CD4^+$ T cells to initiate appropriate Th2 immune responses (Figure 58). These results and the finding of EBI-3 expression during pregnancy leads to the speculation that free EBI-3 might counter-regulate Th1 immune responses similar to the way by which $(p40)_2$ was found to antagonize the function of IL-12. Contrarily, a publication from Zahn et al., which used a murine model of leishmaniasis, demonstrated a diverse cytokine profile in the lymph nodes of infected EBI-3 deficient mice. Secretion levels of IL-4, IL-10 and IL-13 were upregulated while IFN-γ was produced to a lesser extent compared to the wild-type littermates[108].

Among the reams of Th17 studies at least 2 articles were published in nature immunology within the last year, both claiming IL-27 to inhibit naïve $CD4^+$ T cells to differentiate into Th17 cells[90, 109]. Stumhofer used a mouse model of experimental chronic Toxoplasma gondii infection in IL-27R deficient mice that led to autoimmune encephalitis. He demonstrated that in vitro treatment of naïve primary T cells with IL-27 was able to suppress the STAT1 dependent Th17 development induced by TGF-β and IL-6[90]. A similar study was performed by Batten, who analyzed the Th17 immune response of IL-27R deficient mice in several inflammatory models and found in vivo that IL-27 directly acts on effector T cells to suppress the development of Th17 cells. In addition to Stumhofer, Batten revealed that the effect of IL-27 is not only dependent on STAT1 but also independent from IFN-γ[109]. If these findings are brought forward to the B16-F10 model of metastatic melanoma in EBI-3 deficient mice, one can expect the IL-17 levels secreted from tumor bearing EBI-3 deficient $CD4^+$ T cells to be elevated compared to the cytokine secretion from B6 wild-type littermates (Figure 60). This thought bases on the fact that EBI-3 deficient mice in consequence lack IL-27 which if

present is able to down-regulate the IL-17 producing cells. Therefore I analyzed the secretion of IL-17 in my tumor model and found a significant elevation of IL-17 secreted from EBI-3 deficient $CD4^+$ T cells at day 10 after intravenous injection of B16-F10 cells.

This project was aimed at uncovering a mechanism by which the EBI-3 deficient mice escape the metastatic development. Analyzing many possible mechanisms that induce programmed cell death indicated that TNF-dependent apoptosis initiated from $CD8^+$ T cells in vivo has great impact on the immune response in the EBI-3 deficient mice. While proteins from the Bcl-2 family were not involved in the anti-tumor response of EBI-3 deficient mice, the expression of FasL on $CD8^+$ T cells as well as the secretion of TNF-α from these cells was illustrated to be increased in tumor bearing EBI-3 deficient mice (Figure 61 - Figure 67). A co-culture experiment gave additional insight in the killing capabilities of tumor antigen primed EBI-3 deficient $CD8^+$ T cells and proved the important role of TNF-α in this model. The local overexpression of IL-27 by murine tumor cell lines was shown to have a similar effect in activating $CD8^+$ T cells to induce tumor cell lysis as was demonstrated for EBI-3 deficient $CD8^+$ T cells in this thesis[95-99]. Aside from that, no other studies dealt with the influence of EBI-3 in $CD8^+$ T cell-mediated apoptosis of tumor cells.

Previous studies already used activated $CD8^+$ T cells in adoptive transfer models to reduce tumor burden in mice and patients[110, 111]. The adoptive $CD8^+$ T cell transfer I performed was very successful. The analysis of the immune response in recipient mice was enlightening, by revealing that the transferred EBI-3 deficient $CD8^+$ T cells were capable of conquering the inefficient immune response of the B6 wild-type recipients, and in vivo initiating an immune response that resembles the one found in tumor bearing EBI-3 deficient mice. Although this experiment gives reason for optimism, several questions remain to be answered. The $CD8^+$ T cells were isolated from lungs of EBI-3 deficient and B6 wild-type mice at day 5 after intravenous injection of B16-F10 melanoma cells. According to my studies on the activation status of the T cells in this model, the $CD8^+$ T cells were not yet fully activated at the time of the $CD8^+$ T cell transfer. Furthermore, Corthay et al. published his work including a $CD4^+$ T cell transfer that was successful in reducing tumor burden[112]. Since the results obtained from $CD4^+$ T cell analysis in the EBI-3 deficient mice injected with melanoma cells gave strong evidence that these T helper cells are potently activated, I utilized a $CD4^+$ T cell

transfer as an approach against tumor growth. As depicted in Figure 71 the attempt failed. Actually, the disappointing outcome of the $CD4^+$ T cell transfer is not much of a surprise due to the low number of successful treatments with this cell population. $CD4^+$ T cells or T helper cells, which describe their function more precisely, strengthen the effector response created by $CD8^+$ T cells. This knowledge was already used in the treatment of cancer by administering a co-transfer of antigen-primed $CD4^+$ and $CD8^+$ T cells as published by Huang and colleagues[113]. Unfortunately, the effort to clear the B16-F10 induced lung melanoma metastases from B6 wild-type mice by co-injecting $CD4^+$ and $CD8^+$ T cells was unsuccessful as well. In the experimental design I decided to transfer equal amounts of T cells into the recipient mice meaning that each B6 wild-type mouse was treated with $1x10^6$ T cells regardless of which origin. The result of the combined $CD4^+$ and $CD8^+$ T cell transfer might be improved by using the same amount of $CD8^+$ T cells and in addition inject $1x10^6$ $CD4^+$ T cells then injecting a total of two million cells instead of injecting a total amount of one million cells.

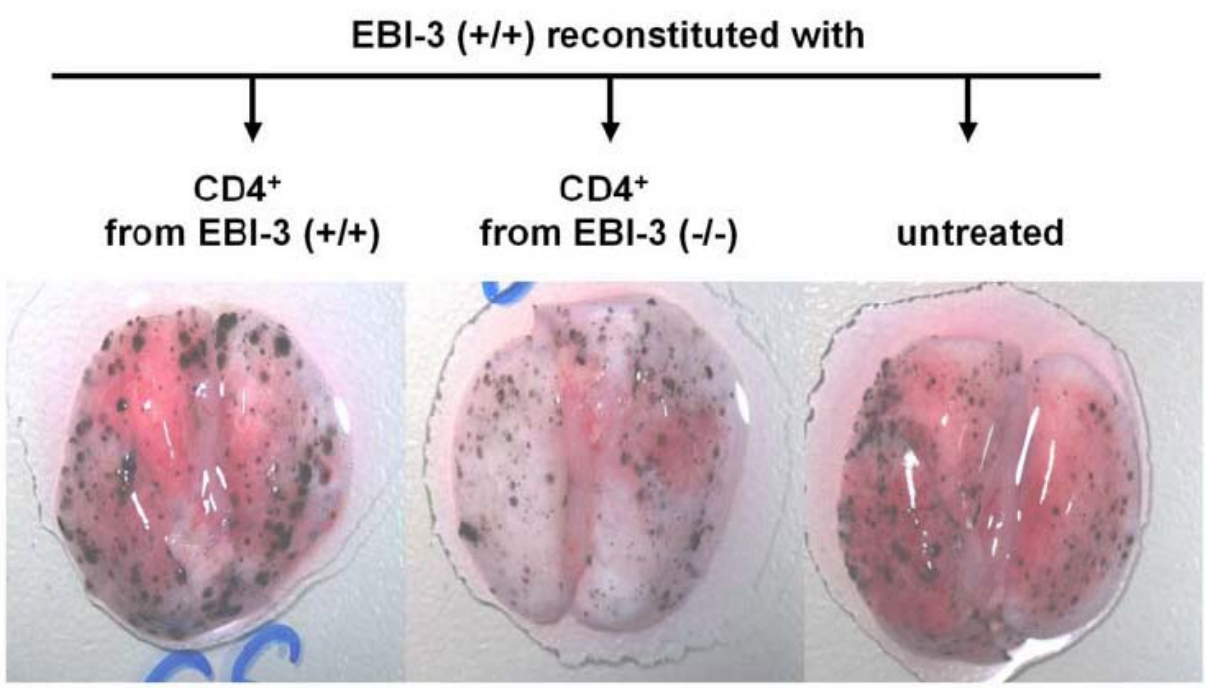

Figure 71: Adoptive transfer of in vivo primed $CD4^+$ T cells.

5.2 Outlook

Regardless of several unanswered questions, the work in this thesis still proves that EBI-3 deficiency results in a protection from lung metastases of B16-F10 induced melanoma by activating $CD8^+$ T cells that induce TNF-dependent programmed cell death of the B16-F10 cells. To incontrovertibly confirm the statement that the lack of EBI-3 is responsible for the retarded tumor growth in these mice, two experimental designs are imaginable. One could either treat EBI-3 deficient mice with commercially available murine recombinant IL-27 or block EBI-3 expression in B6 wild-type mice. In both cases, the effect seen in the treated mice should be reversed to resemble the effect of the respective genetically other mouse type.

The Hunter group published many studies using IL-27 receptor knockout mice that often displayed similar results as obtained from EBI-3 deficient mice. In both cases signaling through the WSX-1 receptor is not possible and might therefore lead to related results[53]. Moreover, the fact that IL-27R deficient mice develop conflictive immune responses dependent on the kind of infection[52, 53], and this is true for EBI-3 deficient mice as well[56, 65, 108], supports the hypothesis of Hunter that EBI-3 does not have a function on its own independently from IL-27. In contrast, EBI-3 is much more widely expressed than p28 and can form homo-dimers[114, 115]. This directs the theory that EBI-3 has a purpose when expressed without p28, although a receptor that upon binding of EBI-3 alone gets functionally activated, is not yet discovered. The generation of a p28 deficient mouse would be the only chance to reveal the in vivo function of EBI-3 in absence of IL-27.

The work presented here suggests EBI-3 as a target for effective therapy of metastatic melanoma. This thesis did not survey human data on this issue. Actually, RT-PCR for EBI-3 in human monocytes indicated that some patients suffer from extremely high expression of EBI-3 in stage IV metastatic melanoma compared to healthy individuals, while other patients do not show increased expression of EBI-3 (data not shown). It remains to study the immune responses in correlation with EBI-3 expression in a higher number of patients bearing metastatic melanoma. For effective treatments, a well compliant EBI-3 antibody or even small interfering RNA needs to be developed to either apply one of the mentioned treatments directly to the patients or to

isolate $CD8^+$ effector T cells and permanently eradicate EBI-3 expression intracellularly before re-injecting these cells into the patient.

6 Abstract

6.1 Abstract English version

This thesis addresses the role of Epstein-Barr virus-induced gene 3 in a murine model of B16-F10 cell induced lung metastases of melanoma. EBI-3 codes for a soluble type 1 cytokine receptor homologous to the p40 subunit of IL-12 that is expressed by antigen presenting cells following activation and together with p28 forms the IL-27.

Intravenous injection of the B16-F10 cell line resulted in a significant reduction of lung tumor metastasis in EBI-3 deficient mice as well as in prolonged survival compared to B6 wild-type littermates. Furthermore, I found that EBI-3 deficient mice had a decreased number of VCAM-1 expressing endothelial cells but changes in VEGF expression were not detected. The immunological finding accompanying this therapeutic effect was the orchestrate priming and activation of T cells by the newly described DC subset, called Interferon-producing Killer Dendritic Cells (IK-DC), in addition to activated and mature conventional DCs. IK-DCs from EBI-3 deficient mice released increased amounts of IFN-γ while conventional DCs expressed MHC and co-stimulatory molecules initiating the secretion of IL-12 thereby inducing augmented $CD4^+$ and $CD8^+$ T cell responses in the lung. This in turn resulted in a TNF-α and TRAIL mediated programmed cell death of B16-F10 melanoma cells in the lungs of EBI-3 deficient mice, whereas other anti-apoptotic mechanisms and T regulatory cells did not seem to influence the anti-tumor immune response observed in the EBI-3 deficient mice. Finally, adoptive transfer of EBI-3 deficient antigen-primed $CD8^+$ T cells into tumor bearing wild-type mice diminished the development of lung metastasis in recipient mice.

Taken together, these data demonstrate that targeting EBI-3 in metastatic melanoma is a promising approach in anti-tumor therapy.

6.2 Abstract German version / Zusammenfassung der Arbeit

In dieser Arbeit wurde die Rolle des Epstein-Barr Virus induzierten Gens 3 in einem Mausmodel des durch B16-F10 Zellen hervorgerufenen metastasierenden Melanoms untersucht. Das von aktivierten antigenpräsentierenden Zellen exprimierte EBI-3 gehört

zur Familie der löslichen Typ 1 Zytokinrezeptoren, weist eine hohe Homologie zur p40 Untereinheit des IL-12 auf und bildet zusammen mit p28 das IL-27.

Die intravenöse Injektion der B16-F10 Zelllinie führte zu einer signifikanten Erniedrigung der Tumormetastasen in den EBI-3 defizienten Lungen sowie zu einer höheren Lebenserwartung dieser Mäuse im Vergleich zu den B6 Wildtypen. Darüber hinaus habe ich in den EBI-3 defizienten Mäusen eine verminderte VCAM-1 Expression auf den Endothelzellen der Lunge gefunden während Änderungen in der VEGF Expression nicht detektiert wurden. Der immunologische Hintergrund, der diesen therapeutischen Effekt hervorrief, konnte durch die T-Zellaktivierung durch die kürzlich neu beschriebene DC Population, welche Interferon-produzierende Killer Dendritische Zellen genannt werden (IK-DC), die zusätzlich von aktivierten und maturierten klassischen DCs unterstützt wurden, erklärt werden. IK-DCs von EBI-3 defizienten Mäusen produzierten höhere Mengen an IFN-γ während die klassischen DCs MHC und co-stimulatorische Moleküle exprimierten, welche die Sekretion von IL-12 initiierten. Das Zusammenspiel der genannten Faktoren induzierte eine verstärkte CD4 und CD8 T-Zellantwort in den Lungen dieser Mäuse. Dies wiederum resultierte im TNF-α und TRAIL abhängigen programmierten Zelltod der B16-F10 Melanomzellen in den Lungen der EBI-3 defizienten Mäuse, wohingegen sowohl weitere anti-apoptotische Mechanismen als auch T regulatorische Zellen keinen Einfluss auf die in den EBI-3 defizienten Mäusen beobachtete Tumorabwehr zu spielen scheint. Schlussendlich konnten EBI-3 defiziente $CD8^+$ T-Zellen, welche zuvor mit Tumorantigen geprimed wurden, adoptiv in B6 Wildtypmäuse transferiert werden, was zeigte, dass diese Zellen in der Lage sind, die Tumormasse in den Empfängermäusen signifikant zu verringern.

Zusammengefasst, demonstrieren diese Daten, dass das Blockieren von EBI-3 im metastasierenden Melanom ein vielversprechender Angriffspunkt in der Tumortherapie darstellt.

7 Bibliography

1. *Parkin, J. and B. Cohen, An overview of the immune system. Lancet, 2001. **357**(9270): p. 1777-89.*
2. *Chaplin, D.D., 1. Overview of the immune response. J Allergy Clin Immunol, 2003. **111**(2 Suppl): p. S442-59.*
3. *http://www.actagainstallergy.co.uk/aaa_couk/631-innate-immunity-and-acquired-immunity.html.*
4. *http://en.wikipedia.org/wiki/lung.*
5. *http://www.thoracic.org/sections/copd/for-patients/anatomy-and-function-of-the-normal-lung.html.*
6. *Watson, J.H., NH; Roberts, JW; Steitz, JA; Weiner, AM, Molecular Biology of the Gene. 4th ed. Vol. II.*
7. *Abbas, A.a.L., AH, Cellular and Molecular Immunology. Vol. 5th edition.*
8. *Strauss, B.S., Hypermutability and silent mutations in human carcinogenesis. Semin Cancer Biol, 1998. **8**(6): p. 431-8.*
9. *Eccles, S.A. and D.R. Welch, Metastasis: recent discoveries and novel treatment strategies. Lancet, 2007. **369**(9574): p. 1742-57.*
10. *Mehlen, P. and A. Puisieux, Metastasis: a question of life or death. Nat Rev Cancer, 2006. **6**(6): p. 449-58.*
11. *Hendrix, M.J., et al., Remodeling of the microenvironment by aggressive melanoma tumor cells. Ann N Y Acad Sci, 2003. **995**: p. 151-61.*
12. *Witte, M.H., et al., Structure function relationships in the lymphatic system and implications for cancer biology. Cancer Metastasis Rev, 2006. **25**(2): p. 159-84.*
13. *Wang, W., et al., Tumor cells caught in the act of invading: their strategy for enhanced cell motility. Trends Cell Biol, 2005. **15**(3): p. 138-45.*
14. *Fidler, I.J., The pathogenesis of cancer metastasis: the 'seed and soil' hypothesis revisited. Nat Rev Cancer, 2003. **3**(6): p. 453-8.*
15. *Minn, A.J., et al., Distinct organ-specific metastatic potential of individual breast cancer cells and primary tumors. J Clin Invest, 2005. **115**(1): p. 44-55.*
16. *Shevde, L.A. and D.R. Welch, Metastasis suppressor pathways--an evolving paradigm. Cancer Lett, 2003. **198**(1): p. 1-20.*
17. *Hill, R., et al., Selective evolution of stromal mesenchyme with p53 loss in response to epithelial tumorigenesis. Cell, 2005. **123**(6): p. 1001-11.*
18. *http://www.who.int/topics/melanoma/en/.*
19. *http://pschyrembel.de/index_101.htm.*
20. *Schallreuter, K.U., et al., Human phenylalanine hydroxylase is activated by H2O2: a novel mechanism for increasing the L-tyrosine supply for melanogenesis in melanocytes. Biochem Biophys Res Commun, 2004. **322**(1): p. 88-92.*
21. *Gray-Schopfer, V., C. Wellbrock, and R. Marais, Melanoma biology and new targeted therapy. Nature, 2007. **445**(7130): p. 851-7.*
22. *Kimura, S., et al., Bcl-2 reduced and fas activated by the inhibition of stem cell factor/KIT signaling in murine melanocyte precursors. J Invest Dermatol, 2005. **124**(1): p. 229-34.*
23. *Sharpless, N.E., INK4a/ARF: a multifunctional tumor suppressor locus. Mutat Res, 2005. **576**(1-2): p. 22-38.*

24. *Perales, M.A., et al., Strategies to overcome immune ignorance and tolerance. Semin Cancer Biol, 2002. **12**(1): p. 63-71.*
25. *Carbone, F.R., et al., Cross-presentation: a general mechanism for CTL immunity and tolerance. Immunol Today, 1998. **19**(8): p. 368-73.*
26. *Curiel, T.J., Tregs and rethinking cancer immunotherapy. J Clin Invest, 2007. **117**(5): p. 1167-74.*
27. *Kaufman, H.L. and M.L. Disis, Immune system versus tumor: shifting the balance in favor of DCs and effective immunity. J Clin Invest, 2004. **113**(5): p. 664-7.*
28. *Schwartz, R.H., Costimulation of T lymphocytes: the role of CD28, CTLA-4, and B7/BB1 in interleukin-2 production and immunotherapy. Cell, 1992. **71**(7): p. 1065-8.*
29. *Smyth, M.J., D.I. Godfrey, and J.A. Trapani, A fresh look at tumor immunosurveillance and immunotherapy. Nat Immunol, 2001. **2**(4): p. 293-9.*
30. *Whiteside, T.L. and R.B. Herberman, The role of natural killer cells in immune surveillance of cancer. Curr Opin Immunol, 1995. **7**(5): p. 704-10.*
31. *Bauer, S., et al., Activation of NK cells and T cells by NKG2D, a receptor for stress-inducible MICA. Science, 1999. **285**(5428): p. 727-9.*
32. *Cerwenka, A., et al., Retinoic acid early inducible genes define a ligand family for the activating NKG2D receptor in mice. Immunity, 2000. **12**(6): p. 721-7.*
33. *Diefenbach, A., et al., Ligands for the murine NKG2D receptor: expression by tumor cells and activation of NK cells and macrophages. Nat Immunol, 2000. **1**(2): p. 119-26.*
34. *Godfrey, D.I., et al., NKT cells: facts, functions and fallacies. Immunol Today, 2000. **21**(11): p. 573-83.*
35. *Sakaguchi, S., Animal models of autoimmunity and their relevance to human diseases. Curr Opin Immunol, 2000. **12**(6): p. 684-90.*
36. *Sakaguchi, S., Regulatory T cells: key controllers of immunologic self-tolerance. Cell, 2000. **101**(5): p. 455-8.*
37. *Hickman, J.A., Apoptosis and tumourigenesis. Curr Opin Genet Dev, 2002. **12**(1): p. 67-72.*
38. *Caruso, D.A., et al., Results of a Phase I study utilizing monocyte-derived dendritic cells pulsed with tumor RNA in children with Stage 4 neuroblastoma. Cancer, 2005. **103**(6): p. 1280-91.*
39. *Espinoza-Delgado, I., Cancer vaccines. Oncologist, 2002. **7 Suppl 3**: p. 20-33.*
40. *Hodi, F.S., et al., Biologic activity of cytotoxic T lymphocyte-associated antigen 4 antibody blockade in previously vaccinated metastatic melanoma and ovarian carcinoma patients. Proc Natl Acad Sci U S A, 2003. **100**(8): p. 4712-7.*
41. *Phan, G.Q., et al., Cancer regression and autoimmunity induced by cytotoxic T lymphocyte-associated antigen 4 blockade in patients with metastatic melanoma. Proc Natl Acad Sci U S A, 2003. **100**(14): p. 8372-7.*
42. *Shimizu, J., et al., Stimulation of CD25(+)CD4(+) regulatory T cells through GITR breaks immunological self-tolerance. Nat Immunol, 2002. **3**(2): p. 135-42.*
43. *Lahn, M., S. Kloeker, and B.S. Berry, TGF-beta inhibitors for the treatment of cancer. Expert Opin Investig Drugs, 2005. **14**(6): p. 629-43.*
44. *Gaffen, S.L. and K.D. Liu, Overview of interleukin-2 function, production and clinical applications. Cytokine, 2004. **28**(3): p. 109-23.*
45. *Sutmuller, R.P., et al., Synergism of cytotoxic T lymphocyte-associated antigen 4 blockade and depletion of CD25(+) regulatory T cells in antitumor therapy*

reveals alternative pathways for suppression of autoreactive cytotoxic T lymphocyte responses. J Exp Med, 2001. ***194****(6): p. 823-32.*

46. *Gordon, M.S., et al., Phase I safety and pharmacokinetic study of recombinant human anti-vascular endothelial growth factor in patients with advanced cancer. J Clin Oncol, 2001.* ***19****(3): p. 843-50.*
47. *Gutheil, J.C., et al., Targeted antiangiogenic therapy for cancer using Vitaxin: a humanized monoclonal antibody to the integrin alphavbeta3. Clin Cancer Res, 2000.* ***6****(8): p. 3056-61.*
48. *Fidler, I.J., Selection of successive tumour lines for metastasis. Nat New Biol, 1973.* ***242****(118): p. 148-9.*
49. *Fidler, I.J., Biological behavior of malignant melanoma cells correlated to their survival in vivo. Cancer Res, 1975.* ***35****(1): p. 218-24.*
50. *Fidler, I.J. and G.L. Nicolson, Organ selectivity for implantation survival and growth of B16 melanoma variant tumor lines. J Natl Cancer Inst, 1976.* ***57****(5): p. 1199-202.*
51. *http://ccforum.com/content/8/3/180/figure/F1.*
52. *Kastelein, R.A., C.A. Hunter, and D.J. Cua, Discovery and biology of IL-23 and IL-27: related but functionally distinct regulators of inflammation. Annu Rev Immunol, 2007.* ***25****: p. 221-42.*
53. *Villarino, A.V. and C.A. Hunter, Biology of recently discovered cytokines: discerning the pro- and anti-inflammatory properties of interleukin-27. Arthritis Res Ther, 2004.* ***6****(5): p. 225-33.*
54. *Colgan, J. and P. Rothman, All in the family: IL-27 suppression of T(H)-17 cells. Nat Immunol, 2006.* ***7****(9): p. 899-901.*
55. *Brombacher, F., R.A. Kastelein, and G. Alber, Novel IL-12 family members shed light on the orchestration of Th1 responses. Trends Immunol, 2003.* ***24****(4): p. 207-12.*
56. *Nieuwenhuis, E.E., et al., Disruption of T helper 2-immune responses in Epstein-Barr virus-induced gene 3-deficient mice. Proc Natl Acad Sci U S A, 2002.* ***99****(26): p. 16951-6.*
57. *Wirtz, S., et al., Protection from lethal septic peritonitis by neutralizing the biological function of interleukin 27. J Exp Med, 2006.* ***203****(8): p. 1875-81.*
58. *Maxeiner, J.H., et al., A method to enable the investigation of murine bronchial immune cells, their cytokines and mediators. Nat Protoc, 2007.* ***2****(1): p. 105-12.*
59. *Doganci, A., et al., The IL-6R alpha chain controls lung CD4+CD25+ Treg development and function during allergic airway inflammation in vivo. J Clin Invest, 2005.* ***115****(2): p. 313-25.*
60. *Sauer, K.A., et al., Isolation of CD4+ T cells from murine lungs: a method to analyze ongoing immune responses in the lung. Nat Protoc, 2006.* ***1****(6): p. 2870-5.*
61. *http://www.miltenyibiotech.com.*
62. *Janeway, C., Immunobiology. 2005.* ***6th edition****.*
63. *Sasse, A.D., et al., Chemoimmunotherapy versus chemotherapy for metastatic malignant melanoma. Cochrane Database Syst Rev, 2007(1): p. CD005413.*
64. *McMahon, G., VEGF receptor signaling in tumor angiogenesis. Oncologist, 2000.* ***5 Suppl 1****: p. 3-10.*

65. *Hausding, M., et al., Lung CD11c+ cells from mice deficient in Epstein-Barr virus-induced gene 3 (EBI-3) prevent airway hyper-responsiveness in experimental asthma. Eur J Immunol, 2007.* ***37****(6): p. 1663-77.*
66. *Banchereau, J., et al., Will the making of plasmacytoid dendritic cells in vitro help unravel their mysteries? J Exp Med, 2000.* ***192****(12): p. F39-44.*
67. *Gerosa, F., et al., The reciprocal interaction of NK cells with plasmacytoid or myeloid dendritic cells profoundly affects innate resistance functions. J Immunol, 2005.* ***174****(2): p. 727-34.*
68. *Shortman, K. and Y.J. Liu, Mouse and human dendritic cell subtypes. Nat Rev Immunol, 2002.* ***2****(3): p. 151-61.*
69. *Chan, C.W., et al., Interferon-producing killer dendritic cells provide a link between innate and adaptive immunity. Nat Med, 2006.* ***12****(2): p. 207-13.*
70. *Taieb, J., et al., A novel dendritic cell subset involved in tumor immunosurveillance. Nat Med, 2006.* ***12****(2): p. 214-9.*
71. *Ullrich, E., et al., Therapy-induced tumor immunosurveillance involves IFN-producing killer dendritic cells. Cancer Res, 2007.* ***67****(3): p. 851-3.*
72. *Shortman, K. and J.A. Villadangos, Is it a DC, is it an NK? No, it's an IKDC. Nat Med, 2006.* ***12****(2): p. 167-8.*
73. *Spits, H. and L.L. Lanier, Natural killer or dendritic: what's in a name? Immunity, 2007.* ***26****(1): p. 11-6.*
74. *Szabo, S.J., et al., Distinct effects of T-bet in TH1 lineage commitment and IFN-gamma production in CD4 and CD8 T cells. Science, 2002.* ***295****(5553): p. 338-42.*
75. *Lucas, M., et al., Dendritic cells prime natural killer cells by trans-presenting interleukin 15. Immunity, 2007.* ***26****(4): p. 503-17.*
76. *Borg, N.A., et al., CD1d-lipid-antigen recognition by the semi-invariant NKT T-cell receptor. Nature, 2007.* ***448****(7149): p. 44-9.*
77. *Heath, W.R., et al., Cross-presentation, dendritic cell subsets, and the generation of immunity to cellular antigens. Immunol Rev, 2004.* ***199****: p. 9-26.*
78. *Allan, R.S., et al., Epidermal viral immunity induced by CD8alpha+ dendritic cells but not by Langerhans cells. Science, 2003.* ***301****(5641): p. 1925-8.*
79. *Belz, G.T., et al., Distinct migrating and nonmigrating dendritic cell populations are involved in MHC class I-restricted antigen presentation after lung infection with virus. Proc Natl Acad Sci U S A, 2004.* ***101****(23): p. 8670-5.*
80. *Bergmann, S. and P.P. Pandolfi, Giving blood: a new role for CD40 in tumorigenesis. J Exp Med, 2006.* ***203****(11): p. 2409-12.*
81. *Tuettenberg, A., et al., Dendritic cell-based immunotherapy of malignant melanoma: success and limitations. J Dtsch Dermatol Ges, 2007.* ***5****(3): p. 190-6.*
82. *Huang, H., et al., CD4+ Th1 cells promote CD8+ Tc1 cell survival, memory response, tumor localization and therapy by targeted delivery of interleukin 2 via acquired pMHC I complexes. Immunology, 2007.* ***120****(2): p. 148-59.*
83. *Dalchau, R., J. Kirkley, and J.W. Fabre, Monoclonal antibody to a human leukocyte-specific membrane glycoprotein probably homologous to the leukocyte-common (L-C) antigen of the rat. Eur J Immunol, 1980.* ***10****(10): p. 737-44.*
84. *Sancho, D., M. Gomez, and F. Sanchez-Madrid, CD69 is an immunoregulatory molecule induced following activation. Trends Immunol, 2005.* ***26****(3): p. 136-40.*

85. *Klemke, M., et al., High affinity interaction of integrin alpha4beta1 (VLA-4) and vascular cell adhesion molecule 1 (VCAM-1) enhances migration of human melanoma cells across activated endothelial cell layers. J Cell Physiol, 2007.* ***212****(2): p. 368-74.*
86. *Marie, J.C., et al., TGF-beta1 maintains suppressor function and Foxp3 expression in CD4+CD25+ regulatory T cells. J Exp Med, 2005.* ***201****(7): p. 1061-7.*
87. *Zheng, Y. and A.Y. Rudensky, Foxp3 in control of the regulatory T cell lineage. Nat Immunol, 2007.* ***8****(5): p. 457-62.*
88. *O'Garra, A. and P. Vieira, T(H)1 cells control themselves by producing interleukin-10. Nat Rev Immunol, 2007.* ***7****(6): p. 425-8.*
89. *Endharti, A.T., et al., Cutting edge: CD8+CD122+ regulatory T cells produce IL-10 to suppress IFN-gamma production and proliferation of CD8+ T cells. J Immunol, 2005.* ***175****(11): p. 7093-7.*
90. *Stumhofer, J.S., et al., Interleukin 27 negatively regulates the development of interleukin 17-producing T helper cells during chronic inflammation of the central nervous system. Nat Immunol, 2006.* ***7****(9): p. 937-45.*
91. *Beutler, B. and F. Bazzoni, TNF, apoptosis and autoimmunity: a common thread? Blood Cells Mol Dis, 1998.* ***24****(2): p. 216-30.*
92. *Blankenstein, T., et al., Tumor suppression after tumor cell-targeted tumor necrosis factor alpha gene transfer. J Exp Med, 1991.* ***173****(5): p. 1047-52.*
93. *Pan, G., et al., The receptor for the cytotoxic ligand TRAIL. Science, 1997.* ***276****(5309): p. 111-3.*
94. *Huang, Z., Bcl-2 family proteins as targets for anticancer drug design. Oncogene, 2000.* ***19****(56): p. 6627-31.*
95. *Hisada, M., et al., Potent antitumor activity of interleukin-27. Cancer Res, 2004.* ***64****(3): p. 1152-6.*
96. *Chiyo, M., et al., Expression of IL-27 in murine carcinoma cells produces antitumor effects and induces protective immunity in inoculated host animals. Int J Cancer, 2005.* ***115****(3): p. 437-42.*
97. *Salcedo, R., et al., IL-27 mediates complete regression of orthotopic primary and metastatic murine neuroblastoma tumors: role for CD8+ T cells. J Immunol, 2004.* ***173****(12): p. 7170-82.*
98. *Shimizu, M., et al., Antiangiogenic and antitumor activities of IL-27. J Immunol, 2006.* ***176****(12): p. 7317-24.*
99. *Oniki, S., et al., Interleukin-23 and interleukin-27 exert quite different antitumor and vaccine effects on poorly immunogenic melanoma. Cancer Res, 2006.* ***66****(12): p. 6395-404.*
100. *Larousserie, F., et al., Analysis of interleukin-27 (EBI3/p28) expression in Epstein-Barr virus- and human T-cell leukemia virus type 1-associated lymphomas: heterogeneous expression of EBI3 subunit by tumoral cells. Am J Pathol, 2005.* ***166****(4): p. 1217-28.*
101. *Kim, T.H., et al., Recombinant human prothrombin kringle-2 inhibits B16F10 melanoma metastasis through inhibition of neovascularization and reduction of matrix metalloproteinase expression. Clin Exp Metastasis, 2006.* ***23****(7-8): p. 391-9.*
102. *Colonna, M., G. Trinchieri, and Y.J. Liu, Plasmacytoid dendritic cells in immunity. Nat Immunol, 2004.* ***5****(12): p. 1219-26.*

103. *Hutson, T.E. and D.I. Quinn, Cytokine therapy: a standard of care for metastatic renal cell carcinoma? Clin Genitourin Cancer, 2005.* ***4****(3): p. 181-6.*
104. *Chaudhry, U.I., et al., Combined stimulation with interleukin-18 and CpG induces murine natural killer dendritic cells to produce IFN-gamma and inhibit tumor growth. Cancer Res, 2006.* ***66****(21): p. 10497-504.*
105. *Villarino, A., et al., The IL-27R (WSX-1) is required to suppress T cell hyperactivity during infection. Immunity, 2003.* ***19****(5): p. 645-55.*
106. *Lin, W.N., et al., Involvement of MAPKs and NF-kappaB in LPS-induced VCAM-1 expression in human tracheal smooth muscle cells. Cell Signal, 2007.* ***19****(6): p. 1258-67.*
107. *Smits, H.H., et al., Different faces of regulatory DCs in homeostasis and immunity. Trends Immunol, 2005.* ***26****(3): p. 123-9.*
108. *Zahn, S., et al., Impaired Th1 responses in mice deficient in Epstein-Barr virus-induced gene 3 and challenged with physiological doses of Leishmania major. Eur J Immunol, 2005.* ***35****(4): p. 1106-12.*
109. *Batten, M., et al., Interleukin 27 limits autoimmune encephalomyelitis by suppressing the development of interleukin 17-producing T cells. Nat Immunol, 2006.* ***7****(9): p. 929-36.*
110. *Klebanoff, C.A., L. Gattinoni, and N.P. Restifo, CD8+ T-cell memory in tumor immunology and immunotherapy. Immunol Rev, 2006.* ***211****: p. 214-24.*
111. *Mackensen, A., et al., Phase I study of adoptive T-cell therapy using antigen-specific CD8+ T cells for the treatment of patients with metastatic melanoma. J Clin Oncol, 2006.* ***24****(31): p. 5060-9.*
112. *Corthay, A., et al., Primary antitumor immune response mediated by CD4+ T cells. Immunity, 2005.* ***22****(3): p. 371-83.*
113. *Huang, H., et al., Synergistic enhancement of antitumor immunity with adoptively transferred tumor-specific CD4+ and CD8+ T cells and intratumoral lymphotactin transgene expression. Cancer Res, 2002.* ***62****(7): p. 2043-51.*
114. *Devergne, O., et al., A novel interleukin-12 p40-related protein induced by latent Epstein-Barr virus infection in B lymphocytes. J Virol, 1996.* ***70****(2): p. 1143-53.*
115. *Maaser, C., et al., Expression of Epstein-Barr virus-induced gene 3 and other interleukin-12-related molecules by human intestinal epithelium. Immunology, 2004.* ***112****(3): p. 437-45.*

8 Abbreviations

APC = antigen presenting cells

APS = Ammoniumperoxidsulphate

BALF = Bronchoalveolar lavage fluid

°C = degree Celsius

CO_2 = carbon dioxide

CTL = cytotoxic T lymphocyte

DC = dendritic cells

DMEM = Dulbecco`s modified eagle medium

DMSO = Dimethylsulfoxid

DLN = draining lymph nodes

DNA = deoxyribonucleic acid

DR = death receptor

EBI-3 = Epstein-Barr virus induced gene 3

EDTA = Ethylendiamintetraacetate

e.g. = for example

EGFR = epidermal growth factor receptor

ELISA = enzyme linked immunosorbend assay

EtBr = Ethidiumbromide

EtOH = Ethanol

FACS = fluorescence-activated cell sorting

FADD = Fas associated protein with death domain

FasL = Fas ligand

FCS = Fetal Calf Serum

Foxp3 = Forkhead box protein 3

G = grams

GITR = glucocorticoid-induced TNF receptor

h = hours

HCl = Hydrochloric Acid

H_2SO_4 = Sulfuric Acid

HSP = heat shock proteins

i.c. = intracardial

IFN = interferon

IK-DC = interferon-γ producing killer dendritic cells

IL = interleukin

IL-6R = Interleukin-6 Receptor

i.p. = intraperitoneal

i.v. = intravenous

Jak = Janus Kinase

$KHCO_3$ = Potassiumhydrogencarbonat

KOH = Potassiumhydroxide

L = liters

LPS = Lipopolysaccharide

$MgCl_2$ = Magnesiumchloride

MHC = major histocompatibility class

min = minutes

mg = milligrams

ml = milliliters

µg = micrograms

µl = microliters

Na_2CO_3 = Sodiumcarbonat

NaH_2PO_4 = Sodiumdihydrogenphosphate

$NaHCO_3$ = Sodiumhydrogencarbonat

Na_2HPO_4 = Di-Sodiumhydrogenphosphate

NH_4Cl = Ammoniumchloride

NaN_3 = Sodium Azide

NFAT = nuclear factor of activated T cells

NFκB = nuclear factor-kappa B

ng = nanograms

NK = natural killer

NKT = natural killer T

OCT compound = optimal cutting temperature compound

PBS = Phosphate buffered Saline

PCR = Polymerase chain reaction
pDC = plasmacytoid dendritic cells
PMA = Phorbol-myristat-Acetate
rpm = rotations per minute
RPMI = Roswell Park Memorial Institute
SDS = Sodium-dodecylsulfate
SEM = standard error of mean
STAT = signal transducer and activator of transcription
TAA = tumor associated antigen
TAE = Tris-Acetate-EDTA
TCCR = T cell cytokine receptor
TCR = T cell receptor
TGF = transforming growth factor
Th = T helper
TLR = toll like receptor
TMB = 3,3,5,5- Tetramethylbenzidin
TNF = tumor necrosis factor
TRAIL = TNF related apoptosis inducing ligand
Tris-HCl = Tris-hydrochloride
Treg = T regulatory
UV = Ultra Violet
VCAM = vascular cell adhesion molecule
VEGF = vascular endothelial growth factor